Oxygen activation during neuronal NOS reaction

Davide Papale

Thesis presented for the degree of Doctor of Philosophy

University of Edinburgh

2008

Alla mia famiglia

"...e un ragazzino
al secondo piano
che canta ride e stona
perché vada lontano
fa che gli sia dolce
anche la pioggia nelle scarpe
anche la solitudine"

Declaration

I declare that the work presented in this thesis is the original work of the author, except where specific reference is made to other sources. It has not been submitted in part, or in whole, for any other degree.

Davide Papale

July 2008

Acknowledgements

Firstly I would like to thank my supervisor, Dr. Simon Daff for his excellent guidance and for being always present during the entire period of my PhD. Then I thank my second supervisor, Prof. Steve Chapman for his professionalism and for his constant support. I would also like to thank all the people of the Chapman/Daff group, past and present, for being such beautiful mates.

In addition I would like to thank Dr. Caroline Miles for the molecular biology work, Dr. Chris Mowat and Ms. Chiara Bruckmann for all the crystallography.

ABSTRACT

Nitric oxide synthase (NOS), a cytochrome P450-like oxygenase, catalyzes nitric oxide (NO) production in a two cycle reaction: the first step leads to the production of N^G-hydroxy-L-arginine (NOHA), the stable enzyme-bound intermediate, while the second cycle results in the production of NO and L-citrulline. The three mammalian isozymes are homodimeric enzymes and each monomer is composed of a reductase and an oxygenase domain. The oxygenase domain contains the arginine binding site and needs one heme (protoporphyrin IX) ligated by a cysteine thiolate, and one H_4B molecule. Enzyme substrates are O_2, L-arginine (or NOHA) and NADPH, which provides electrons for the activation of oxygen. H_4B is an essential cofactor for NO production by NOS and its roles are in dimerization and as an electron donor/acceptor. In each cycle the generally accepted reaction sequence that involves the heme iron is:

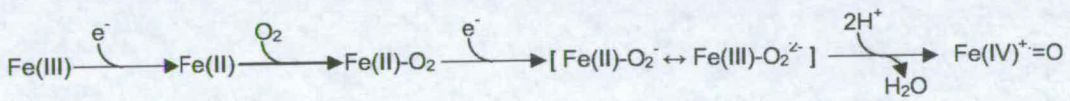

the first electron is transferred from the reductase domain, and the second electron donated by H_4B. Amino acid residues in the distal portion of NOS heme domain are involved in the stabilization and activation of the oxygen-heme complexes formed during NO production. An amino acid residue with the ability of forming hydrogen-bonds at a suitable distance from the space where substrate and oxygen-heme complexes interact may introduce species stabilization during the course of oxygen activation. With this in mind a mutant of $nNOS_{oxy}$ was generated where glycine 586 was replaced by a serine residue (G586S $nNOS_{oxy}$). It was then expressed and purified as the truncated heme domain and spectroscopic (UV-Vis) characterization of the

mutant to verify that it retained its structural integrity was performed. The way the mutation affects the binding of a variety of compounds, such as substrates, substrate-analogues and diatomic ligands, was tested and compared with that characterizing the wild type.

Stopped Flow experiments monitoring Oxy-Ferrous compound formation and decay were performed and analyzed in a comparison with the wild type $nNOS_{oxy}$. We report the formation of a novel reaction intermediate during G586S $nNOS_{oxy}$ reaction in the presence of H_4B and substrate, subsequent to the formation of the Oxy-Ferrous compound. The nature of the newly detected species has been investigated repeating stopped flow experiments in a variety of conditions, such as the absence of substrate and replacing H_4B with amino-H_4B, a strong inhibitor of NOS activity. The fact that the new intermediate was not detected when substrate-bound G586S $nNOS_{oxy}$ reacts in the presence of amino-H_4B, points to how its formation relies on the second electron being donated to the oxy-ferrous compound (from H_4B). In order to assess whether the mutation affects the reduction potential of the G586S mutant, potentiometric titrations were conducted in the presence and absence of the substrate, evidencing that the mutant enzyme retains the heme native electrical properties.

Finally crystals of the G586S mutant with L-arginine bound in the catalytic site were grown and the X-Ray structure solved. This showed that the newly introduced serine 586 is at a suitable distance from the substrate guanidinium group to form a hydrogen-bond: this causes a repositioning of the substrate itself, which in turn justifies the different affinities and catalytic behaviour compared to those of the wild type $nNOS_{oxy}$.

Amino Acids

Alanine	A	Ala	Methionine	M	Met
Cysteine	C	Cys	Asparagine	N	Asn
Aspartic Acid	D	Asp	Proline	P	Pro
Glutamic Acid	E	Glu	Glutamine	Q	Gln
Phenylalanine	F	Phe	Arginine	R	Arg
Glycine	G	Gly	Serine	S	Ser
Histidine	H	His	Threonine	T	Thr
Isoleucine	I	Ile	Valine	V	Val
Lysine	K	Lys	Tryptophan	W	Trp
Leucine	L	Leu	Tyrosine	Y	Tyr

Standard Units

m	Metre	°C	Celsius
Å	Angstrom	l	Litre
g	Gram	V	Volt
s	Second	M	Molar

Kinetic Parameters

k_{cat}	Maximal turnover rate constant
K_M	Michaelis constant
K_d	Dissociation constant
k_{sat}	Observed rate constant at saturating concentrations of substrate

k_{red}	Rate constant for first-electron transfer
k_{red2}	Rate constant for second-electron transfer
k_{autox}	Rate constant for oxy-ferrous decay
k_{obs}	Observed rate constant
$k_{1,2,3}$	Rate constants for the first, second or third phases of a multi phase reaction

Textural Abbreviations

Abs.	Absorbance
CaM	Calmoduline
cGMP	Cyclic guanosine monophosphate
cNOS	Constitutive NOS
CYP	Cytochrome P450
Da	Dalton
dH_2O	Deionised water
DMSO	Dimethyl Sulfoxide
ε_x	Extinction coefficient at wavelength x nm
E. coli	*Escherichia coli*
EDRF	Endothelium-derived relaxing factor
EDTA	Ethylenediaminetetraacetic acid
E_m	Midpoint potential
eNOS	Endothelial NOS
EPR	Electron Paramagnetic Resonance

FAD	Flavin Adenine Dinucleotide
FMN	Flavin Mononucleotide
H_4B	Tetrahydrobiopbterin
hd	Heme Domain
iNOS	inducible NOS
NADH	β-Nicotinamide adenine dinucleotide
NAME	N-Nitro-L-Arginine Methyl Ester
NIO	N-iminoethyl-L-ornithine
NADPH	β-Nicotinamide adenine dinucleotide phosphate
nNOS	neuronal NOS
NO	Nitric oxide
NOHA	N-Hydroxy-arginine
NOS	Nitric Oxide Synthase
NOS_{oxy}	NOS oxygenase domain
OTTLE	Optically Transparent Thin Layer Electrode
ox	Oxidised
P450 BM3	Cytochrome P450 monooxygenase from *Bacillus megaterium*
P450 cam	Cytochrme P450 monooxygenase from *Pseudomonas putida*
PDB	Protein data bank
red	Reduced
SDS-PAGE	Sodium dodecylsulphate-polyacrylamide gel electrophoresis
SHE	Standard hydrogen electrode
RMSD	Root mean square deviation
Tris	Tris(hydroxyl)aminomethane
UV	Ultra Violet

vis	visible
WT	Wild type

TABLE OF CONTENTS

Chapter 1

INTRODUCTION

1 INTRODUCTION

1.1 Nitric Oxide

Nitric oxide (NO) is a signalling molecule that is involved in a multiplicity of physiological processes: in fact the number of pathways in which it plays a role is growing rapidly since the first discovery of its role as a vascular tone regulator. Its tasks range from cytotoxic agent during immune response, to neurotransmitter diffusing between synapses. Its versatility is due to its size, reactivity and absence of charge, among others. The capability to diffuse across hundreds of microns and to form complexes with transition metals explain why NO is such an eclectic factor and why it acts as a mediator for such a large number of targets belonging to cascades with both eventual protective and destructive effects. On the other hand it is quite surprising to find that a molecule, which is commonly known as a very unstable air pollutant, is central to so many biological processes.

The importance of NO as a topic of research arose when, in 1986, it was identified as the previously called endothelium-derived relaxing factor (EDRF) by two groups researching independently (1,2). New evidence for its involvement in pathologies have been detected since that moment with an impressive pace. The following examples of NO implication are just a tiny selection to represent its ubiquity.

Nitrosylation is a protein post-translation modification analogous to phosphorylation that can modify the activity of a protein (3). The most known nitrosylation, although not the only possible, is S-nitrosylation. This is the reaction of NO with certain cysteine residues in a protein. Targets of this modification can be proteins with an essential role in an organism such as haemoglobin (4) and serum albumin (5).

Malfunctioning protein nitrosylation, and obviously its reverse reaction, denitrosylation, have been associated with pathologies such as myocardial ischemia, atherosclerosis, inflammation, and cancer.

One of the most important enzymes targeted by the action of NO is the soluble Guanylyl Cyclase, the enzyme that converts guanosine triphosphate (GTP) into cyclic guanosine monophosphate (cGMP). The importance of this interaction derives from the huge number of processes in which cGMP has a role: among others it acts as an effector of smooth muscle relaxation, regulator of synaptic transmission and platelet aggregation inhibitor (6,7). These and other processes are modulated through the action of cGMP-dependent enzymes, such as protein kinases, phosphodiesterases and ion channels. NO react with guanylyl cyclase by binding to its prosthetic heme group enhancing cGMP production by up to 400-fold. In fact, as NO production is sensitive to the increase of calcium concentration, it is basically the linking step between the entrance of calcium into the cytoplasm and the production of cGMP and all the effects due to it (figure 1.1).

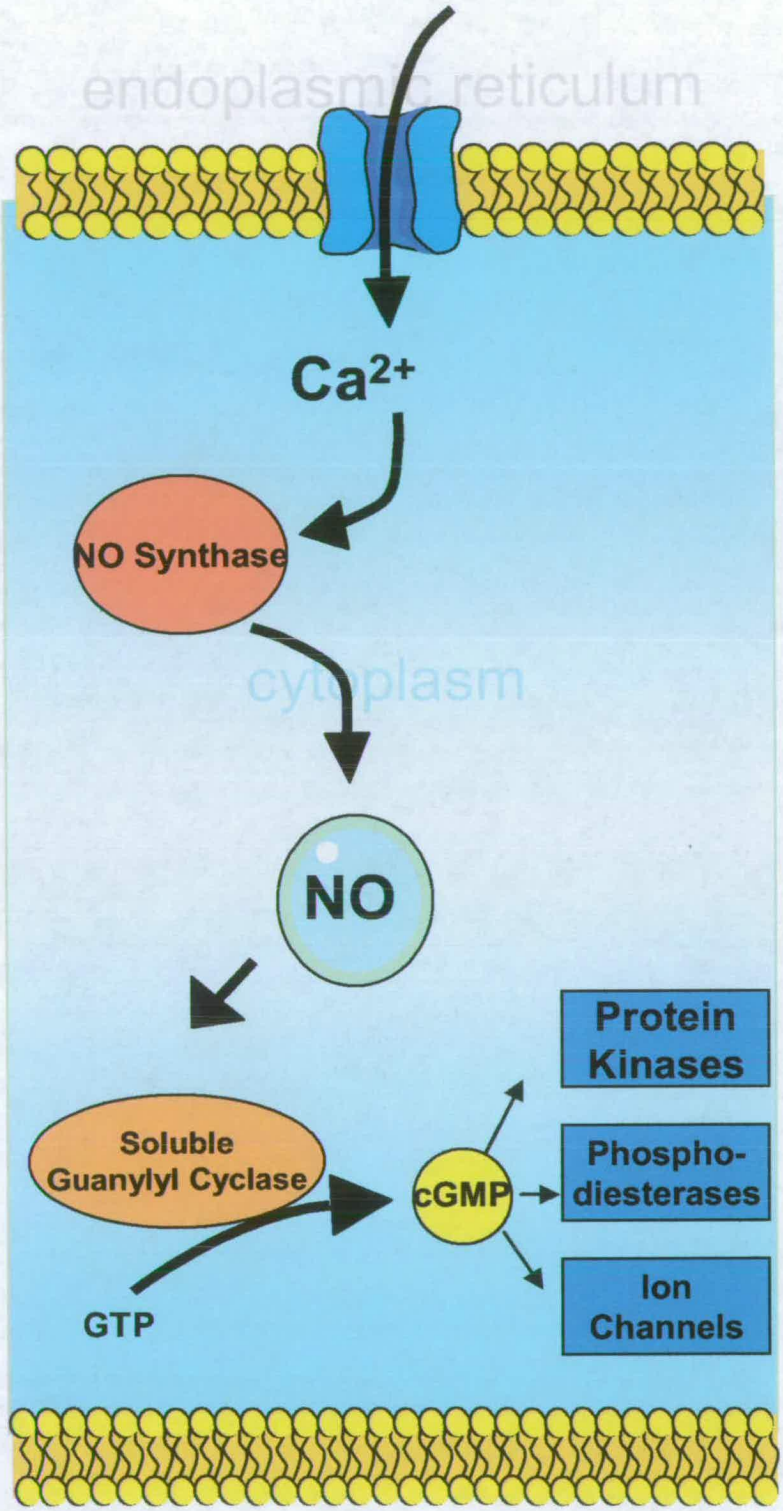

Figure 1.1: Diagram illustrating the cascade of events that connect the entrance of calcium into the cell and the reactions triggered by cyclic GMP

1.1.1 Physical and chemical properties of Nitric Oxide

NO is a colourless gas which turns blue on condensing to the liquid phase (8). The electronic configuration of NO is $(\sigma_s)^2 (\sigma_s^*)^2 (\pi_{x,y})^4 (\sigma_z)^2 (\pi_{x,y}^*)^1$ and the Molecular Orbital energy level diagram is shown in figure 1.2.

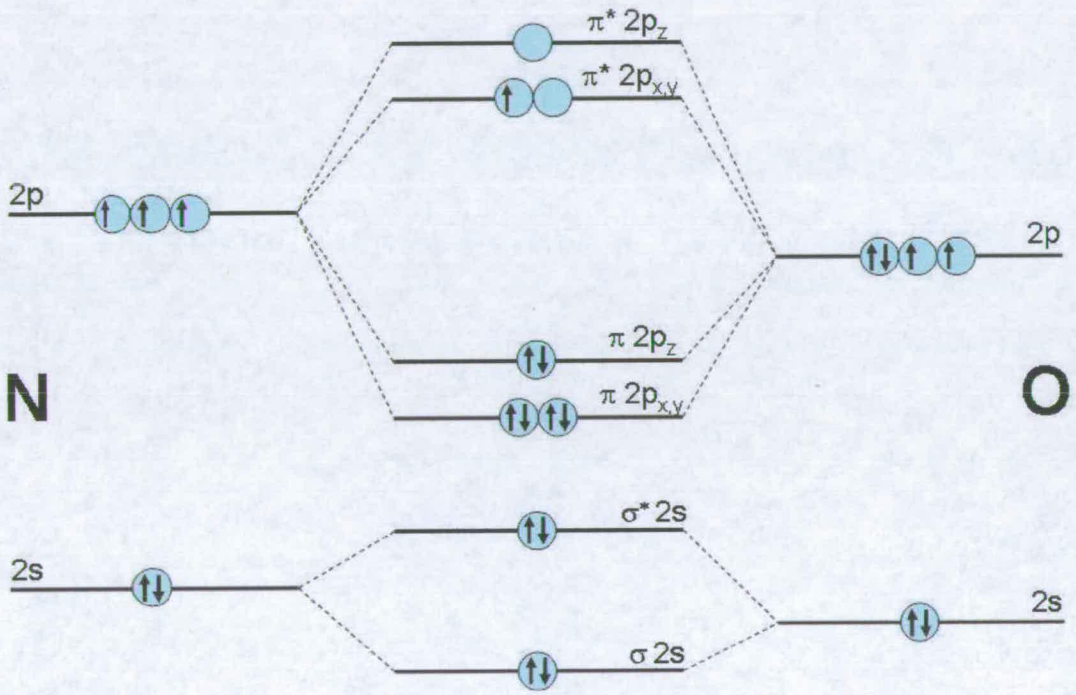

Figure 1.2: Molecular-orbital energy-level diagram for nitric oxide.

The last unpaired electron takes position in a π^* orbital, this is responsible for the main physical and chemical features of NO. The bond order equals 2.5 and suggests that NO is less stable than NO^+ (nitrosyl cation), which has a bond order of 3 and a

shorter bond length (1.06 Å compared to 1.15 Å). The ionization energy of the reaction $NO \rightarrow NO^+$ is, as expected, much lower than that for $N_2 \rightarrow N_2^+$: this is consistent with the fact that the odd electron is positioned in an antibonding orbital and is shielded from the nucleus by the inner electrons. When complexed with metals, NO can be considered to be either an electron donor or acceptor, binding as either NO^+ in a linear geometry or as NO^- in a bent geometry, both via the nitrogen. The most common metal-nitrosyl complexes are with Fe, Ru and Ni. The small difference in electronegativity between oxygen and nitrogen gives the bond a tiny polar character, with the electrons being more probably found around the oxygen atom. Nevertheless NO could be described as an almost non polar molecule.

1.1.2 Biological NO synthesis

Nitric oxide in organisms is enzymatically produced by means of the reaction described in figure 1.3 (9).

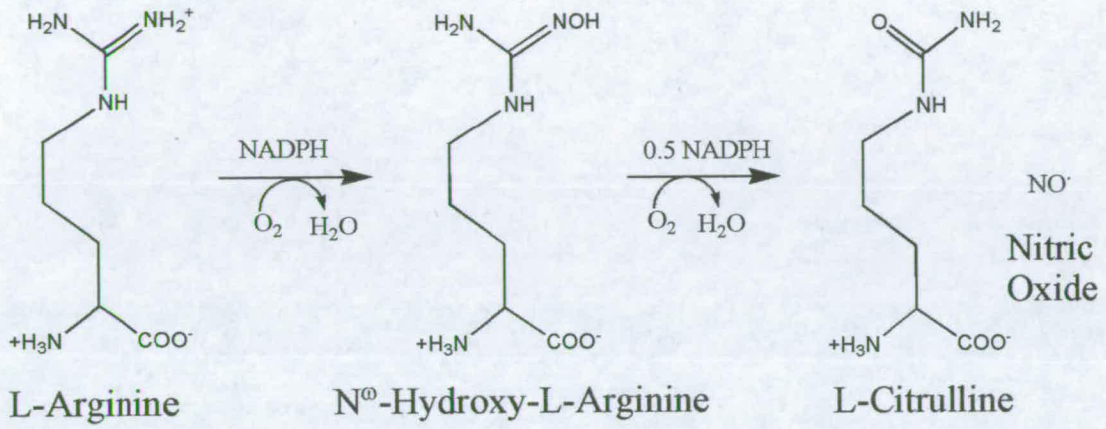

Figure 1.3: Enzyme catalyzed production of NO.

L-Arginine, once bound into the catalytic site, can undergo a first oxidation, that, with the consumption of molecular oxygen and 2 electrons, leads to the formation of N$^{\omega}$-Hydroxy-L-Arginine (NOHA). This reaction intermediate stays bound to the catalytic site and undergoes a second reaction, which is performed with the consumption of 1 electron equivalent and 1 molecule of oxygen. This leads to the production of L-Citrulline and nitric oxide. Both steps of the reaction require the reductive activation of an oxygen molecule. The reaction requires the presence of a number of cofactors and conditions; these will be described and analyzed in the catalytic cycle chapter.

1.2 Nitric Oxide Synthase

The group of enzymes that produce nitric oxide in eukaryotes and in some prokaryotes are called Nitric Oxide Synthases (10). The mammalian NOSs are big dimeric proteins in which each monomer is made of two domains, with a specific connecting region between the two (figure 1.4).

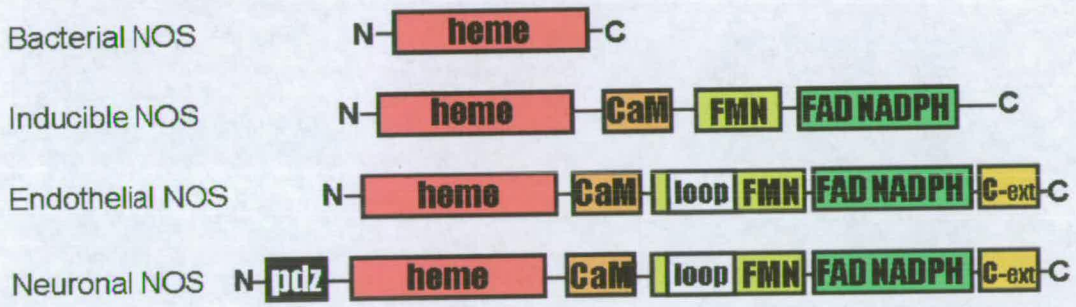

Figure 1.4: Modular composition of the different NOS isoforms, according to protein sequence. In red is the heme domain while the reductase domain is in yellow/green. The connecting portion is composed of a CaM binding region (orange). There is a loop (white) within the FMN domain of endothelial and inducible NOSs and a C-terminal extension to both. Neuronal NOS is the only one having a PDZ-binding domain. The bacterial NOS consists of a heme domain, and requires an electron-providing partner. Only the two constitutive NOSs have a C-terminal regulatory extension (dark yellow).

The N-terminal domain is called the oxygenase or heme domain and binds the prosthetic group heme, the substrate L-arginine, the cofactor (6R)-5,6,7,8-Tetrahydrobiopterin (H_4B) and is the portion of the protein where the actual production of NO happens. The C-terminal portion is called the reductase domain and has the function of providing electrons to the heme domain through the bound

cofactors NADPH, FAD and FMN (figure 1.5). The connecting region is a flexible domain capable of binding the small protein calmodulin (CaM) in

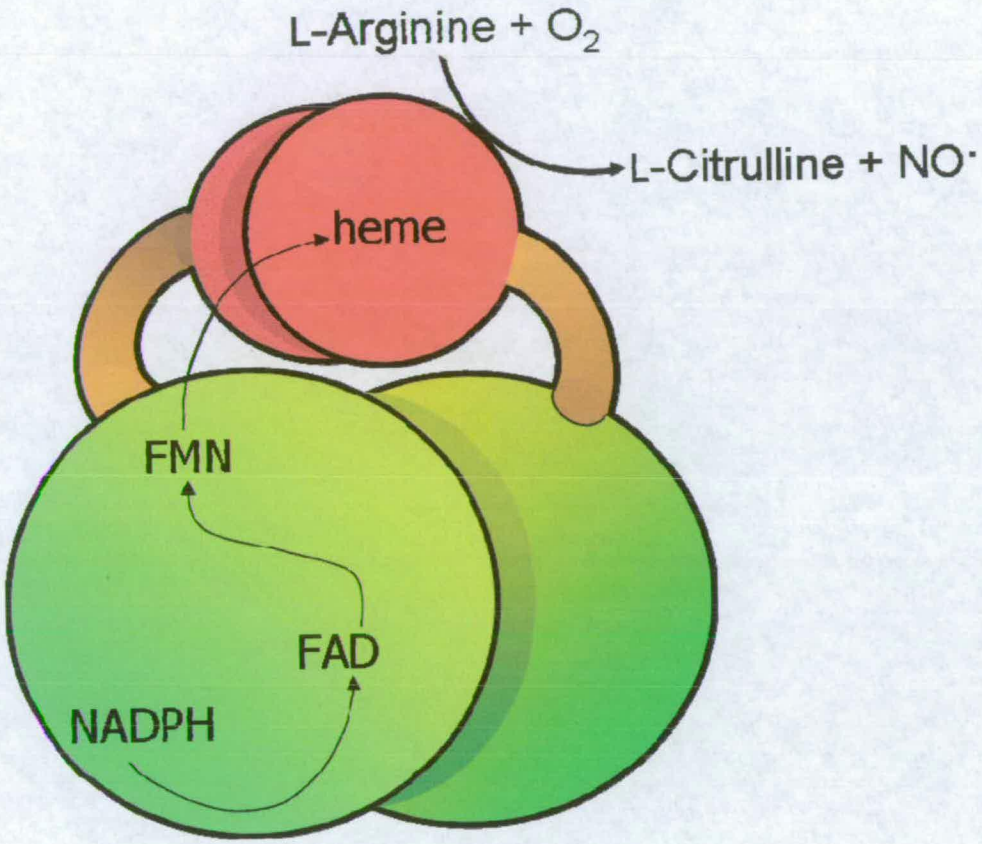

Figure 1.5: Diagram showing the electron flow through the NOS domains during production of NO. In the dimer each reductase domain passes electrons to the heme domain of the other subunit.

the presence of calcium. This is quite a common regulating cofactor which in fact locks the protein in a conformation that allows the communication between the two domains, a condition required for the enzyme to be active. In only one type of mammalian NOS, (nNOS) there is an N-terminal region, located upstream from the heme domain, which forms a PDZ- binding domain (11), the acronym deriving from the first letter of the first three proteins were it was discovered. This region interacts

with other proteins or intracellular structures in the organization of signal transduction complexes. The NOS dimer is formed by a large interface involving the heme domains of each monomer (12), resulting in an overall quasi-globular enzyme. Bacterial NOSs are essentially formed exclusively by the heme domain of animal NOSs, lacking therefore a N-terminal PDZ domain, the CaM binding intermediate region but, most importantly, the reductase domain. They therefore require an external source of electrons (13).

In animals three distinct isoforms of NOSs have been identified, probably descending from a common ancestor, considering the high sequence identity of 50 to 60% between them (15). These are neuronal NOS (nNOS), inducible NOS (iNOS) and endothelial NOS (eNOS), or, respectively, NOS I, II and III. The three isoforms can be divided in two other groups; nNOS and eNOS are the two constitutively produced enzymes whose activity is regulated by the binding of CaM (16). In the other group, iNOS has a very high affinity for CaM such that, when present, it is bound in an irreversible way and allows the enzyme to be always active (17). Hence, the activity of the inducible form is primarily regulated at the level of its expression, and specifically this is started as a response to inflammatory stimuli (18).

The length of the polypeptide chains of the two main domains are quite similar within the mammalian NOS isoforms, with the heme domain of about 500 residues and the reductase of about 700 (from residue 221 to 724 and from 743 to 1429 in nNOS respectively). The overall mass of a neuronal NOS dimer is consequently of about 160 kDa. All the isoforms of NOS have been successfully expressed in a variety of expression systems and new bacterial isoforms are continuously being discovered and characterized (14, 15). The X-ray crystal structures of the isolated

heme domains are available for all isoforms in a number of conditions (e.g. binding substrates or other ligands into the catalytical site) and for many bacterial NOSs (13, 19-22). The structure of the isolate neuronal NOS reductive domain has also been determined (23). On the other hand the structure of an entire mammalian holoenzyme has not been achieved yet, due to the large size of the protein and the flexibility of portions of it.

1.2.1 Reductase domain

The NOS reductase domain is composed of two subdomains, the FMN-domain and the FAD/NADPH-domain, positioned in this order along the polypeptidic chain in the direction N-terminus to C-terminus. A flexible portion between them allows the insertion of the globular FMN domain into the C shaped FAD/NADPH domain (figures 1.7 and 1.13).

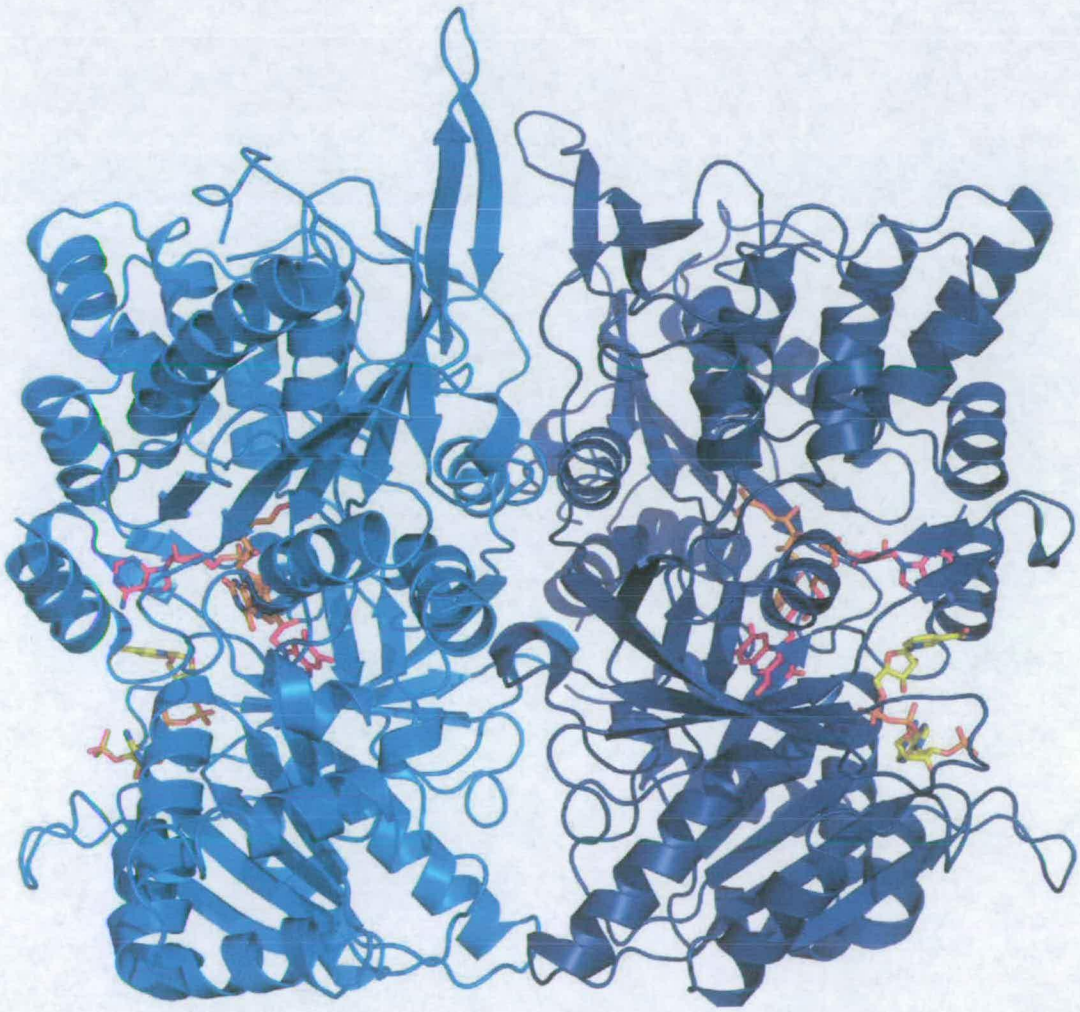

Figure 1.7: NOS reductase domain dimer as it appears in X-ray crystal structure. Buried into the polypeptide chain are the NADPHs (yellow), FADs (red) and FMNs (orange) (23, PDB file: 1TLL).

The reductase domain is structurally and functionally related to a family of diflavin reductases, including cytochrome P450 reductase. It is thought to derive from the fusion of two genes because of structural similarities between the members of this family and singularly expressed proteins that resemble either FMN or NADPH/FAD domains such as flavodoxins (24) and ferredoxin $NADP^+$ reductases (25) respectively. The substrate (NADPH) and the two cofactors, FAD and FMN (figures 1.8 and 1.9), define the domain's role as an electron supplier to the heme domain. They act as electron flow carriers, swinging between different reduction states. More specifically, the stablility of the partially reduced forms of FAD and FMN (figure 1.10) allow single electron donation to the heme starting from the two-electron donor, NADPH in the sequence NADPH→FAD→FMN (figure 1.11) (16, 26, 27).

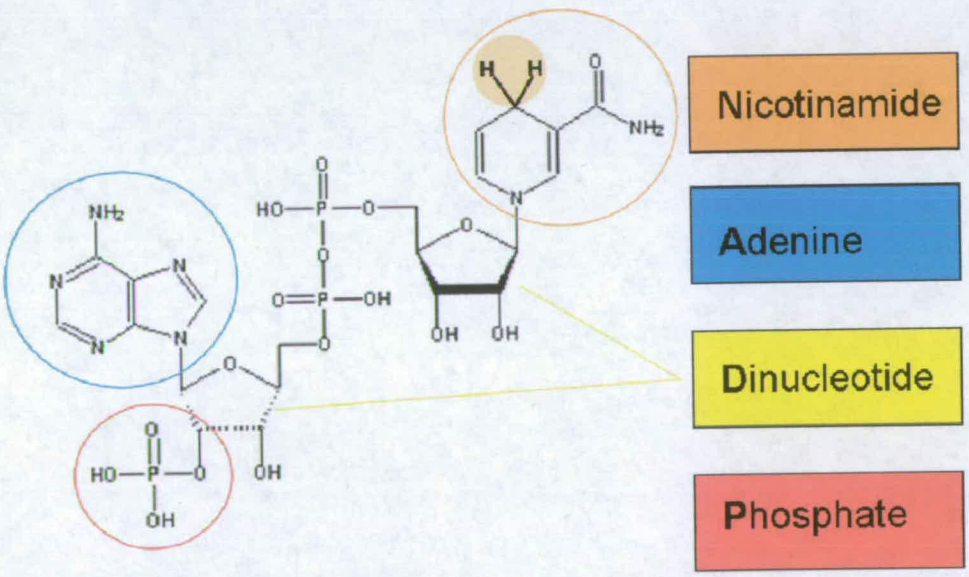

Figure 1.8: NADP(H) structure described with details on each group. Highlighted in orange is the site of hydride transfer.

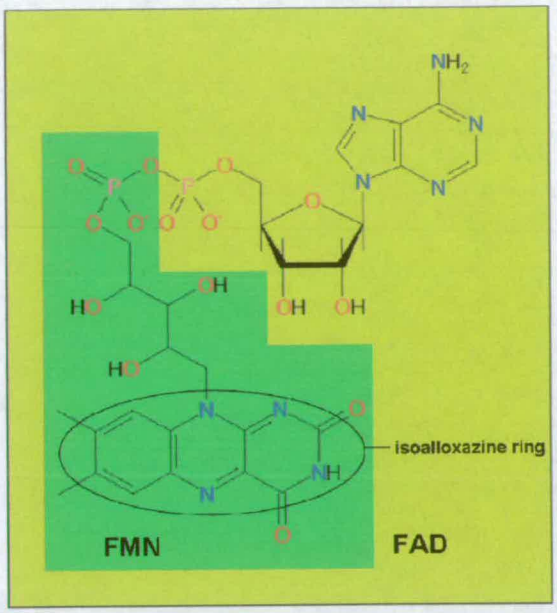

Figure 1.9: Diagram of Flavin Mononucleotide (FMN, on dark green background) and Flavin Adenine Dinucleotide (FAD, entire structure) showing the common part and the isoalloxazine ring which support the different oxidation states of the cofactors.

Essential tools in the study of electron flow through the reductase domain are external electron acceptors, which interact with specificity at different sites. The one-electron acceptor ferricyanide, given its small size, is capable of accepting electrons from either FAD or FMN. Its reduction rate is then useful to assess the rate at which NADPH reduces FAD.

Figure 1.10: Different oxidation states assumed by the isoalloxazine rings of FAD and FMN.

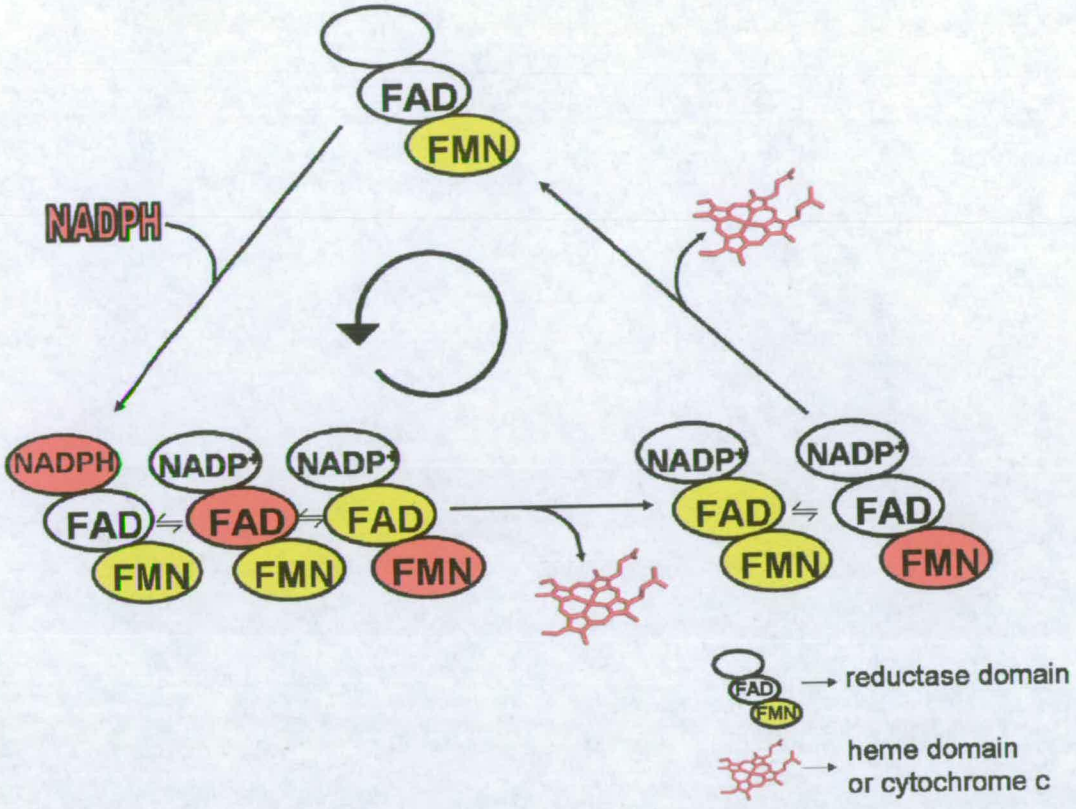

Figure 1.11: The catalytic cycle of NOS reductase domain. The different oxidation states of the cofactors are described by a colour code, being white oxidized, yellow semiquinone and red hydroquinone forms. The sign representing an equilibrium means that all the species are present according to a statistical distribution.

Cytochrome *c* on the other hand, cannot react with the FAD of NOS, while it can irreversibly accept electrons from the FMN, mimicking the electron donation to the NOS heme domain (29, 30).

The role of NOS reductase domain is to enable the two-electron donor, NADPH to reduce the heme, which is a strict one-electron donor.

The first step of the process is the binding of NADPH. The main interactions holding it to the protein consist of a network of hydrogen bonds between the protein itself and the negatively charged phosphate substituent. While the binding of the adenine moiety is quite strict. The nicotinamide ring of NADPH can be positioned either in a

productive conformation, stacking the with FAD isoalloxazine ring, or in an unproductive one, far from it. The isoalloxazine ring of FAD must be stacked either with the nicotinamide ring or with a conserved phenylalanine residue (F1395 in rat nNOS), and the mechanism of displacing each other partitions the enzyme into an active or inactive state as a consequence (figure 1.12) (31, 76). This mechanism, as well as the secondary structure of the NADPH and FAD binding portion, is shared by the large family ferredoxin–$NADP^+$ reductase (FNR) proteins, to which the reductase domain belongs.

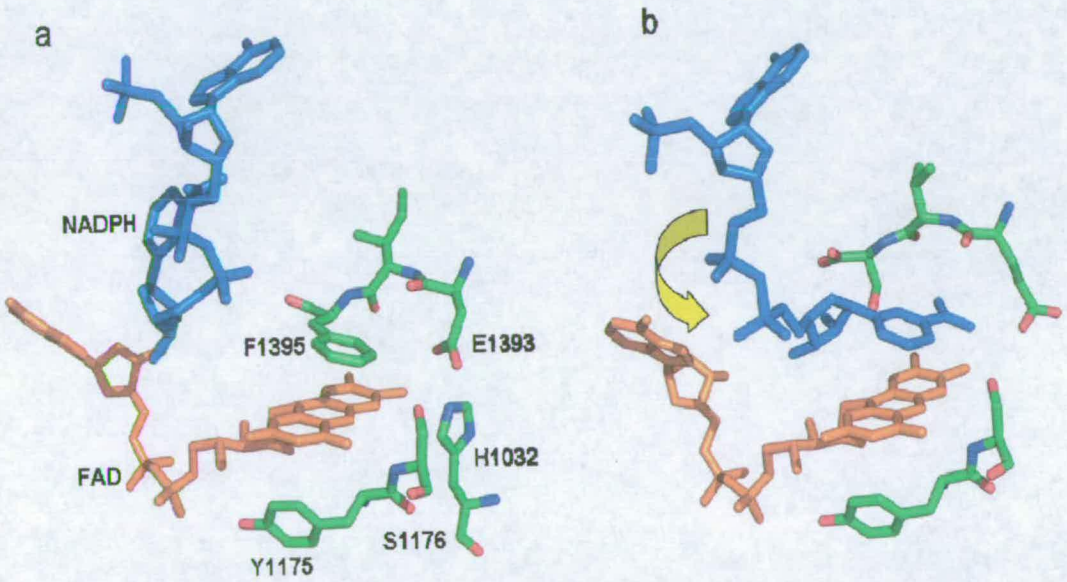

Figure 1.12: The reaction of NADPH with FAD: a) the NADPH/FAD domain of rat nNOS (32) and b) FNR Y308S mutant (33), showing NADPH binding in unproductive and productive conformations respectively. The mutation engineered on FNR enhanced the stacking of the nicotinamide on FAD achieving a much ordered structure. The corresponding F1395 residue of nNOS must move before stacking can occur.

FNR generally catalyzes, hydride transfer from FAD to NADP(H), i.e. in the opposite direction of NOS reductase domain: a shift in the reduction potential of the FAD makes this possible. Being distributed into a productive or unproductive conformation at equilibrium, a portion of the enzyme is into the active form and can give rise to the first step of the electron flow, the double reduction of the FAD to its hydroquinone state. This, although buried in the core of the reductase domain, is in an optimal position to interact with FMN (figure 1.13). The two different subdomains are kept together by means of salt bridges formed by conserved residues. The FMN subdomain has a globular shape and is surrounded by the convex surface formed by the FAD/NADPH subdomain such that the isoalloxazine rings are held in an aligned position at a distance of 4.8Å that is compatible with electron transfer (figure 1.13). In its binding site, FAD forms a hydrogen bond with a conserved serine residue (figure 1.12), which helps to stabilize its semiquinone form, allowing the passage of one electron at time to the FMN. On the other hand, the FMN semiquinone form is extremely stable. Two aromatic residues (Phe809 and Tyr889 in nNOS) stack both sides of the isoalloxazine ring and a carbonyl group of the backbone (belonging to Gly810 in nNOS) forms a hydrogen bond with the N5 nitrogen of the ring system (figure 1.14).

These interactions help to prevent the complete oxidation of FMN. Consequently the cofactor uses only the semiquinone and hydroquinone forms as it shuttle one electron at a time to the heme domain.

All NOS isoforms are active exclusively when as dimers. The dimers are stabilized by interactions between the heme domains of the two monomers and allow the passage

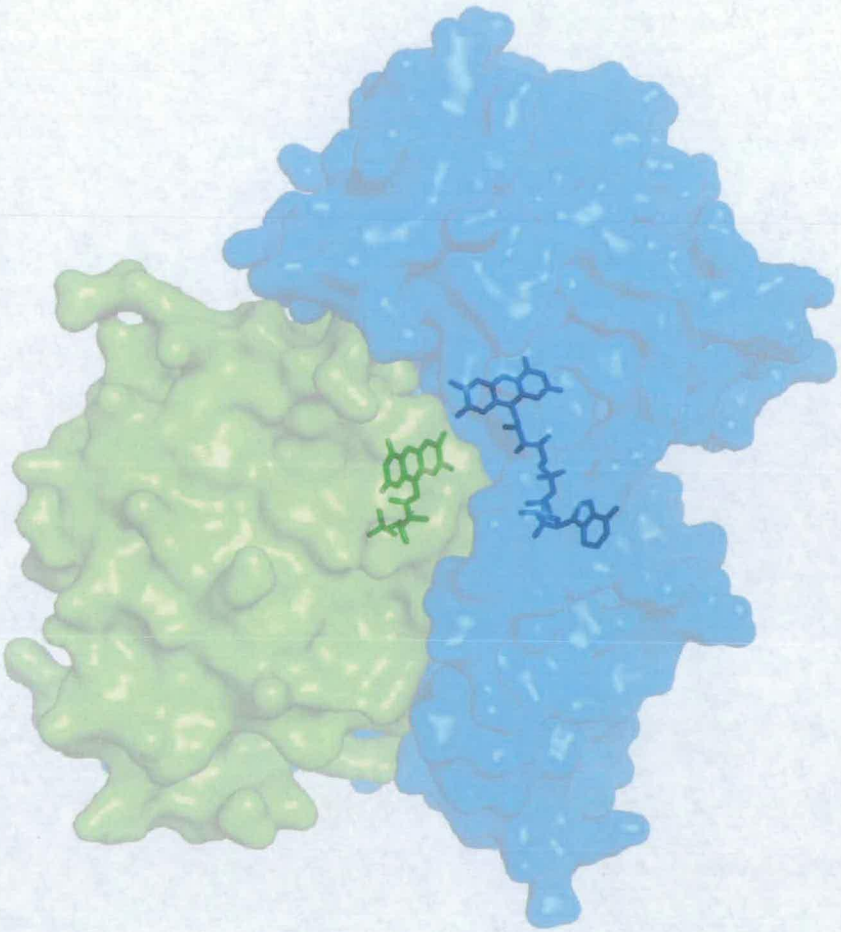

Figure 1.13: The Flavins of nNOS reductase domain are only 4.8 Å apart. FMN domain (in green) and NADPH/FAD domain (in blue), in this X-ray crystal structure (23, PDB file 1TLL).

of electrons from the reductase domain of one monomer and the heme domain of the other monomer that constitute the dimer (34).

Structural investigations have taking into consideration the length of the protein segment that connects the reductase and the heme domains as well as the quaternary structure arrangements between the two monomers (23) have shown that the distance from the FMN cofactor to the accepting heme could be 70 Å. Consequently the FMN subunit has to undergo a large structural rearrangements in order to donate an electron to the heme, for which the distance limit is about 15 Å.

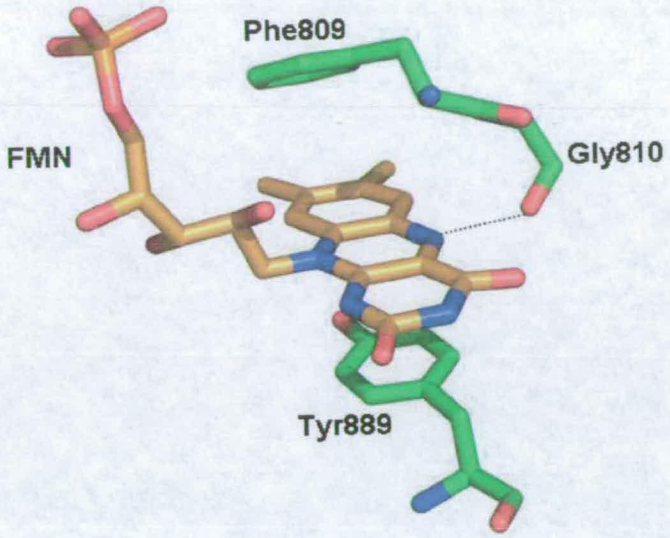

Figure 1.14: FMN in its binding site, being stacked by Phe809 and Tyr889, and forming a hydrogen bond with carbonyl group of Gly810. This tight net of interactions stabilizes the reduced forms of FMN.

As already said, the region connecting the two domains has the role of binding CaM which is of key importance in activating the enzyme for NO production. The CaM binding region was first identified by structural homology with other CaM binging proteins (35, 36).

Binding was shown to occur by the protection of the cleavage site from trypsinolysis in the presence of CaM (37). CaM is a small protein (less then 17 KDa) formed by 4 helix-loop-helix Ca^{2+} binding regions arranged in a double globular structure (figure 1.15). In the presence of a Ca^{2+} atom, two helixes are held in perpendicular to one another resulting in the exposure of hydrophobic residues, which are capable of interacting with recognition sites on NOS. The binding of CaM to NOS has different features and effects depending on the isotype of NOS. The main difference being between iNOS and constitutive NOSs (cNOSs). The latter have an affinity for the

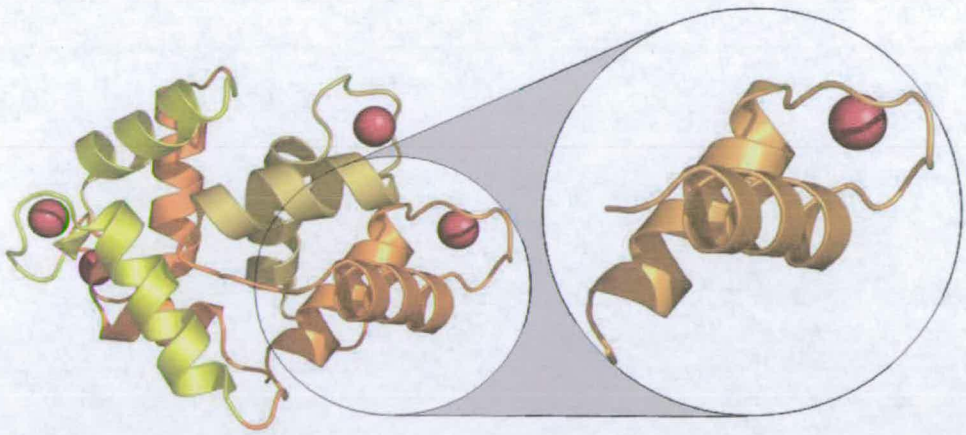

Figure 1.15: Structure of Calmodulin binding 4 atoms of Ca^{2+} (red spheres). On the right the enlargement shows that in the presence of Ca^{2+} the two helixes of each motif assume a perpendicular position.

CaM-Ca^{2+} complex in the range of nM, while that of iNOS is ten fold higher (K_D= 0.1 nM). Furthermore CaM binding to iNOS is virtually Ca^{2+} independent and irreversible (38, 39).

The different affinities of constitutive NOSs and inducible NOS for CaM rely not only on a different CaM-binding region sequence. There are at least two elements that differentiate the structure of the various isoforms reductase domains: these are an autoregulatory region which sequence is positioned within the FMN-binding subdomain of cNOSs and a C-terminal extension of various lengths (figure 1.4). Both elements exert their regulatory role with a mechanism that involve the interaction with CaM and its binding to NOS. Due to the flexibility of at least a portion of both elements none of the reductase domain structure published so far tell us about the exact position they have in the different functional conformations of

NOS. The determination of their involvement during the regulation of the enzyme activity is consequently not entirely revealed.

The autoregulatory region is an insert of 40-50 amino acids that lowers the affinity of constitutive NOSs for CaM with the result of making the enzyme sensitive to intracellular changes in Ca^{2+} concentration (16, 28). The insert is in fact in a competition with CaM to bind the region between the two flavin domains. In addition, a role for the autoregulatory insert as a suppressor of electron flow to the heme domain apart from CaM involvement has been inferred (16): a truncated form of NOS lacking the insert, showed in fact a suboptimal production of NO even in CaM free condition, differently from the wt which has none.

The C-terminal extension is present in all the three isoforms of NOS but has a different length, being 21, 33 and 42 residues long in the inducible, neuronal and endothelial forms respectively. The deletion of the extension produces an enzyme with higher reductase efficiency in the absence of CaM; the mutant activity has no difference with that of the wt when CaM is present (77, 78). The role of the tail is consequently that of an interflavins electron-flow repressor in the CaM-free NOS.

Further investigations analyzing a NOS reductase domain mutant lacking both the insert and C-terminal extension have been made (79); on the basis of this work a model relying on the concerted interaction of the two elements with CaM has been proposed. According to the model two different conformations are assumed by the reductase domain: a locked one where electron flow is allowed within the reductase domain, and an open one which lets electron flow to the heme domain. The switch between the different conformations is determined by the oxidation state of NADP(H): when oxidised ($NADP^+$) is then released and no longer interacting with

the C-terminal extension, which in turn is no longer capable to contact the autoregulatory insert. The loss of this contact determines the conformational change that arranges the reductase domain in order to donate electrons to the heme domain (open).

Activation of electron transfer by CaM binding is independent of the heme domain, being performed by the purified reductase domain by its own as well. CaM binding doesn't affect the reduction potentials of FAD and FMN (42), indicating that the triggering effect is based on a deep structural rearrangement that shortens the distance from FMN to heme, probably by inducing a degree of conformational mobility.

1.3 Heme domain

The heme domain of NOS is the N-terminal portion of the protein, (although the neuronal isotype has a preceding 300 residue PDZ-binding domain, which function is in holding together multi-protein complexes) and has a length of about 400 amino acids, which binds a b type heme via a conserved cysteine residue through the central iron atom (figure 1.16). The heme domains of the different NOS isotype have a strong structural homology, ranging from 50 to 60 % for each couple comparison, and consequently they share the same overall fold and topology (19).

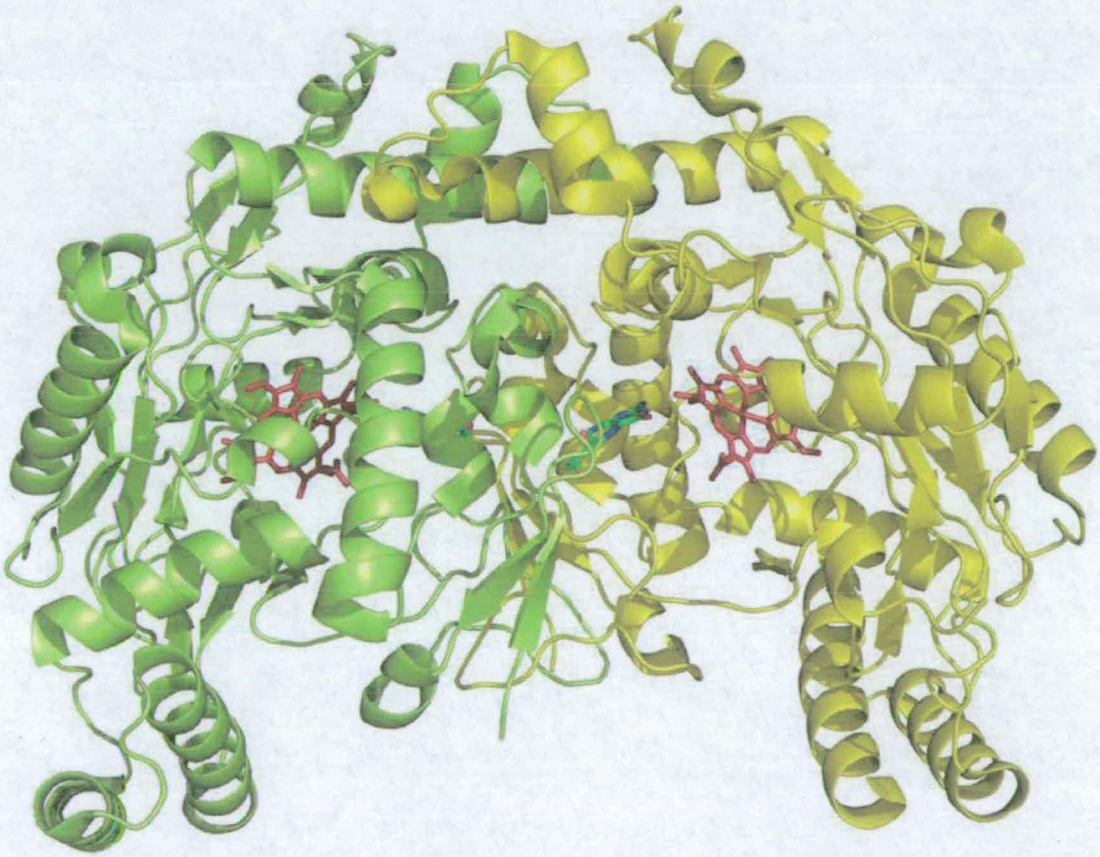

Figure 1.16: A NOS heme domain dimer showing the heme (red) and H_4B (green with oxygens and nitrogens in red and blue respectively). The H_4Bs lie within the dimer interface, which is approximately vertical in the above diagram (PDB file: 1OM4).

Considering the heme domain as being composed of subdomains is not entirely correct, as the different portions contact each other through surfaces wide enough not to be considered hinges. Nevertheless it is quite useful to describe the domain as composed by three discrete portions (figure 1.17). The biggest one is that providing the residues that interact with the substrate: it has the shape of a crescent with a cleft for the substrate just in the middle of the concavity (43).

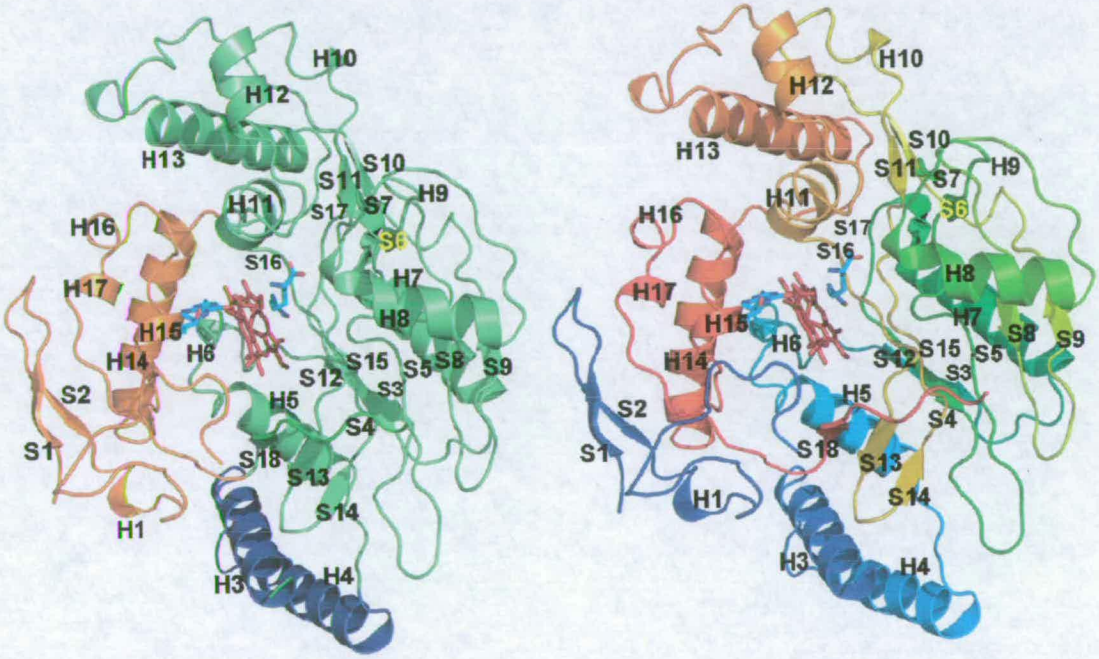

Figure 1.17: Structures of eNOS heme domain monomers showing different details through colour code. On the left panel the three subdomains are shown as green, yellow and blue: the substrate-binding, H_4B binding and two-helix bundle respectively. On the right panel the colours of the ribbon diagram fade one into the other gradually according to the primary structure, starting with blue at the N-terminal and ending with red on the C-terminal. In both structures H_4B and arginine are shown respectively on the left and right side of the heme (PDB file: 3NOS).

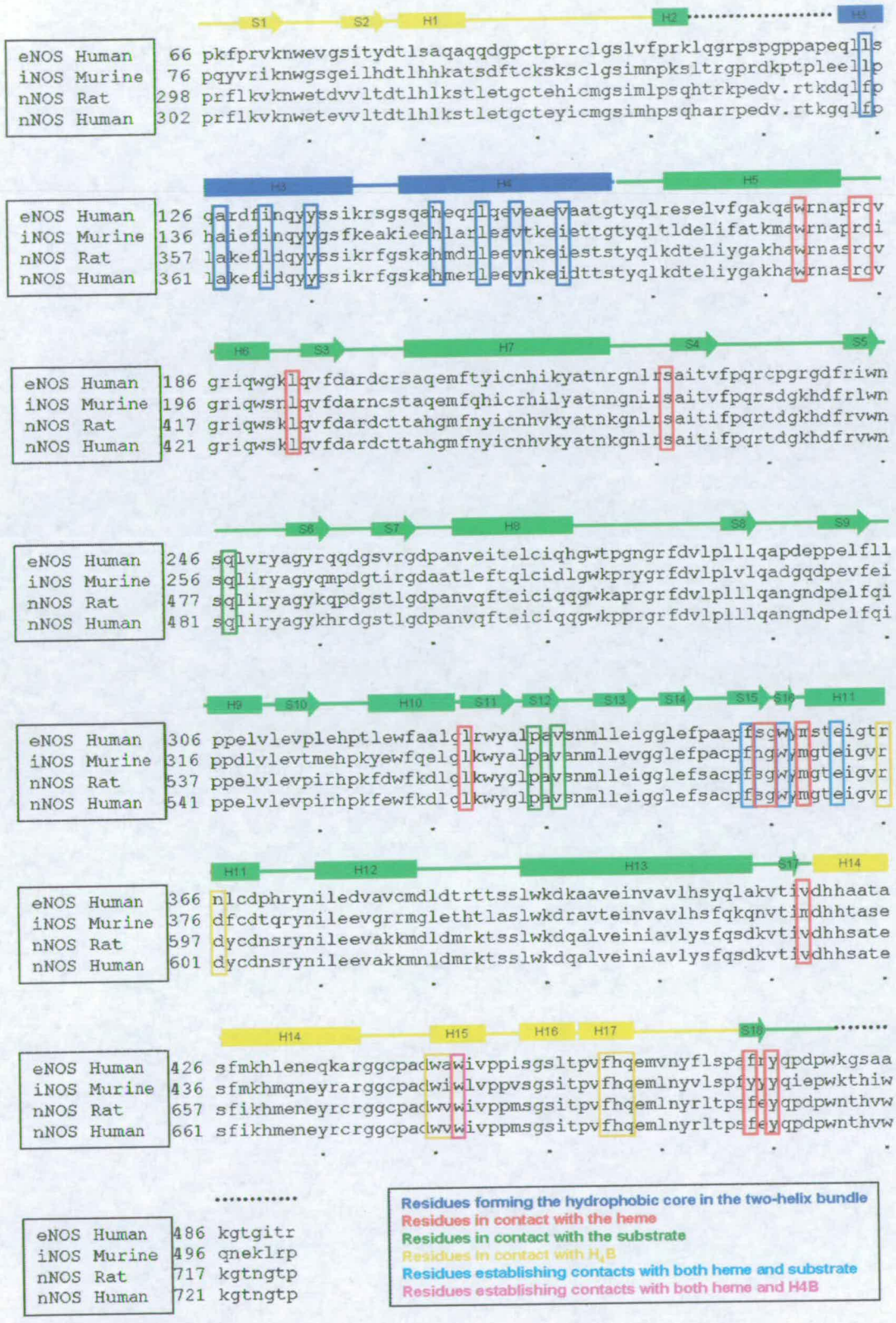

Figure 1.18: Alignment of the sequences of different NOS heme domains, coupled with the secondary structures formed. These are in accordance with the colour code of figure 1.17 left panels: arrows stand for β-strands and rectangles for α-helices (43).

Diagonally below the heme there is the second and smaller subdomain, mainly composed of helices, which provdes the residues contacting H_4B. The outer surface of this subdomain composes most of the dimer interface, providing a link between structural rearrangement upon H_4B binding and dimerization. Finally below the heme plane and on the other side from the H_4B-binding portion, there is a conserved two-helix bundle. This has limited interactions with the other two portions and may act as a structural reinforcement exploiting the strong hydrophobic interactions between the two helices.

In detail, the residues that interact with the proximal side belong to a mostly N-terminal portion mainly composed of helices (H5, H6 figure 1.19) and a loop that provides the thiolate ligand to the heme iron (Cys415 in rat nNOS).

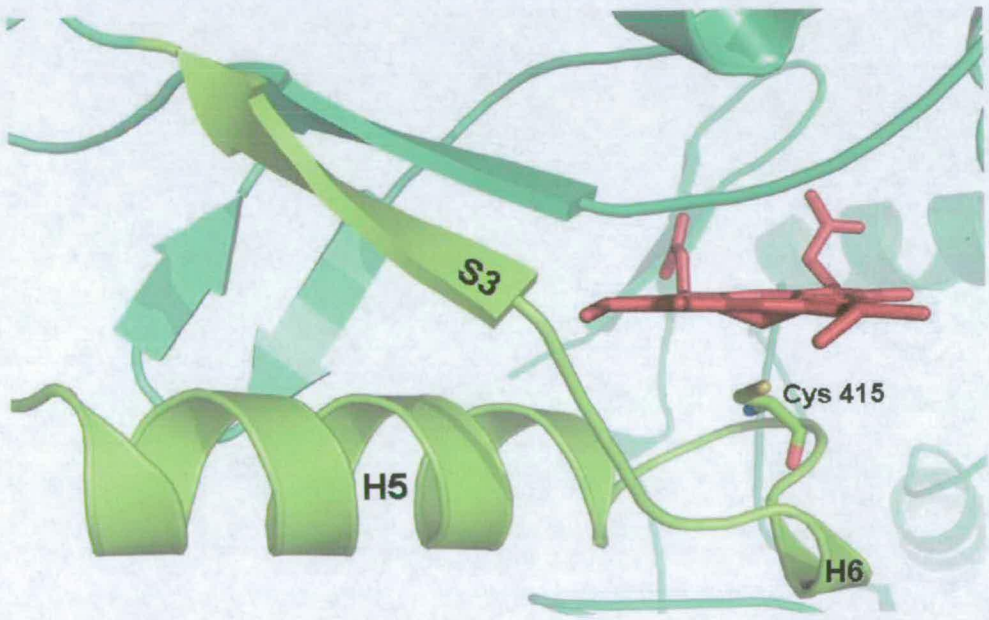

Figure 1.19: The α–β motif formed by H5 and S3 positions the iron coordinating residue, Cys415 in nNOS.

The substrate-binding pocket is formed by residues of the large central β-sheet, particularly belonging to the segment S11-S16 (Val567, Pro565, Tyr588 and Ile593 in rat nNOS). The heme is surrounded all around its plane by a number of hydrophobic residues (Leu424, Leu559, Trp587, Met589, Val649, Phe704 and Tyr 706) (figure 1.20).

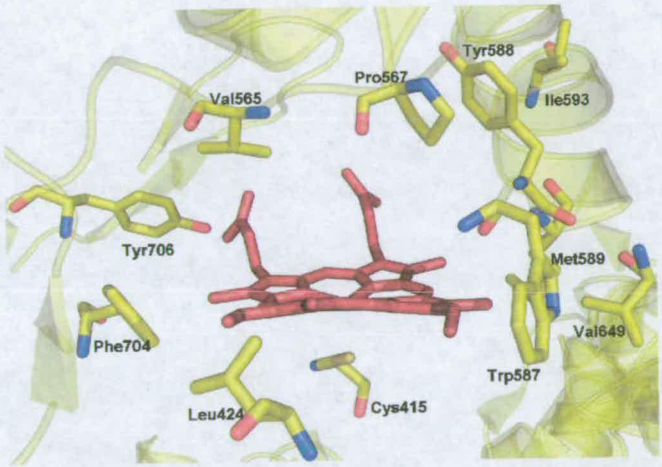

Figure 1.20

Furthermore two aromatic residues stack the heme from above and beneath (Phe584 and Trp409 respectively in rat nNOS) keeping their rings on planes that are parallel to the heme plane (figure 1.21).

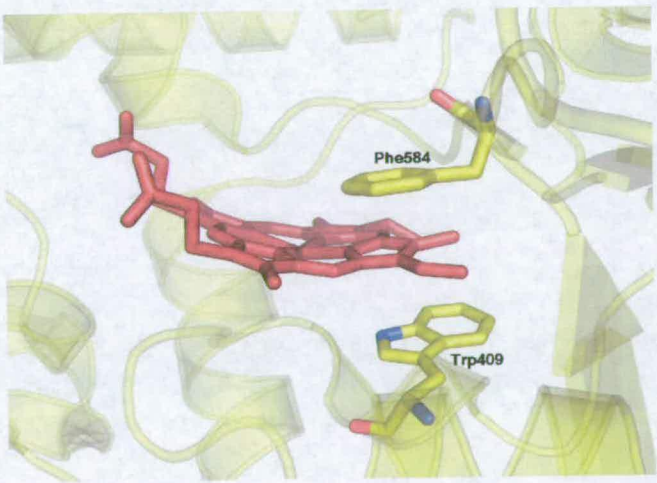

Figure 1.21

1.3.1 Pterin binding site

The requirement of H_4B (figure 1.22) is a peculiarity of NOSs. Both the N and

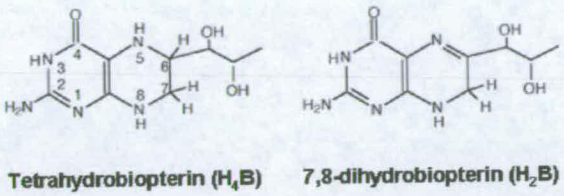

Figure 1.22: Structures of H_4B and H_2B.

C-terminal portions of the heme domain can be found in different conformations depending on the domain being a monomer or a dimer. They are mobile and flexible in the first case, but when H_4B is present and the heme domains dimerize the portions are gathered around the pterine in a multiple residue interaction.

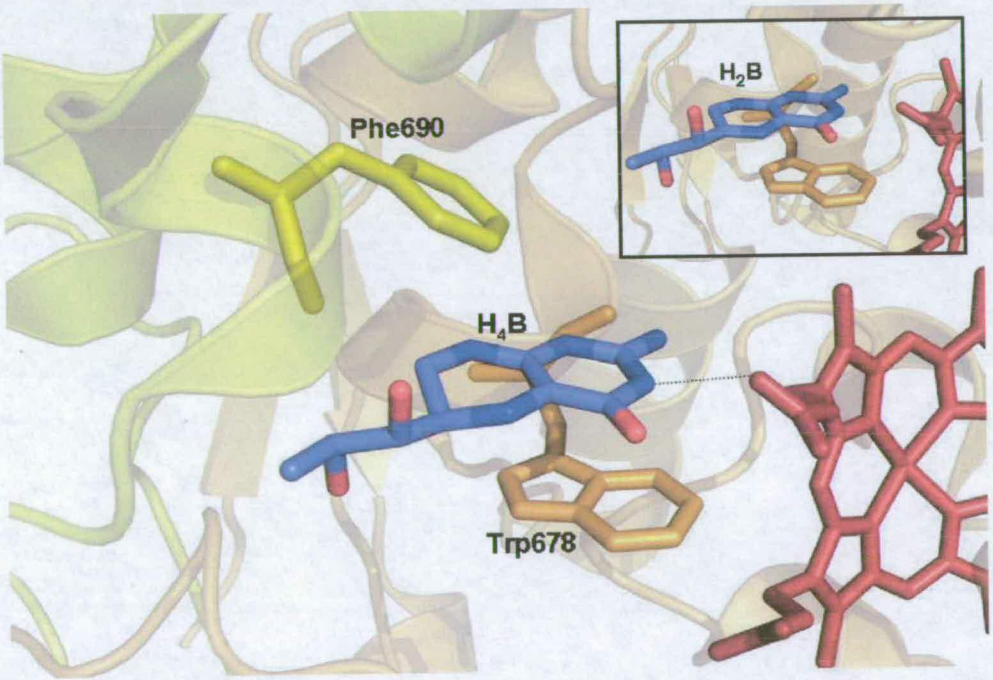

Figure 1.23: H_4B buried in the dimer interface, is stacked by a tryptophan (orange) and a phenylalanine from the facing monomer (yellow). The heme propionate H-bonds with the 3N of the pterin ring (figure H). In the insert is shown H_2B replacing H_4B: the planar geometry assumed by its C6 is not as stable as the tetrahedral one present in H_4B.

H_4B assumes a buried position deep into the dimer interface due to hydrophobic interactions (figure 1.16 and 1.22). The pterine is very unstable in solution, undergoing facile double electron oxidation. Its role in NOS catalysis is as a one electron donor/acceptor, thus the interactions in the binding site need to stabilize the reduced and the partially oxidised form. The stabilization is obtained through a series of interactions of a different nature (figure 1.23). The first type of interaction is the stacking of a conserved tryptophan (Trp678 in nNOS) which is thought to stabilize the H_4B radical by mean of π^- cation interaction. When mutation of this residue was performed, even though the protein retained its conformation, formation of the H_4B radical was slowed down and the overall reaction disrupted (45, 46). An additional stacking of the pterin rings is with a phenylalanine of the other subunit, illustrating the importance of dimerization for binding of the cofactor. In addition there is a series of H-bonds between the heteroatoms of the pterin rings and the surrounding environment, the most important of which is the one between the N3 and heme propionate. This is thought to be the preferential path for electron transfer from H_4B to the heme-bound oxygen (80). When completely oxidised, as H_2B (figure H) the pterin has a different spatial geometry. The C6 on the second ring assumes a trigonal planar geometry that, different from the tetrahedral of the reduced form, clashes with the environment. The inconvenient geometrical interaction probably exerts a restriction that prevents H_4B from oxidising (figure 1.23) (80).

1.3.2 The active site

The substrate channel in NOS has a funnel shape, wide at the entrance and narrow going toward the heme (22). The interactions formed by the substrate into the channel position it over the heme plane: the nitrogens of the guanidinium group are not equally distant from the heme iron, being the proximal the one that undergoes the attack of the iron-oxo species (figure 1.24).

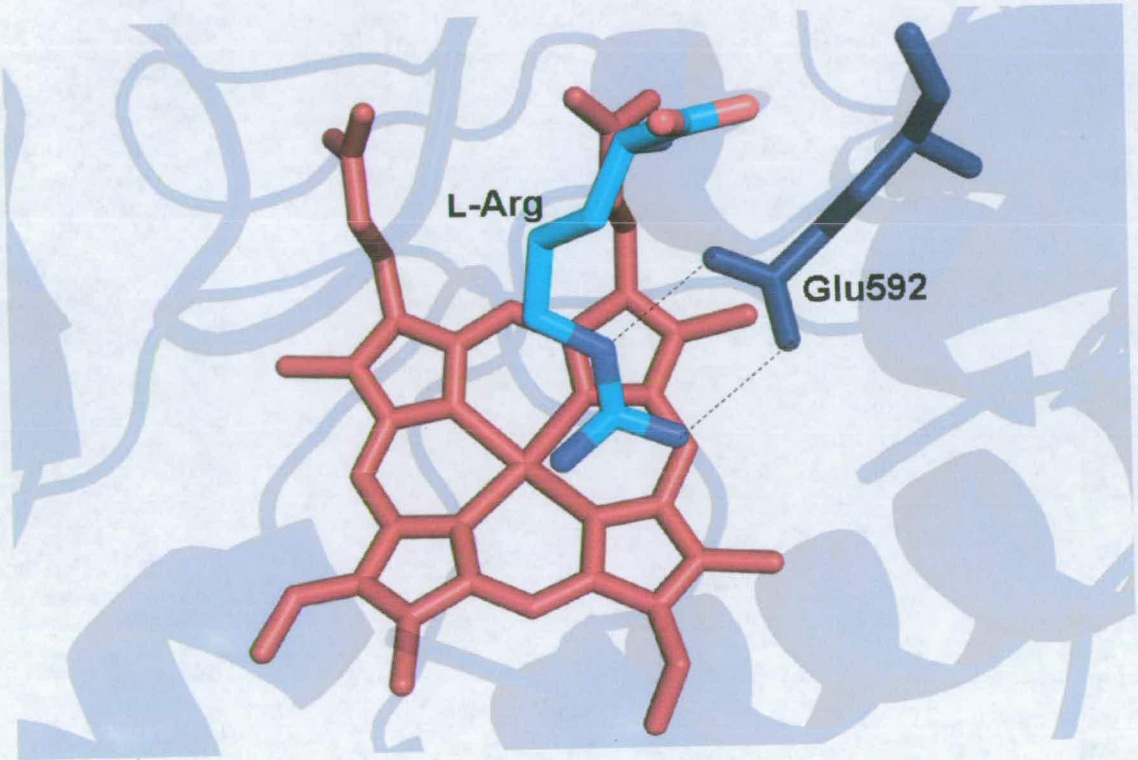

Figure 1.24: The substrate, arginine positioned over the heme plane (PDB file:1OM4).

Residues interacting with the guanidinium group are extremely conserved among the isotypes of NOS, the key role in positioning the substrate belonging to a glutamate residue (Glu592 in nNOS). Both oxygens of its carboxy terminal form H bonds with two nitrogens of the guanidinium group, that close to the α-carbon and the distal one (figure 1.25). The latter forms also an H bond with the backbone corresponding to a

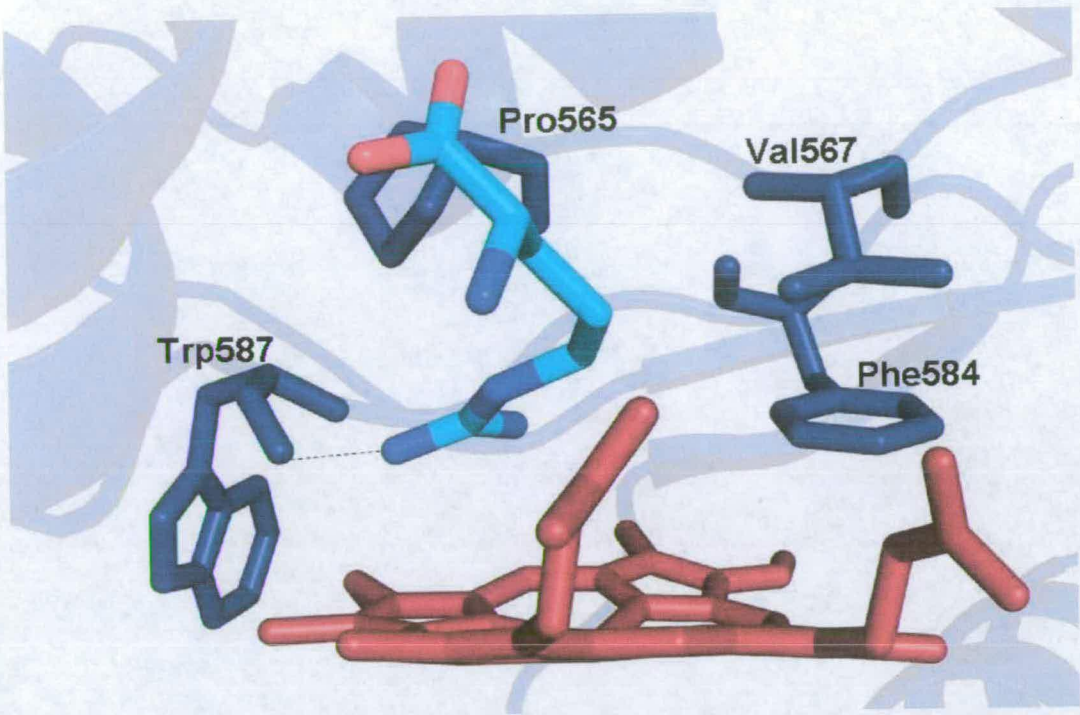

Figure 1.25: Residues limiting the pocket for the guanidinium group of arginine in nNOS (PDB file:1OM4).

conserved tryptophan (Trp587 in nNOS). The space around the distal guanidinium nitrogen is evidently tight, and not even a methyl group on this nitrogen is tolerated. The allocation of the proximal guanidinium nitrogen is slightly wider: inhibitors with up to three carbons on this side are accepted into the cavity, limited by conserved proline, valine and phenylalanine (Pro565, Val567 and Phe584 in rat nNOS) (figure 1.25). The α-carbon moiety of the substrate lies in a lateral pocket, in respect to the main channel, designed to accommodate L-amino acids only. A range of inhibitors simply bulkier or without the amino acid substituents extend out of the lateral pocket along the main channel and bypass this part. The interactions happening at this level determine the specificity of inhibitors in respect to the isotypes. The H bonds formed between the protein and the terminal α-carbon of the substrate involve the hydroxyl

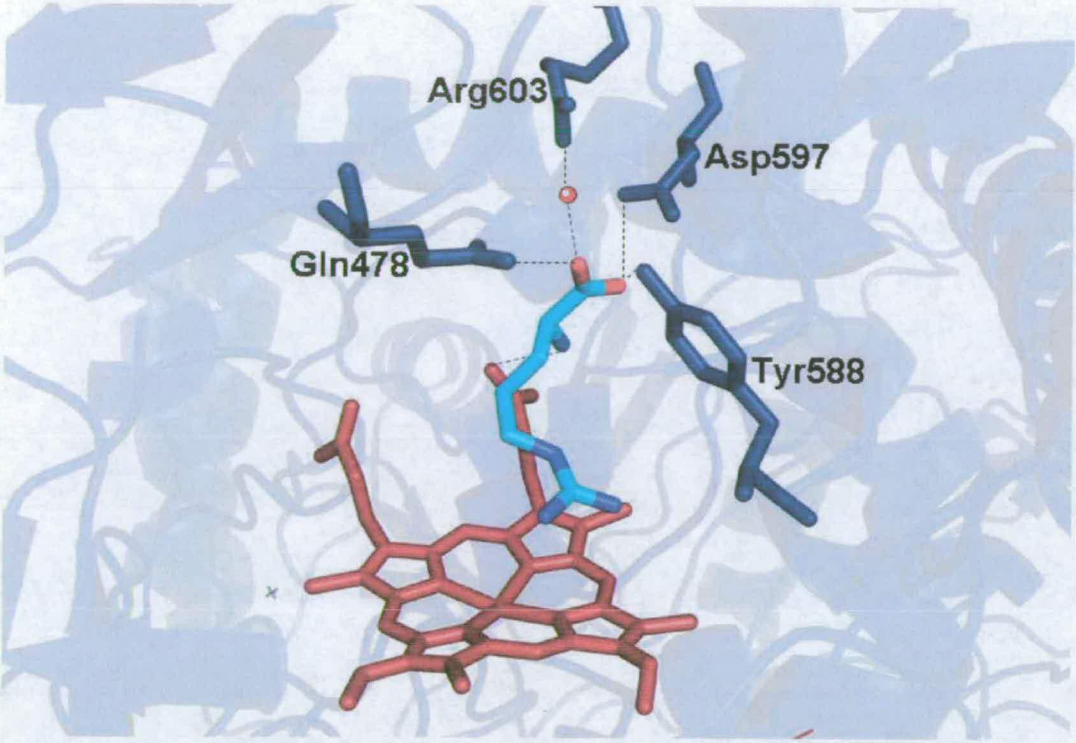

Figure 1.26: Residues forming the pocket that binds the carboxylate of arginine.

of Tyr588, the carboxylate of Asp597, Lys478 and a water molecule held by Arg603 with the carboxylate of the substrate; the α amino-group on the other hand interacts with the previously mentioned Glu592 and the heme propionate (figure 1.26).

1.4 Cytochrome P450

Cytochromes P450 are a large family of enzymes named after the peculiar absorption peak formed upon CO binding (47, 48). They usually perform mono-oxygenation reactions, namely the insertion of an atom of oxygen, in order to hydroxylate a variety of substrates, exploiting the activation of molecular oxygen (figure 1.27).

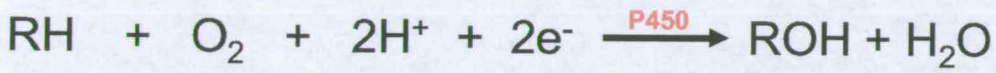

Figure 1.27: The generic mono-oxygenation reaction catalyzed by P450s.

This reaction if uncatalyzed would require extremely high temperatures to happen. Hydroxylation of non-activated hydrocarbons often increases their hydrophilicity, facilitating their excretion from the organism. Also, hydroxylations performed by P450s are key steps in various synthetic and metabolic pathways (49, 56). A digression into P450s forms a usefull introduction to the NOS reaction due to the similarities of the reactions performed and of the active site cofactors, both of which are a *b*-type heme with a thiolate iron ligand. However, it should be noted that the structures of NOS and P450s are entirely unrelated.

The involvement of P450 in progesterone metabolism, demonstrated in 1963 (49), triggered a chain reaction of growing interest that led to the present situation, where the structures of many members of the family have been solved in a variety of conditions (50-52) and the catalytic cycle is known in detail for a large part of it (53, 54). Focusing on the structure shows how P450s and NOSs have achieved the performance of a similar reaction through convergent evolution. P450s are in fact

made of mainly helical structures, unlike NOSs, and share the same global folding and tertiary structure even when the sequence homology is low (e.g. 15 %) (figure 1.28). The heme is generally sandwiched by four helices that provide the catalitically important conserved residues, such as the cysteine that coordinates to the iron (figures 1.29 and 1.30). Having a cysteine as fifth ligand, is a feature shared by P450s and NOSs. The strong electron donating nature of the thiolate is thought to activate molecular oxygen bound to the ferrous heme iron.

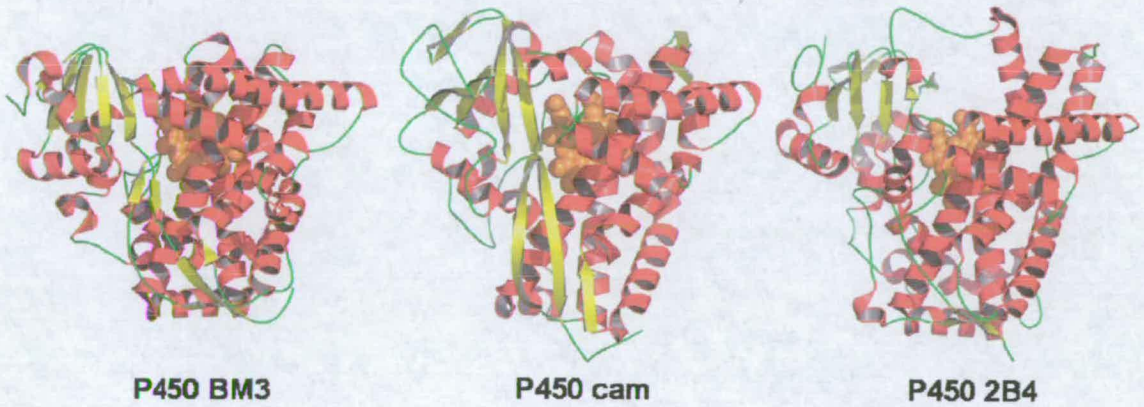

Figure 1.28: Three different examples of P450 enzymes sharing the overall helices predominance, particularly for what concern the engaging of the heme (in orange).

A small pocket above the heme is always present in P450s and allows a molecule of water to coordinate to the iron during the resting state of the enzyme (figure 1.29); this water is often displaced by the substrate binding, causing a change in the spin state of the iron.

It is difficult to generalize about the substrate binding site given the huge variety of substrates processed by the family members. The examples in figure 1.30 show how wide can be differences in size and shape, ranging from a small molecule such as NO

(P450nor) (81) to a large one like epithilone (P450epok) (82). Even when the substrates are similar, a high homology is not obvious; this the case of P450cin and P450cam, hydroxylating cineole and camphor respectively having an identity of only 26% (83, 84).

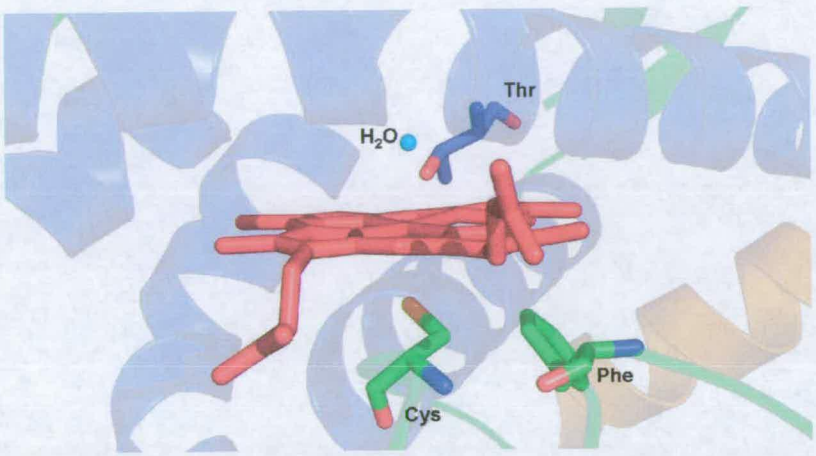

Figure 1.29: The P450s heme is coordinated by Cys on the proximal side, and H_2O on the distal side. A catalytically important Thr residue is within H-bonding distance of the bound H_2O.

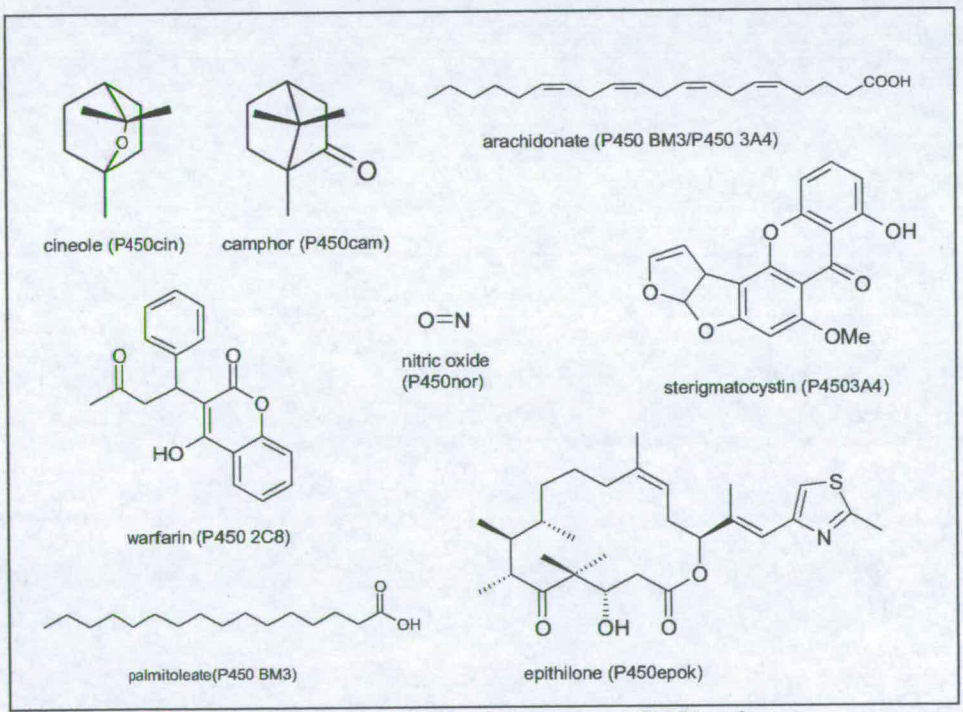

Figure 1.30: Examples of molecules that serve as P450 substrates

1.4.1 Supporting redox partner

P450s can be divided in two main groups depending on the way they have their electrons supplied (except there are several unique combinations not belonging to any of the class) (figure 1.31). Class I P450s have a redox partner made of two components delivering the electron equivalents generated by NADH dehydrogenation. The first component, Ferredoxin Reductase, binds NADH and uses FAD as a cofactor to accept the hydride. Electrons are passed to a second protein, the iron-sulphur cluster containing Ferredoxin. The electrons are then transferred to the heme of P450. This arrangement is common in bacterial and mitochondrial P450 systems; in bacteria the complex are usually soluble (P450cam (85)), while in mitochondria are commonly bound to the membrane (P450scc (86)). Class II P450s have Cytochrome P450 reductase as a redox partner. This protein closely resembles the NOS reductase domain. It binds FAD and FMN and uses them to deliver NADPH-derived electrons to the heme. This system is common to microsomal proteins, being the complex bound to the cytoplasmic side the endoplasmic reticulum (P450 2C5 (87)). When a homologue of Cytochrome P450 reductase and a P450 are fused together in a unique enzyme they are called a Class III P450, a minor group.

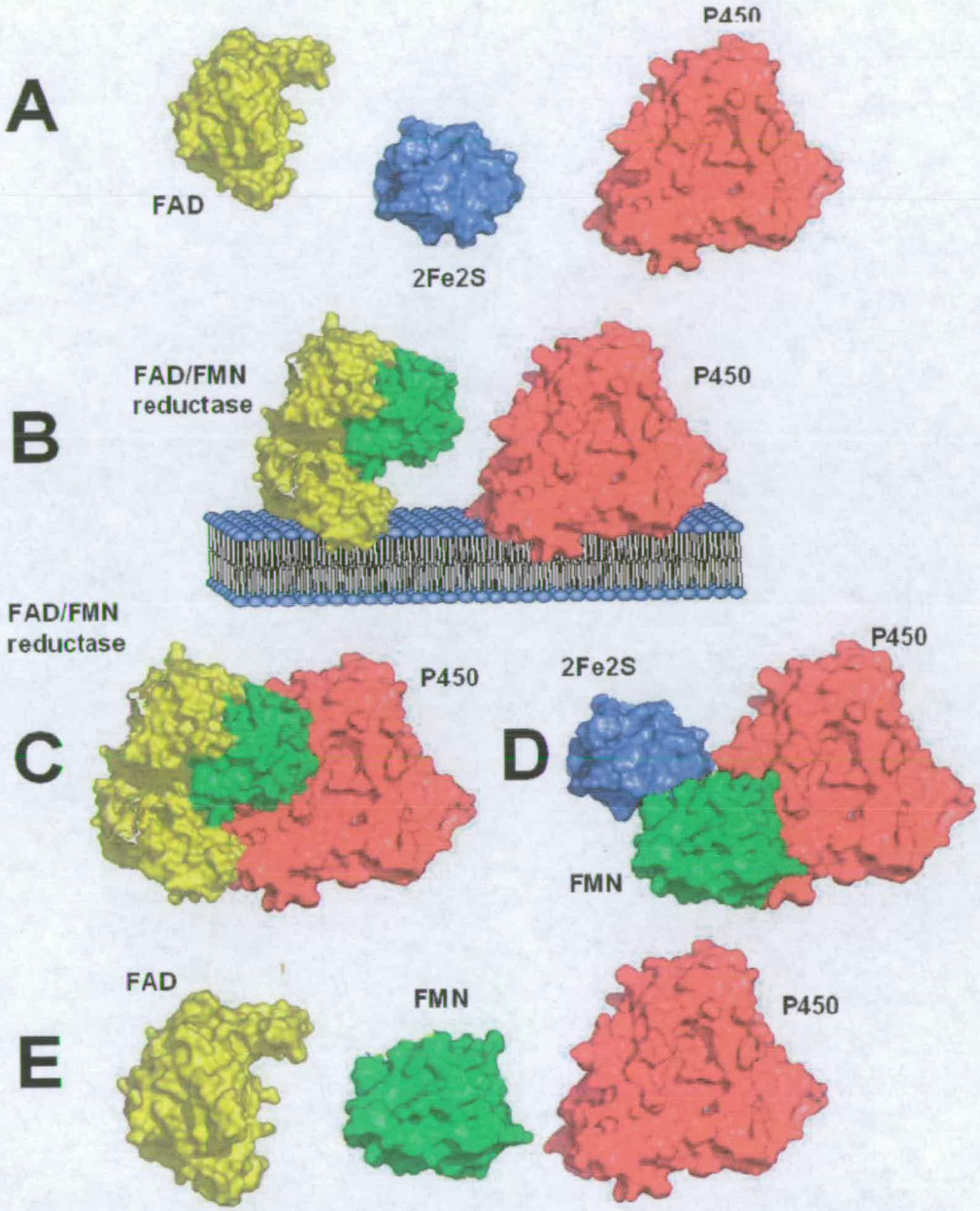

Figure 1.31: Representation of the different classes of cytochrome P450. P450 domains are in red and redox partner components in yellow (FAD domain), green (FMN domain) and blue (Iron-sulphur cluster). A: class I system comprised of FAD, iron sulphur and P450 subunits. B: class II system comprised of FAD/FMN reductase and P450 subunits. C: class III system formed by fused FAD/FMN reductase and P450 domains. Panels D and E: other unique combinations of redox cofactors such as P450 Rhf and P450 cin.

1.4.2 The catalytic cycle of P450

In order to perform the reaction, the first aim for the P450 is the activation of molecular oxygen that otherwise, in its triplet state, would not react with the singlet-state majority of substrates. Metals are commonly used for this purpose by enzymes, being in this case the heme-iron that binds the oxygen and stabilizes the highly reactive transients as the reaction proceeds. In addition to the oxygen binding, two sequential one-electron reductions are necessary for P450 to perform its reaction: these steps produce a series of intermediates that lead to the formation of the reactive species. A diagram showing all the steps of the reaction is shown in figure 1.32.

1) Substrate binding. The first step of the reaction is the binding of the substrate that nearly in all the cases displaces the loosely bound sixth iron ligand, a molecule of water (52, 88, 89). In P450s the binding of substrate has the effect of causing a heme spin state shift from low to high, but most importantly and differently from NOS, the displacement of the water has a destabilizing effect on the ferric form of the enzyme causing a heme reduction potential shift of about +100mV. The enzyme swings then from a substrate-free state where uncoupled hydride consumption is prevented, to a substrate bound one where the heme reduction is viable.

2) First electron transfer. The first electron, as well as the second, is provided by the redox partner-bound NAD(P)H. Molecular oxygen, which has high affinity only for the ferrous heme, then binds. In some P450 enzymes the heme reduction may induce structural rearrangements that bring the substrate closer to the heme, as an additional control element of the reaction coupling (90).

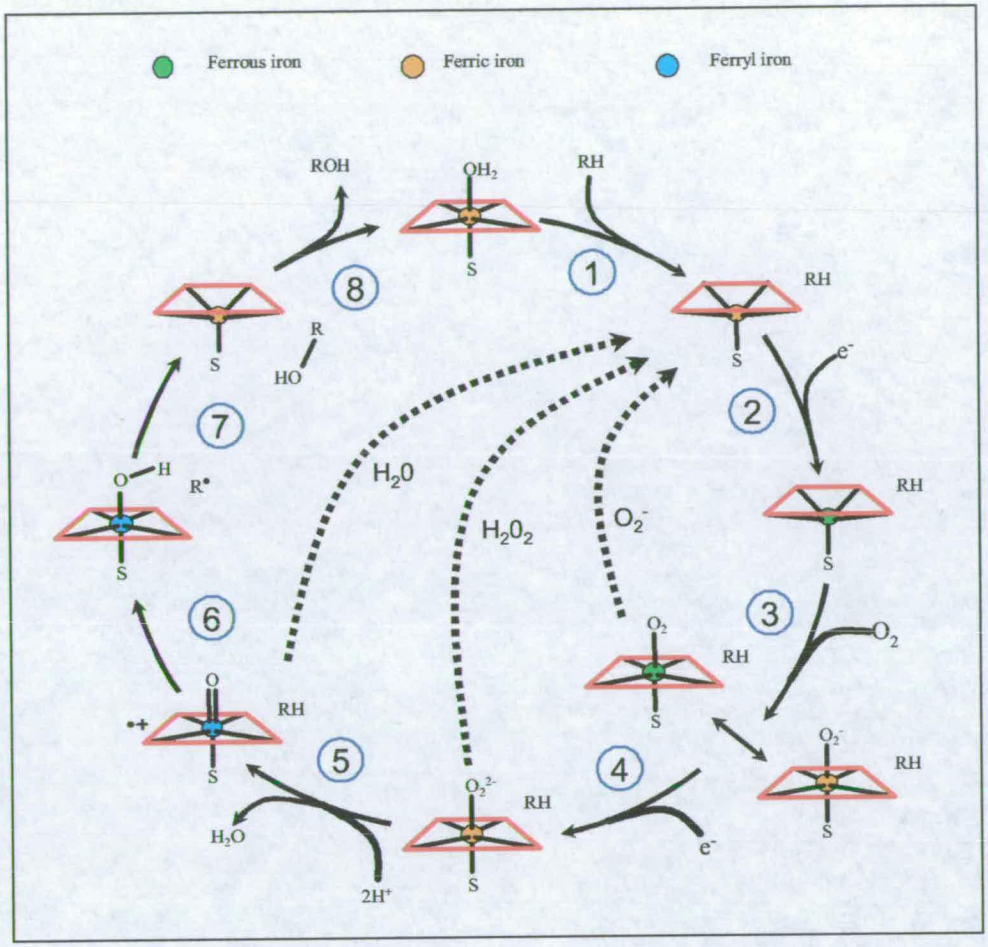

Figure 1.32: General scheme of the P450 reaction: **1**: substrate binding, **2**: first electron transfer, **3**: Oxygen binding, **4**: second-electron transfer, **5**: formation of oxy-ferryl species, **6/7**: rebound mechanism for oxygen insertion and **8**: product dissociation. The 1, 2 and 4 electron uncoupling pathways to superoxide, peroxide and water are shown as dotted lines.

3) Oxygen binding. Molecular oxygen binds rapidly to the ferrous heme. The complex could be described either as oxy-ferrous (Fe^{II}-O_2) or as the isoelectronic superoxy-ferric form (Fe^{III}-O_2^-).

4) Second electron transfer. As already mentioned a second electron is accepted and gives rise to the formation of a peroxy-ferric species (Fe^{III}-OO^{2-}). In some atypical P450 reactions the latter is the reactive compound towards the substrate. This is the case in P450 aromatase, which performs the removal of a methyl group as a step in

the synthesis of some steroids. The enzyme performs a three-step reaction, the third of which cannot be explained by the action of the usual P450 oxy-ferryl compound (92).

5) Protonation. The reaction proceeds via a double protonation, the first of which produces a hydroperoxy-ferric intermediate (Fe^{III}-OOH^-). The hydroperoxyferric compound has also been suggested to be in some cases the reactive species, being reactive enough to perform the oxygenation especially when the second protonation is slow (91). However it is generally accepted that the hydroperoxyferric species is protonated and subsequently decays by loss of a water molecule to form a highly reactive carbocationic oxy-ferryl species (Fe^{IV+}), known as Compound I.

6) and 7) Oxygen insertion. The oxy-ferryl compound is thought to abstract a hydrogen atom from the substrate, creating, on one side a substrate radical species, and on the other a hydroxyferric heme. The hydroxylation step is then a rapid radical-recombination, resulting in ferric heme. This global mechanism is called Rebound and is graphically described in figure 1.33.

8) Product dissociation. The hydroxylated product is released from the ferric heme which binds a new molecule of water as sixth ligand.

Of all the intermediates shown in the catalytic cycle (figure 1.32), the oxyferrous compound arising from the binding of molecular oxygen to ferrous enzyme is the last one that can be observed with classic spectroscopic techniques (UV-Vis spectroscopy) in physiological conditions. The identity of the subsequent intermediates is only inferred. These were initially derived from comparison with structurally and functionally similar enzymes, in particular Chloroperoxidase (CPO) and Horseradish Peroxidase (HRP). In the last two decades there has been made an

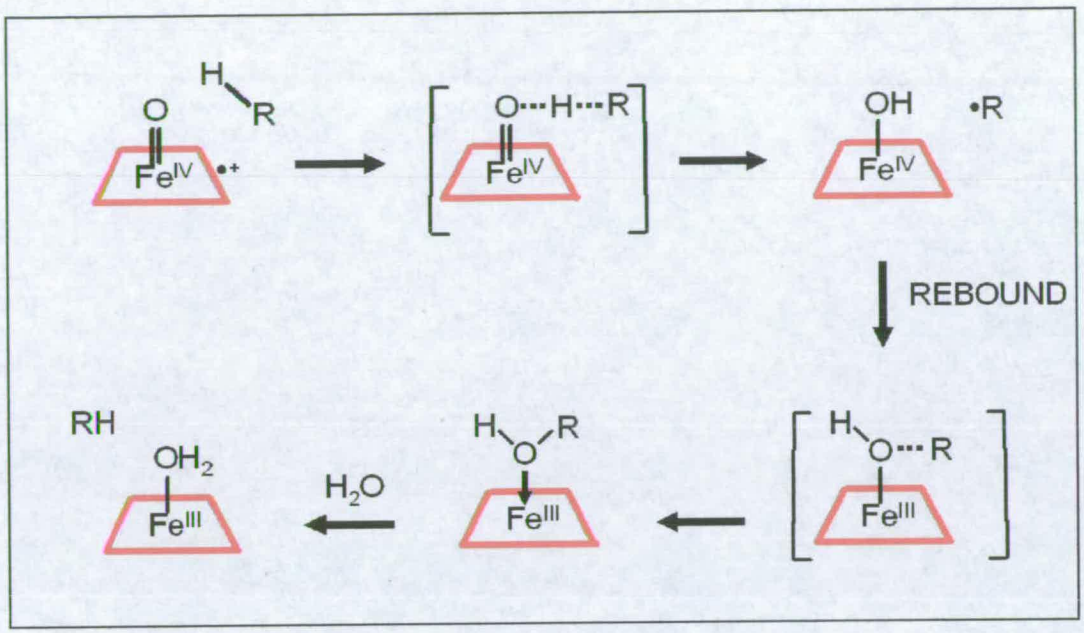

Figure 1.33: Graphical description of the rebound mechanism of oxygen insertion. The oxy-ferryl binds substrate and abstracting a proton fenerate a substrate radical; this radical rebinds the heme-hydroxyl group hrough the oxygen before being released in its hydroxilated form.

extensive spectroscopical characterization of the intermediates produced by the second electron transfer: peroxyferric, hydroperoxyferric and oxyferryl compounds. Electron Paramagnetic Resonance (EPR), Electron-nuclear Double Resonance (ENDOR) and Raman Spectroscopy have been giving information about the identity of the compounds forming during the course of the reaction, especially when these techniques are coupled with stabilizing conditions such as low temperature and mutagenesis (93-95).

In a recent work (96) structures of three transients formed during the oxygen activation process in P450cam have been determined by freeze-trapping the different complexes. *Schlichting et al.* exploited the ordered and contemporaneous manner

with which the enzyme in the crystals initiates the subsequent steps of the reaction and obtained a homogeneous sample of intermediates. They used short-wavelength X-ray irradiation to solve the structure of the ferrous and oxygen bound enzyme so as to avoid further reduction during data collection. On the other hand they used long-wavelength X-ray irradiation on the oxyferrous low-temperature stabilized enzyme crystal, with the intent of triggering the second electron delivery to detect the newly formed intermediate, the putative oxyferryl compound. The electron density map they have obtained upon this treatment suggests the presence of a mixture of species: the comparison with the dioxygen-bound enzyme indicates that the predominant species in this case has a single oxygen atom bound to the heme iron.

1.4.3 The catalytic role of a conserved Threonine

TheP450 family is very large and there are many differences between the members, compared with the few conserved characterizing common features. One of these is the extensive presence of a conserved threonine residue (Thr 268 in P450 BM3 and Thr 252 in P450cam) (figure 1.29). This residue belongs to the helix above the heme that provides the pocket where a water molecule is acting as a sixth ligand in the resting state enzyme; the water is in fact within H-bonding distance of the threonine. Many roles have been proposed for this residue such as oxygen activator, proton provider, electron donor, element of recognition for the substrate and heme-water ligand (97-101). The results of part of the work that aimed to clarify the role of this residues are sometimes controversial: e.g. the threonine was mutated to alanine and showed evidence for the involvement of this residue in the binding of oxygen during its activation course (97). On the other hand a recently published structure of the

oxygen-bound enzyme indicates that no hydrogen bond is formed between the threonine and the oxygen (102). Hence further investigation is needed to identify the role of this key threonine, taking in consideration the possibility that it may have different roles in the different members of the family.

.

1.5 Catalytic Reaction of NOS

The conversion of L-Arginine to NO takes place in two steps: first the formation of of L-NOHA and then the conversion of this to L-Citrulline and NO (figure 1.34). Both steps begin with the stepwise activation of molecular oxygen, through the formation of complexes with the heme. The reactive species are formed in order to hydroxylate the substrate in the first cycle and perform an oxidative scission on it in the second one. The present chapter will give a detailed description of the intermediates formed and of the efforts made to reveal their identities.

Figure 1.34 shows the two cycles of the reaction in terms of the heme states formed (62). In the text, as well as in the scheme through different background colours, the reaction will be divided into three phases for convenience of explanation. The phases are: 1) first electron transfer and oxy-ferrous species formation (yellow) 2) electron transfer from H_4B (orange) 3) formation of reactive heme-oxy species, monoxygenation and NO release (red). While in the scheme the two cycles are assumed to be identical for simplicity, within the text the differences will be discussed.

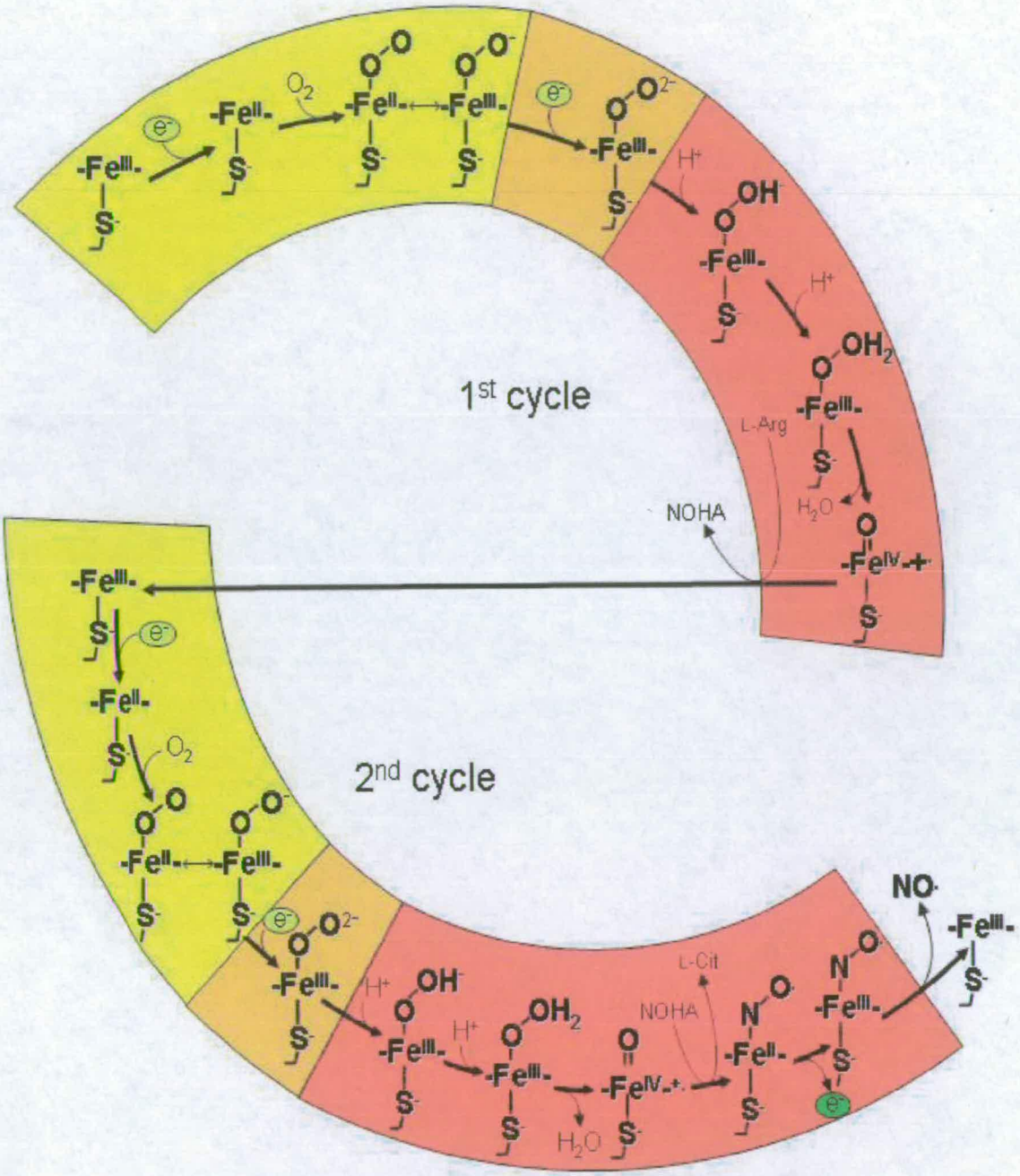

Figure 1.34: Overall scheme of the reaction. The three phases described in the text are here divided by colour code, being yellow, orange and red the first, second and third respectively. The electron transfers are shown in green, reductions being light green and oxidation darker green.

1.5.1 First electron transfer

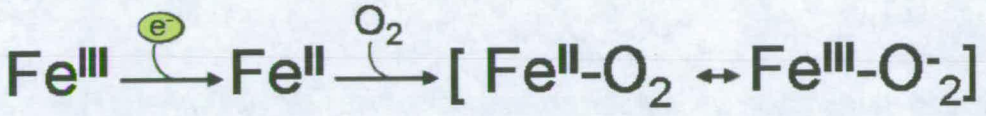

In contrast to the P450 reaction, in NOS substrate binding does not act as an enhancer of the first electron transfer by modifying the heme reduction potential; neither does H_4B. On the other hand the binding of substrates arginine or NOHA determine a shift from mixed low/high to entirely high in the spin state equilibrium of the heme: this is due to the displacing of a weakly bound water molecule acting as a distal sixth axial ligand to the iron heme. This is reflected in a Soret peak shift from 400 nm, that of substrate-free enzyme, to 395 nm (figure 1.35).

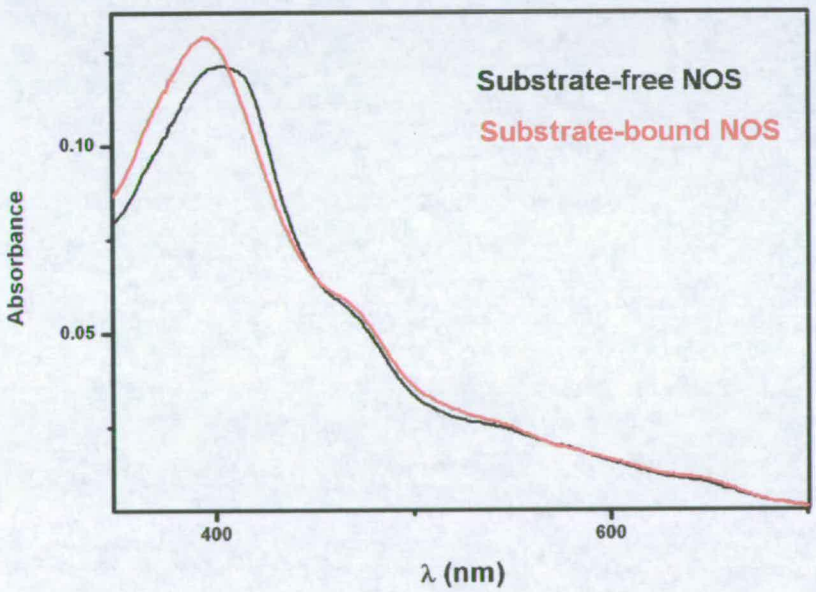

Figure 1.35: NOS spin-state shift from mixed low/high to high upon substrate binding

The electron provided by the reductase-bound FMN reduces then the heme ferric iron (Fe^{III}) to its ferrous form (Fe^{II}) (58, 59). This transformation results in a shift of the UV-Vis spectrum with the Soret peak going from 395 nm to 414 nm (figure 1.36); also a smaller but broad peak in the region of 560 nm forms in place of the two slight bumps at 530 and 650 nm that characterize the ferric heme spin state. The ferrous form has a dramatically increased affinity for oxygen and at this point oxygen binds to the iron on the distal side of the heme plane to form the oxy-ferrous compound. There is a red shift in the Soret maximum to 425 nm and some flattening in the 500/600 nm region (Figure 1.36). On the other hand when the substrate-free enzyme in its ferrous form is mixed with oxygen there is no accumulation of the oxyferrous compound. This indicates that in absence of substrate the rate at which the oxyferrous compound decays is faster than its rate of formation, suggesting a stabilizing role for the substrate (63).

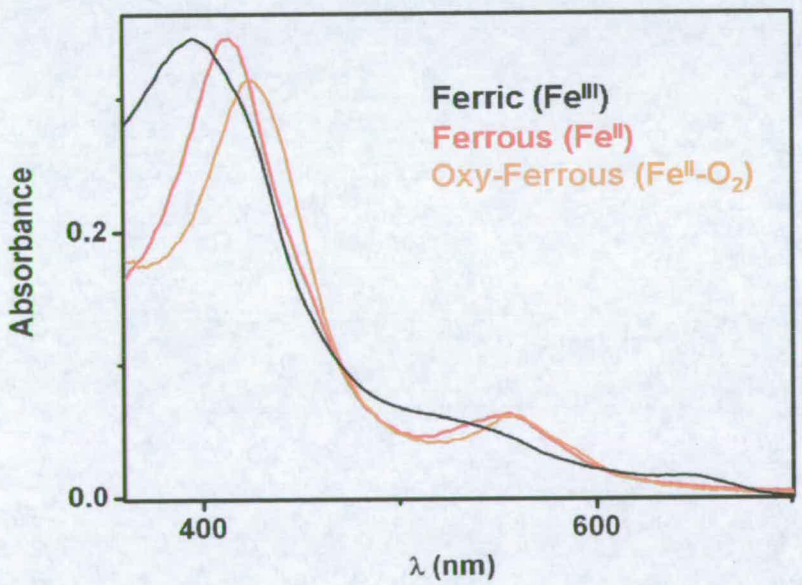

Figure 1.36: UV-Vis spectra of $nNOS_{oxy}$ ferric (black), ferrous (red) and oxyferrous (yellow) forms.

In NOS the peak of the oxyferrous compound is slightly red-shifted if compared with those formed by the majority of P450s: those are ranging around 418-420 nm (e.g. oxyferrous compound of P450cam and P450LM) (103, 104). Nevertheless there are some cases where the similarities are unambiguous (e.g. Oxy-Ferrous compound of substrate bound Cytochrome P450 SCC) (60). This species is named either Oxy-Ferrous (Fe^{II}-O_2) or Ferric-Superoxy (Fe^{III}-O_2^-) and is a resonance form of the two isoelectronic compounds. Its formation is first order dependent on oxygen concentration.

In the absence of either substrate or pterin, or both, the enzyme is directed into an uncoupled unproductive cycle, that is the usage of part or all the electrons for the formation of a compound other than the product; in case of a substrate-free enzyme, regardless of the presence of pterin, the autooxidation of the heme oxy-ferrous species produces superoxide anion (O_2^-) (62). In the presence of H_4B the rate of the oxyferrous compound decay varies greatly depending on the presence of substrate; in the substrate-free NOS the oxyferrous compound decays more quickly (>160 s^{-1}) than it does as part of a productive cycle in the presence of substrates (22 and 4.9 s^{-1} in the presence of arginine and NOHA respectively) (63). Finally when both H_4B and substrate are present, the oxyferrous complex undergoes further reduction.

1.5.2 Second electron transfer

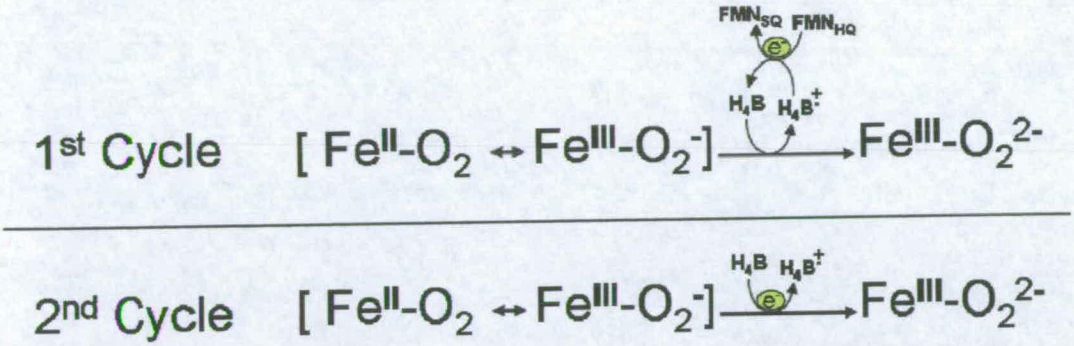

The events involving the oxy-heme compounds in the course of the reaction are no longer producing accumulating intermediates from now on. This is reflected in the fact that none of the transients are detectable by UV-Vis spectrometry, and hence after the identification of the oxy-ferrous compound by means of its UV-Vis spectrum, the next species we can identify is the resting ferric heme formed after the completion of the reaction, this being either the hydroxylation of arginine or the final cleavage that produces NO and citrulline.

Nevertheless, it is accepted that the second electron delivery leads to the formation of a Ferric-Peroxy species, this being the first of a series of compounds in a "black box" of which we can observe only the final result, either in the first or second cycle. A glimpse into the "black box" is provided by very low temperature studies. *Davydov* and co-workers (64) induced the second electron delivery to a competent NOS oxy-ferrous heme through γ-irradiation at 77 K. Both EPR, but particularly ENDOR characterization confirmed the identity of the newly formed transient to be that of a Ferric-Peroxy heme species, hydrogen bonding to a water molecule just above the

heme plane. The ENDOR spectrum resembles that formed upon identical treatment at 77 K of a P450cam mutant where the mutation induced loss of the water molecule binding in the distal pocket (65). In the cryoreduction of the wild-type oxy-ferrous compound a protonated form of the Ferric-Peroxy compound was generated, while the lack of a protonating facility in the mutant produced the same species as observed in NOS.

The identification of the second electron source during oxygen activation in NOS involved a huge amount of work. The requirement of NOS for H_4B in order to produce NO suggested a possible unusual role of the pterin as donor of the second electron: the first evidence for this hypothesis was given by the detection of a H_4B radical ($H_4B^{\cdot}$) after Rapid Freeze Quenching when arginine-bound Ferrous NOS was mixed with oxygen; the formation of the radical occurred at the same rate as the decay of the oxy-ferrous species (69). Radical formation was detected at 0.75 per heme, coupled tightly with oxy-ferrous decay in a monophasic reaction. To countercheck the role of H_4B, a number of different reaction-conditions have also been investigated. In the presence of amino-H_4B (an analogue which promotes enzyme dimerization but has no capability to donate an electron) the enzyme forms the oxy-ferrous compound, which autooxidises slowly (63). When H_4B is replaced by 5-methyl-H_4B the enzyme retains its capability to perform an arginine hydroxylation in a single turnover cycle, but the formation of the pterin radical happens 3-fold faster than with H_4B (70). This is coupled with a 3-fold faster rate of oxy-ferrous decay.

The role of H_4B in the second cycle of the reaction has been clarified only recently, due to the difficulties to detect its radical form: only a small fraction of radical per heme (about 3% of the heme content) was detected during a single-turnover reaction

of NOHA-binding NOS (69). The difficulties in detecting the H_4B radical may be due to its fast disappearance, being quickly reduced back during the last part of the reaction.

When reacting with the oxyferrous complex in the presence of arginine, H_4B donates an electron forming a H_4B^+ radical that is ultimately reduced back to H_4B during catalysis, possibly by a NADPH derived electron. In the presence of NOHA H_4B oxidizes and then is promptly reduced back by the ferrous NO-complex formed at the end of the monoxygenation step. This process is essential to explain how the formation of NO and ferric enzyme ultimately occurs. The ferrous NO-complex is too stable to release NO spontaneously. Therefore there is a double role for H_4B as an electron donor and as an acceptor during the second cycle reaction (67).

1.5.3 Formation of the ultimate reactive species

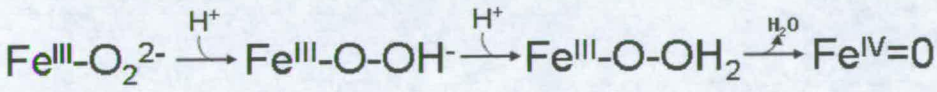

Although theoretically the Ferric-Peroxy compound could be reactive towards both arginine and NOHA, is generally accepted that this compound undergoes a double protonation and through the loss of a water molecule produces what is considered the ultimate reactive species. This is also the putative reactive species of most P450 reactions, the Oxy-Ferryl also called Compound I (Fe^{IV}). Unlike in other molecular oxygen activating enzymes (67, 74), the Ferric-Hydroperoxy compound resulting from the first protonation has never been observed, not even after low temperature reduction and annealing of the Ferric-Peroxy compound. This could strengthen the

hypothesis that the Ferric-Peroxy complex is the active species. Nevertheless after cryoreducion the two-proton delivery is inferred from the detection of a species that can be formed exclusively through two consecutive protonations and the production of a water molecule: a heme-substrate adduct where the substrate is already hydroxylated and coordinated to the ferric iron through the oxygen of the hydroxyl (figure 1.37). The only way for this to happen is that a double protonation weakens the oxygen-oxygen bond in the Ferric-Peroxy complex until it breaks producing water, the overall process leading to the formation of Compound I: the latter can then attack the arginine nitrogen to form the adduct observed (64, 65). If the attack on nitrogen were performed before the breakage of the O-O bond by means of the

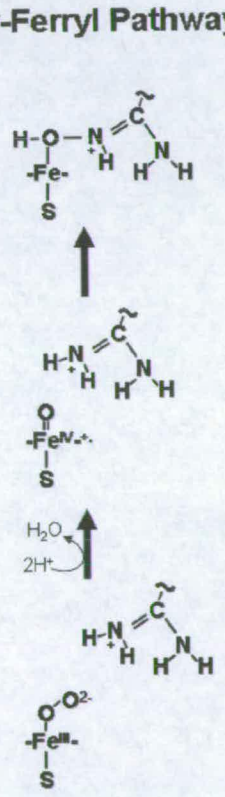

Figure 1.37: Oxy-ferryl pathways for the attack on the substrate. There are evidences for the formation of the adduct on the top of panel.

distal oxygen, the presence of the heme-NOHA intermediate would be difficult to justify (also at 200 K NOHA, after its production, coordinates with the Ferric heme to form an unstable complex) (figure 1.37). The Fe-O distance in the adduct increases stepwise until NOHA is released, remaining enzyme-bound in the catalytic site to undergo the final part of the reaction.

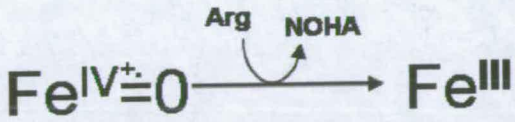

In the second cycle the attack is performed on the hydroxylated nitrogen of NOHA and NO is synthesized through the utilization of this nitrogen (75). Once produced NO is bound to the Ferrous heme which is then oxidised before it can be released.

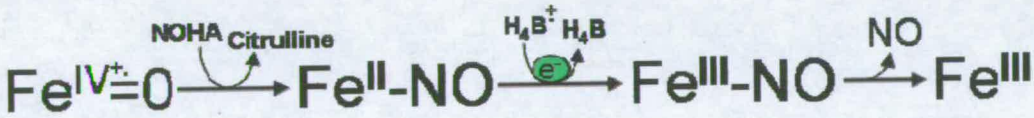

The affinity of NO for the Ferrous heme is much higher and its release would not be possible, forming a dead-end complex instead. For this reason NOS has two different electron-sources. Optimization of electron delivery from the Reductase Domain, in order to provide the second electron as well, would in fact increase the fraction of enzyme forming the unproductive Ferrous-NO heme due to the possibility of the Ferric-NO complex being reduced.

1.6 Aims of the project

The aim of this research is to further understand the final part of the reaction performed by NOS that leads to NO production. As thoroughly discussed in the Introduction the reactive species formed in the heme domain catalytic site have been identified only up to the formation of the Oxy-Ferrous compound. The events taking place thereafter are not obvious due to the lack of accumulation of the intermediates forming. A higher resolution picture of the species succession during NOS reaction could lead to a wider knowledge of the elements that determine oxygen reactivity. This type of information is essential in the attempt to develop specific NOS-inhibitors. Drug development based on the reaction mechanism comprehension is important in relation to the large number of diseases in which anomalous NO production is involved.

Different approaches have been used to gather information about the identity of the intermediates formed upon oxygen activation into the NOS catalytic site. Analysis of the catalytic reaction has been performed at very low temperature in the attempt to trap and characterize the intermediate (64, 69). Also H_4B-analogues have been used to characterize reactions triggered by the second electron delivery (63, 70).

Our approach in the understanding of the NOS reaction involves a preliminary analysis of the enzyme catalytic site: amino acid residues in the distal portion of NOS heme domain are involved in the stabilisation and activation of the oxygen-heme complexes formed during NO production. The interactions they form with the transforming species have the task to promote oxygen binding, prevent uncoupled reactions and assist punctual O-O bond breakage. Inspection of the distal side of the

catalytic domain reveals a striking hydrophobic character of the residues which may interact during the reaction: surprisingly there are no residues capable of hydrogen-bonding to heme-bound oxygen. The reaction performed by NOS is similar to that performed by cytochrome P450, where hydrophilic residues play a key role during the activation of oxygen. An amino acid residue with the ability of forming hydrogen-bonds at a suitable distance from the space where substrate and oxygen-heme complexes interact may introduce species stabilization during the course of oxygen activation. With this in mind a series of mutant of $nNOS_{oxy}$ were generated, expressed and purified. They were then tested for their catalytic behaviour by means of stopped flow experiments. The identification of a mutant showing the capability to stabilize at least one new intermediate of the reaction is the main aim of this project.

Chapter 2

Materials and Methods

2 MATERIALS AND METHODS

2.1 Mutagenesis

All neuronal NOS heme domain constructs were created by Dr. Caroline S. Miles, Institute of Cellular and Molecular Biology, University of Edinburgh. The NOS G586S heme domain mutant characterised was generated by site-directed mutagenesis using the Kunkel method (105). The *E.coli* strain BL21 was used for the expression of both wild type and G586S mutant constructs using plasmid pCRNNR (106). During the creation of both wild type and G586S constructs, an N-terminal histidine tag was added to the plasmid in order to purify the enzymes exploiting their affinity for nickel.

2.1.1 Cell transformation

30 µl of competent cells BL21 E.Coli were gently defrosted on ice before 5 to 10 ng of plasmidic DNA in a volume of 1 to 5 µl were added and mixed. The mixture was incubated for 30 minutes on ice and then heat shocked at 42°C for exactly 30 seconds in a water bath before being quickly placed on ice again. Pre-warmed SOC medium (see table 2.1) (250 µl) was added before transferring the vial at 37°C for 1 hour in a shaker at 225 rpm. Eventually, different aliquots (10 to 100 µl) of the transformation mix were plated onto two LB plates containing 25 mg/ml carbenicillin and 35 mg/ml chloramphenicol: a flame sterilised loop was dragged across the surface of the cells-mix and used to streak out the agar plate. The plates were incubated overnight at 37 °C in order to promote the growth of bacterial colonies.

2.2 Expression and Isolation

Cell cultures for line-maintenance were prepared for both wild type and G586S mutant enzyme. Small amounts of cells were picked from the colonies on LB-agar plates with a sterile wire loop and dispersed into 30 ml of sterile TB augmented with 25 mg/ml carbenicillin and 35 mg/ml chloramphenicol in sterelin tubes.

Table 2.1: Growth Media and Agar

Luria Bertani Broth (LB)	For 1 litre: 10 g Bacto Tryptone 5 gYeast Extract 5 g NaCl
Terrific Broth (TB)	For 1 litre: 20 g Bacto Tryptone 10 gYeast Extract 4 ml Glycerol 2.6 g KH_2PO_4 4.3 g K_2HPO_4
Prepared using MilliQ ultrapure water (of resistivity 18 Ω cm^{-1}) and autoclaved sterilized.	
LB Agar Plates	15 gL^{-1} agar dissolved in LB Autoclaved agar was allowed to cool to room temperature. Prior to setting, agar was augmented with 25 mg/ml carbenicillin and 35 mg/ml chloramphenicol and poured into Petri dishes.
S.O.C. Medium	For 1 litre: 5 g Bacto Tryptone 5 gYeast Extract 0.58 g NaCl 0.19 g KCl 1.2 g $MgSO_4$ 2.0 g $MgCl_2$ 3.6 g Glucose

The cells were then incubated overnight at 37.5 °C and 150 rpm in an orbital shaker/incubator. From these starter-cultures small stocks for future use were prepared by adding 77 µl DMSO to 1 ml of cells dispersion (7% DMSO by volume). DMSO stocks were then stored at -80°C until required and kept at low temperature while in use. The DMSO stocks were replaced periodically using cells colonies from freshly prepared LB agar plates.

Aliquots of 2 ml from the starter cultures were inoculate in each flask containing larger quantity of TB media: typically 40 x 350 ml TB augmented with 25 mg/ml carbenicillin and 35 mg/ml chloramphenicol in 1 litre baffled flasks were used. The flasks were kept at 37.5 °C and 150 rpm in an orbital shaker/incubator until the optical density (O.D.) of the culture was in the region 0.5 – 0.8 (~6 hours). IPTG (24 mg/ml) and ATP (113 mg/ml) were then added to induce overexpression. The temperature was lowered to 20°C for a period of 20 hours.

The cell rich media was eventually collected and the cells harvested through centrifugation at 15 000 rpm for 15 minutes at 4°C (Sorvall RC-5B centrifuge with a SLA 3000 head). The cell pellets were collected and stored at -20°C until required.

2.3 Extraction and Purification

2.3.1 Cell Extraction

Cells stocks were defrosted and suspended in Resuspension/Lysis buffer (table 2.2) allowing approximately 40 ml buffer for 25 g of cell pellet. Lysis of the *E. coli* cells was obtained through air-bubble generation by ultrasonication using a Sanyo Soniprep 150.

Typically 8 sonication turns of 20 second each at 15 microns applied to a 40 ml cell suspension were required to lyse cells. The beakers containing the cell suspension were kept on ice to prevent overheating between one sonication and the other. Eventually the lysate was pooled and cell debris separated by centrifugation at 20 000 rpm for 1 hour at

Table 2.2: Purification Buffers

Resuspension/Lysis Buffer	50 mM Tris-HCl (pH 7.5) 0.5 mM EDTA 10% glycerol 20 µM H_4B/aminoH_4B 1 mM dithiothreitol 25 mM phenylmethylsulfonyl fluoride (PMSF) 20 mM imidazole 0.1mM L-arginine 0.3 M NaCl protease inhibitor (1 tablet/50ml buffer)
Elution Buffer	50 mM Tris-HCl (pH 7.5) 0.5 mM EDTA 10% glycerol 20 µM H_4B/aminoH_4B 1 mM dithiothreitol 150 mM imidazole 0.1mM L-arginine 0.3 M NaCl
Gel Filtration Buffer	50 mM Tris-HCl (pH 7.5) 20 µM H_4B/aminoH_4B 1 mM dithiothreitol
Prepared using MilliQ ultrapure water (of resistivity 18 Ω cm^{-1}) and pH adjusted using HCl	

4°C (Sorvall RC-B5 centrifuge with a SS34 head). The supernatants containing the over-expressed $nNOS_{oxy}$ were collected and kept on ice prior to the chromatographic steps of purification.

2.3.2 Column Chromatography

All protein purification steps were carried out in a cold-room at 4°C using purification buffer A.

The purification profiles for the wild type and G586S $nNOS_{oxy}$ constructs are the same.

Nickel Sepharose Affinity Chromatography: Ni^{2+} Sepharose prepacked column is formed by agarose beads cross-linked together bringing immobilized chelating groups binding in turn nickel (Ni^{2+}). The high affinity of the six-histidine tag on both $nNOS_{oxy}$ for Ni^{2+} make the binding very selective and allows an extremely high degree of separation from all the other proteins in the lysate. We exploited this affinity during the first step of $nNOS_{oxy}$ purification: the lysate was loaded onto a HisTrapHP 5 ml Column (Amersham) using a FPLC system (Åkta Purifier), the flow being very slow (0.5 ml/min) to maximize the protein binding. The column was then washed with Resuspension/Lysis buffer until the UV Absorbance at 400 nm was stable. Elution was then performed using Elution Buffer, allowing high concentration imidazole to displace the histidine tag in Ni^{2+} binding then letting the protein flow through the column. The red/brown coloured fractions were collected, and a further selection was made to increase the purity of the enzyme retaining only the fractions showing high content in heme (UV-Vis absorbance at 400 nm). To prevent the inclusion of heme-containing

deleted forms of the enzyme SDS-PAGE analysis (paragraph 2.5.1.2) was carried out on the fractions collected : only the fractions showing a highly pure presence of the 80 KDa monomer were pooled.

G-25 Size Exclusion Chromatography: Gel filtration was used as last step of purification to eliminate the excess imidazole present due to elution from the agarose-Nickel column. The G-25 size exclusion chromatography beads contain pores of a precisely regulated size allowing only small molecules to enter into the beads. As a result molecules with a bigger size than that of the pores (e.g. enzymes) pass through the column faster than small molecules (e.g. imidazole) which path is considerably longer. To prepare the column freeze dried G-25 sephadex was suspended in Gel Filtration Buffer (table 2.2) and packed by gravity. The column was then thoroughly washed with the same buffer prior to use. The collected fraction from agarose-Nickel column in a volume not greater than 30 % of the G25 column volume was loaded onto the top of the column and eluted by addition of more buffer. The red-coloured imidazole free fractions were collected.

2.3.3 Dialysis

When substrate-free nNOSoxy was needed, the enzyme solution collected from Gel filtration column was dialysised overnight (12 kDa exclusion limit) at 4 °C into 5 litres of Gel Filtration Buffer enriched with 0.5 M imidazole: in this way residual L-arginine bound to the enzyme was displaced by imidazole. Dialysis against Gel Filtration Buffer in order to remove imidazole was then repeated several times until UV-Vis spectrum of substrate free enzyme was detected.

2.4 Concentration and Storage

Concentration of the purified protein was obtained via centrifugation using a FALCON 6-300 centrifuge at 2000 rpm and Amicron Centriprep concentrators with a membrane size of 30 kDa. Protein concentration was spectrophotometrically measured and concentration was repeated until in the region 100 μM. The enzyme solution was then divided into aliquots, flash frozen in liquid nitrogen and stored at -80°C until required.

2.5 Characterisation

2.5.1 Purity Determination

The purity of the protein was measured at several stages by both analysis of UV/vis peak ratios and by SDS-PAGE (Sodium Dodecyl Sulfate-Poly Acrylamide Gel Electrophoresis).

2.5.1.1 Peak Ratios

UV/vis spectra of the enzyme were recorded over the range 200 – 800 nm using a Shimadzu UV-2101PC spectrophotometer. The solution was put in quartz cuvette with a 1 cm path length in a total volume of 1 ml (typically 10 μl of purified protein diluted in 990 μl gel filtration buffer). The purity was measured through the ratio of absorbances values at 280 nm (global content of proteins) and at 395-410 nm depending from the conditions of purification (Soret peak for heme in nNOS). The ratio A_{280}:A_{400} for purity higher than 95% was found to be about 2:1 (figure 2.1).

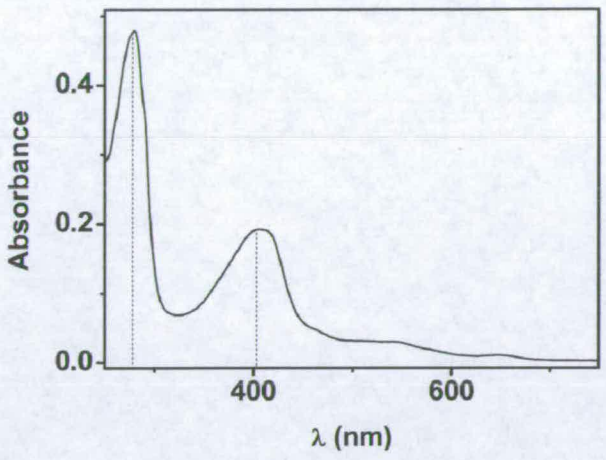

Figure 2.1: UV-Vis spectrum showing $nNOS_{oxy}$ Soret peak (400 nm) and global protein content peak (280 nm).

2.5.1.2 Gel Electrophoresis

SDS-PAGE (Sodium Dodecyl Sulphate - PolyAcrylamide Gel Electrophoresis) was performed using NuPAGE® Novex 4-12 % Bis-Tris pre-cast polyacrylamide gels in combination with SeeBlue Plus 2® molecular weight markers.

Assessment of the purity and integrity of the enzyme was carried out through gel electrophoresis at different stages of the expression/purification. The protein samples or cell pellets were diluted using buffers as described in table 2.3 and boiled for 3 minutes to denature the protein and allow SDS binding. SDS bind with a constant ratio to the proteins as a function of their mass (1.4 g SDS:1g protein) and shields their charges, the different distances at which every protein migrate depending only on its mass.

Table 2.3: SDS PAGE buffers and stains	
Sample Buffer	25 µl NuPAGE® LDS 4x Sample preparation buffer pH 8.4 25 µl diluted protein sample (>1 µM) or 25 µl lysed cell pellet (0.03 gml^{-1}) 50 µl dH_2O
Running Buffer	NuPAGE® MES SDS 20x Running buffer pH 7.0
Coomassie Stain	50 ml dH_2O 40 ml Methanol 10 ml Acetic Acid 1 ml Coomasie Brilliant Blue
Destain	50 ml dH_2O 40 ml Methanol 10 ml Acetic Acid
Prepared using MilliQ ultrapure water (of resistivity 18 Ω cm^{-1}).	

The central reservoir was filled with running buffer ensuring that the buffer-level was beyond the sample loading wells. Aliquots of each sample ranging from 5 to 15 µl were loaded into the wells, reserving one well for SeeBlue Plus 2® molecular weight markers (5 µl). An electric field (150 V, 120 mA and 60 W) was applied to the gel for the time necessary for the dye front to reach the bottom of the gel (approximately 1 hour).The voltage was then removed and the polyacrylamide gel was stained in coomassie (Table 2.3) approximately for 15 minutes and destained for at least 1 hour to remove excess of blue. Coomassie blue binds to the protein forming a blot, and the comparison between the positions of the blots with the markers give an indication about the presence of proteins and their size (figure 2.2).

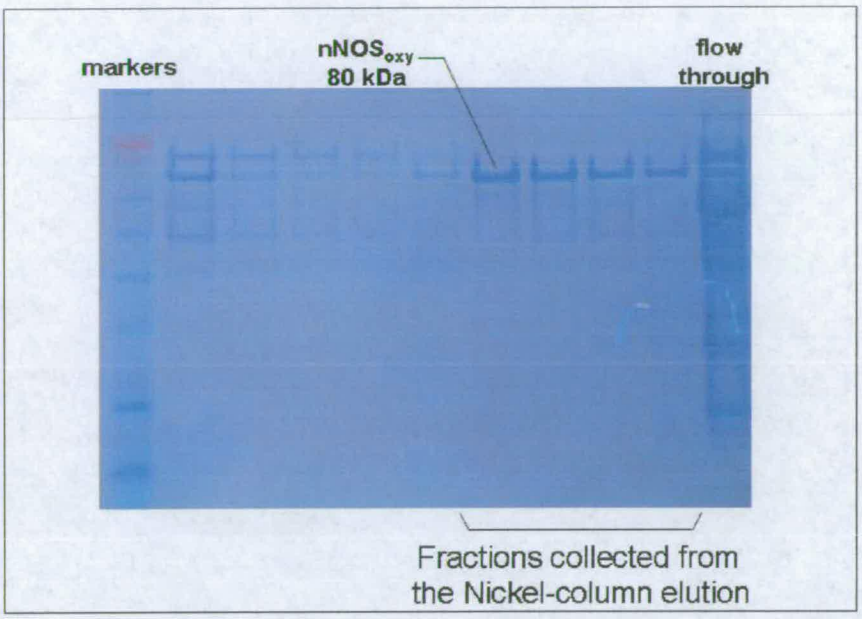

Figure 2.2: Coomassie stained SDS-PAGE of the elution from the Nickel column. In the first lane there are size markers, while in the last one there is a sample of flow through from the washing step. The fractions with a predominant presence of $nNOS_{oxy}$ were collected.

2.5.2 Enzyme Concentration

Enzyme concentrations were determined spectrophotometrically exploiting the absorbance difference between the ferrous and the ferrous CO-binding forms being the extinction coefficient $\varepsilon_{444\text{-}467} = 55,000\ M^{-1}cm^{-1}$ (118) (figure 2.3). Protein solution was diluted with gel filtration buffer to the volume of 1 ml in a 1 cm path length quartz cuvette and UV/vis spectra were recorded over the range 250 – 800 nm with a Shimadzu UV-2101PC spectrophotometer. Protein samples were reduced using sodium dithionite ($Na_2S_2O_4$) and bubbled with CO to form the ferrous-CO complex and spectra were recorded of both species. The reduced-enzyme spectrum was subtracted from that of

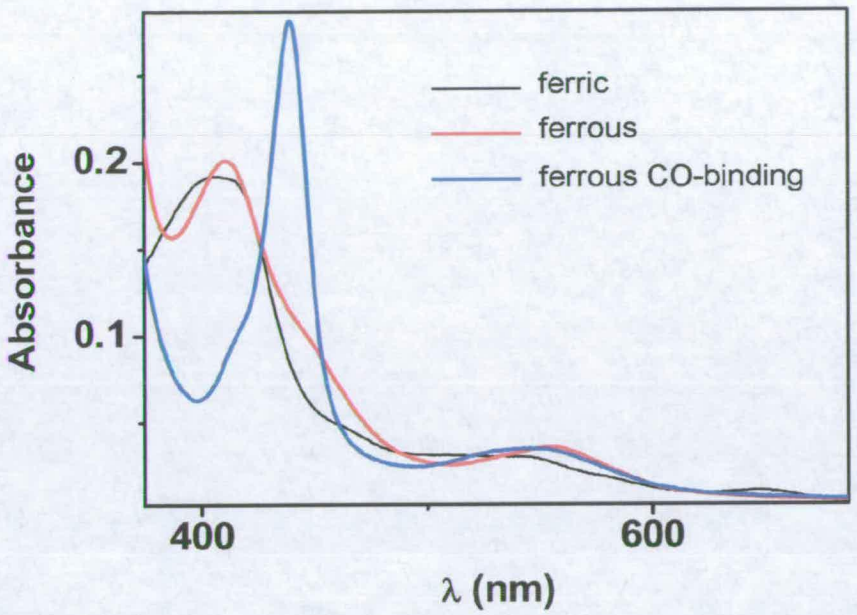

Figure 2.3: UV-Vis spectra of oxidised (black), reduced (red) and reduced CO-binding (blue) $nNOS_{oxy}$ The spectrum resulted from subtracting the reduced one from the CO-binding was used to calculate the enzyme concentration.

CO-binding form and concentration were calculated according to the Beer-Lambert Law ($A = \varepsilon cl$).

2.6 Dissociation constants determination

Difference spectrophotometry measurements were conducted to quantify the affinities of substrates, substrate-analogues and diatomic molecules. Optical spectra were recorded over the range of 250-800 nm using a UV-1601 Shimadzu spectrophotometer at 20°C. 1ml solutions of $nNOS_{oxy}$ were prepared in a quartz cuvette with a path length of 1 cm in gel filtration buffer supplemented with H_4B. Standard solutions of substrates and other compounds were prepared at high concentration in the same buffer and

sequentially added having a final change in the sample volume of less than 5%. Manipulation of the spectra obtained was performed to determine the dissociation constants (K_d): from each spectrum corresponding to the enzyme partially bound to the substrate, the substrate-free enzyme spectrum was subtracted. In the resulting spectrum the difference absorbance between two evident peaks was determined, and the series of differences ($\Delta\Delta$Abs) plotted against substrate concentration. The wavelengths of the selected peaks varied depending on the ligands and on the enzyme used. The points were fitted to a Michaelis-Menten-like rectangular hyperbola and values of K_d were extrapolated (concentration of substrate at which half of the maximum concentration of the complex enzyme-substrate is observed) using Microcal Origin 7.0 software. In the cases, where in the first trial, the affinity of the compound appeared to be extremely high, accuracy in the method was increased using imidazole as a competitive heme ligand. In this way apparent K_ds for every compound were obtained: by using the imidazole concentration and its affinity for $nNOS_{oxy}$ in the formula: $K_{d\ apparent} = K_d (1+[imidazole]/K_i)$, real K_ds were obtained. For the titrations of CO and NO affinity, their concentrations were worked out optically through the difference spectrum of CO/NO binding ferrous/ferric P450 BM3 (ε_{445}=92.000 cm^{-1} and ε_{418}=108.000 cm^{-1} respectively).

2.7 OTTLE Potentiometric Titrations

OTTLE (Optically Transparent Thin Layer Electrode) potentiometric measurements were performed at 25 °C using a Cary UV/vis spectrophotometer and Autolab PGSTAT10 potentiostat. All buffers and mediators used are shown in tables 2.7 and 2.8.

Table 2.7: OTTLE Titration Buffers

Buffer A	50 mM Tris 500 mM KCl 10 % glycerol pH 7.5
Buffer B	50 mM Tris 500 mM KCl pH 7.5
Buffer C	50 mM Tris 500 mM KCl 1mM Laurate pH 7.5
Prepared using MilliQ ultrapure water (of resistivity 18 Ω cm^{-1}) and pH adjusted using HCl	

Table 2.8: OTTLE Titration Mediators

Mediator	E_m (mV) vs SHE
2-Hydroxy-1,4-Napthoquinone	- 145
Flavin Mononucleotide	- 200
Benzyl Viologen	- 310
Methyl Viologen	- 430
Prepared using MilliQ ultrapure water (of resistivity 18 Ω cm^{-1}) and pH adjusted using HCl	

$nNOS_{oxy}$ G586S midpoint potentials (E_m) were calculated in the absence and presence of saturating concentrations of L-Arginine (10 mM).

2.7.1 Sample Preparation

All protein samples for OTTLE experiments were prepared in a Belle Technology glove box where O_2 levels were maintained at < 5 ppm by nitrogen flow. The buffers used were previously degassed by nitrogen bubbling for at least 1 hour. Enzyme samples were degassed as well by introducing them into the anaerobic box at least 1 hour prior to use.

L-Arginine Free G586S: A sample of concentrated pure enzyme was diluted to 100-150 μM in 0.5 ml of buffer A (table 2.7). Any remaining trace of oxygen was removed by running the sample down a G-25 gel-filtration column pre-equilibrated with buffer A: enzyme sample had then a volume of about 1 ml and concentration was 50-75 μM.

L-Arginine-bound G586S: The preparation of the enzyme solution was identical to that of substrate free enzyme, except for the presence of L-Arginine 10 mM in buffer A in all the steps where it was used.

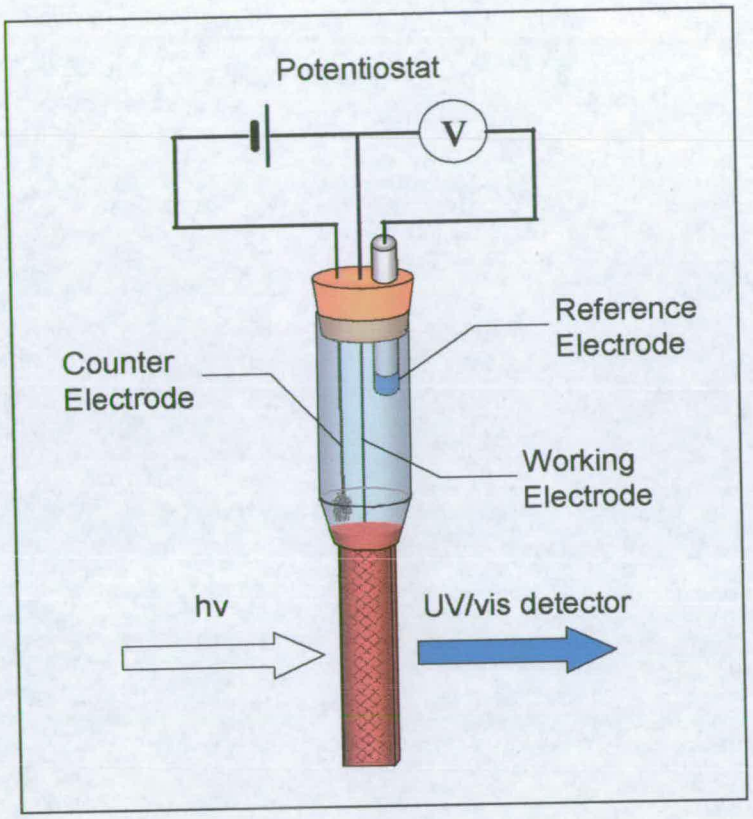

Figure 2.8: OTTLE cell showing a diagrammatic representation of the potentiostat and electrodes.

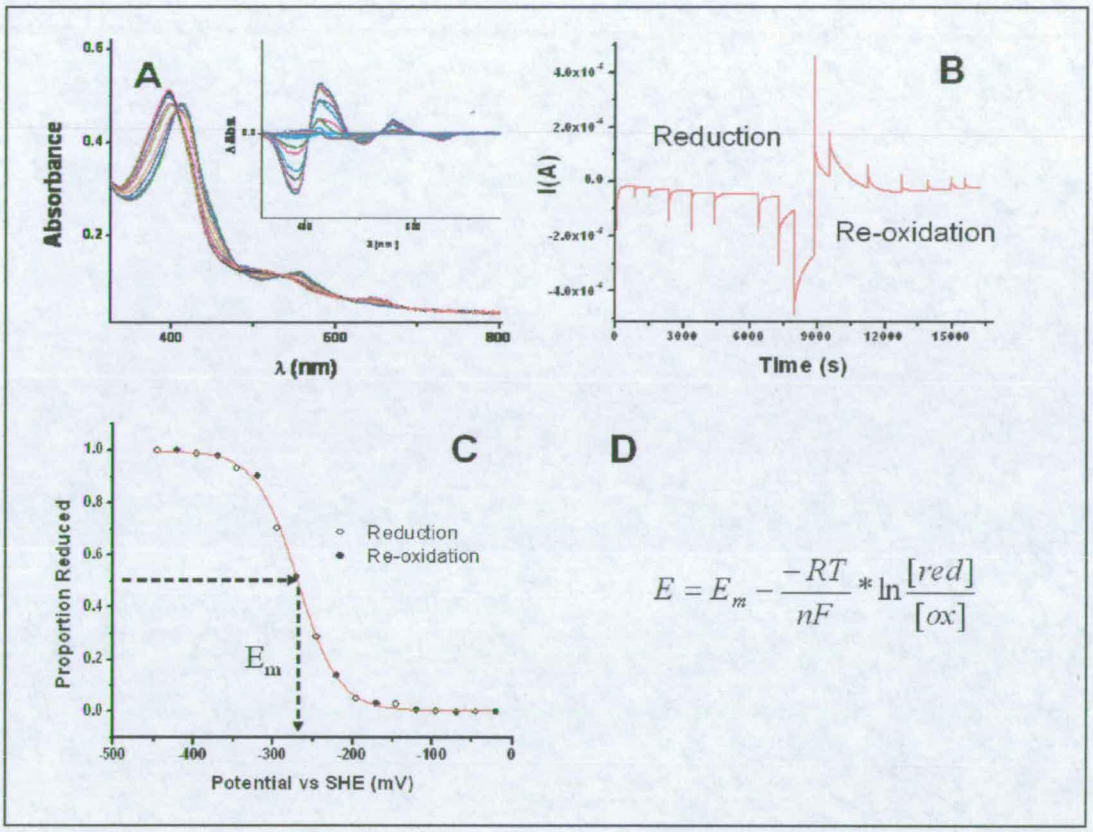

Figure 2.9: Panel **A** shows the changes in spectra observed during reduction and reoxidation of $nNOS_{oxy}$. Inset shows the difference spectra {oxidised}-{reduced}. Panel **B** shows a current vs time plot for reduction and re-oxidation. Panel **C** shows a plot of proportion reduced vs applied potential and the 1e- Nernst plot fit for this data. Panel **D** shows the Nernst equation.

2.7.2 Mediators

A range of mediators (Table 2.8) chosen according to their midpotential were added to the enzyme sample in order to facilitate electron transfer under the applied voltage. They were dissolved into the anaerobic box in degassed buffer A to a concentration of ~2 mM and then added to the samples for a final concentration of ~2 μM.

2.7.3 Potentiometry

The OTTLE experiments were conducted in modified quartz EPR cell with a path length of 0.3 mm provided with a Pt/Rh (95/5) gauze working electrode (wire diameter 0.06 mm, mesh size 1024 cm^{-1}, Engelhardt, UK), a platinum wire counter electrode and a Ag/AgCl reference electrode (model MF2052, Bioanalytical Systems, IN 47906, USA). Enzyme samples were injected with a Hamilton 0.1 mm syringe into the lower and thinner part of the cell. The upper part of the cell was filled with OTTLE buffer B. The different content of glycerol (10 %) between the two buffers used prevented the mixing between the enzyme sample (glycerol) and the glycerol-free buffer at their interface. The cell was then sealed and located into a carry 50 Probe spectrophotometer out of the anaerobic box to monitor the changes in the spectra. The three electrodes were connected to an Autolab PGSTAT potentiostat and an initial potential more positive than the predicted enzyme mid-potential was applied through the working electrode. The applied potential was the lowered stepwise (50 mV) until complete reduction was observed and back to a completely oxidized form. The enzyme samples were allowed to equilibrate until no current was detected before a new potential was applied. Spectra were recorded for each applied potential and interpreted as the partition of the enzyme

into the two redox states. Difference spectra were calculated and plotted against applied potentials (corrected according to the standard hydrogen electrode (SHE), that is $Potential_{Ag/AgCl}$ + 205 mV). E_m values, the potential at which the enzyme is equally distributed into the ferric and ferrous forms were determined by fitting the data to the Nernst equation (Microcal Origin 7.0) (Figure 2.9).

2.8 Pre-Steady-State Kinetics

Pre-steady-state kinetic measurements were all carried out at 10°C using an Applied-Photophysics stopped-flow spectrophomoter (SX.17MV) connected with either a diode-array or a single wavelength detector: diode array was used to monitor the absorbance changes on the entire UV-Vis spectrum while the single wavelength detector was used to measure faster processes once the optimal wavelength was found this having a smaller dead-time. The stopped flow apparatus was located into an anaerobic glovebox (Belle Technology; $[O_2] < 5$ ppm). Reagent concentrations and enzyme redox states were monitored by absorption spectroscopy on a Cary 50 Biospectrophotometer into the anaerobic box too. The general scheme for a stopped flow experiment was the monitoring of the oxy-ferrous complex formation by mixing ferrous enzyme and oxygen saturated buffer, and its decay. For all stopped-flow experiments the buffer used was Gel Filtration buffer (table 2.2) supplemented with 10 mM substrate (L-Arginine or NOHA) when needed. Buffer was made anaerobic by bubbling with nitrogen for 2 h before being left to equilibrate in the anaerobic box overnight. The O_2 concentration in the oxygen containing buffer was measured exploiting the absorbance change caused by oxidation

of electrochemically reduced methyl viologen (ϵ_{600} = 13,000 $M^{-1}cm^{-1}$) taking into consideration that each methyl viologen molecule donates 1 electron and that oxygen reduction to water requires 4 electrons. Typically, the final concentration of enzyme used for all pre-steady state kinetic experiments was ~ 10 μM and saturating concentrations of substrates were 20 mM. Ferrous nNOSoxy was generated by a concentrated solution of sodium dithionite and verified spectrophotometrically. Sodium dithionite was brought into the anaerobic box in powder form and dissolved in anaerobic buffer. Excess reductant in the ferrous enzyme solution was removed by passage down a 1.5 x 20-ml Sephadex G-25 (Sigma) size separation column immediately prior to use. Data were analyzed using Origin 7 (Microcal). Averaged traces from three or more measurements were used for analysis.

2.9 Protein crystallization

Crystallization of the G586S mutant for of NOS heme domain was carried out either by hanging drops or sitting drops vapour diffusion methods (126-128), using 24 wells Linbro® Plate and Cryschem™ plates, respectively (both from Hampton Research). Hanging drops (4 μl volume) were prepared by adding 2 μl of 7-9 mg/ml protein (in 50 mM pH 7.5 Tris / HCl, 0.2 M NaCl, 10 % glycerol, 1 mM dithiothreitol (DTT), 20 μM H_4B to 2 μl of well solution. Crystals were obtained at room temperature with a well solution comprising 0.1 M MES pH 5.8 / 6.0, 22-24% PEG 3350, 0.2 M ammonium acetate, 25 mM L-Arg, 35 μM SDS, 5 mM GSH, 2% isopropanol (all from Sigma).

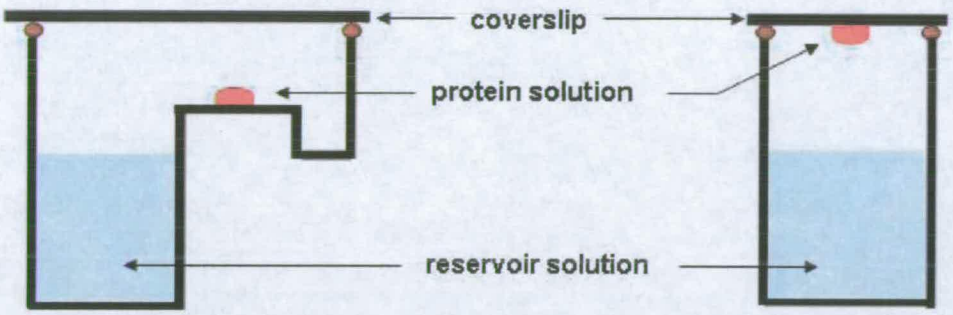

Figure 2.10: Sitting drop (left) and hanging drop (right) crystallization methods

NOS crystals needed to go through steps of mother liquor exchange with a cryo-protected solution in order to not be damaged by the solvent change. Crystals were immersed in cryo-protectan solution stepwise (six steps) with an increasing amount of cryo-protectant.

The cryo-protectant solution consisted of 0.1 M pH 5.8 / 6.0 MES, 25% PEG 3350, 100 mM ammonium acetate, 10 % glygerol, 10% threaolose, 5% mannitole, 5% sucrose, 2% isopropanol and then flash cooled in liquid propane (130).

Best dataset was collected (by C. Bruckmann) to 2.59 Å resolution, at the European synchrotron radiation facility (ERSF) in Grenoble, France on beam line BM14 using Mar Research charged camera detector (CCD) detector (wavelength 0.9737 Å) at 100 K. Crystal were found to belong to space group $P2_12_12_1$ with cell dimensions $a = 51.9630$ $b = 110.8470$ $c = 164.6270$ $\alpha=\beta=\gamma= 90$.

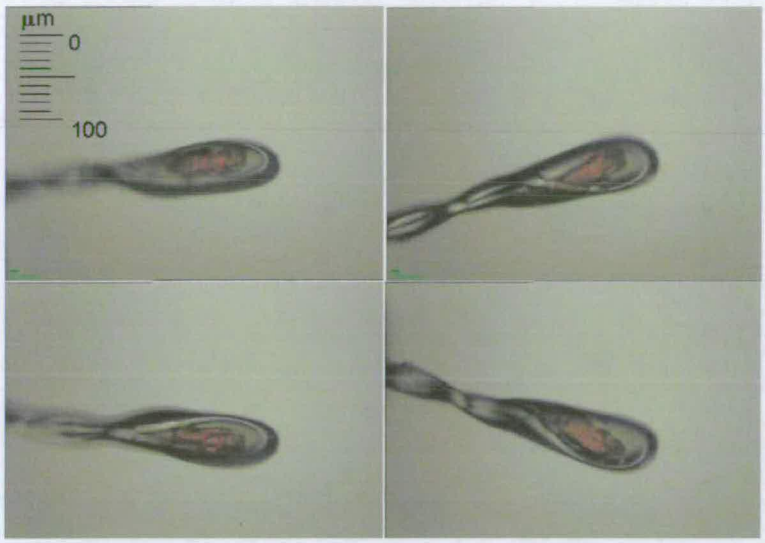

Figure 2.11: Crystal snapshots. Beam line BM14

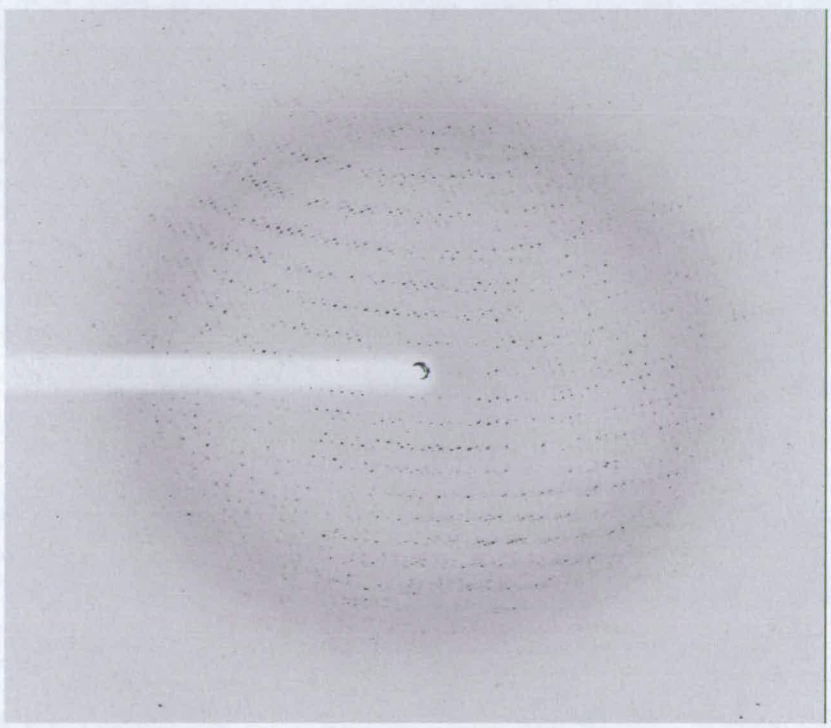

Figure 2.12: Diffraction pattern of NOS G586S mutant crystal. Oscillation range 1.0°, Exposure time 30.0 s; detector distance 269.4 mm; resolution at edge 2.5 Å; resolution at corner 3.54 Å.

Data processing was carried out (by C. Bruckmann) using MOSFLM (120) and SCALA (121). The structure was solved by molecular replacement using PHASER (122) and the wild-type NOS structure (PDB entry 1OM4), stripped of water, as a starting model. Electron fitting was carried out using the programs TURBO-FRODO (123) and COOT (124) and structure refinement was carried out using Refmac 5 (129) and Phenix(125).

Chapter 3

CHARACTERIZATION OF G586S $nNOS_{oxy}$ THROUGH UV/ VISIBLE SPECTROSCOPY AND LIGAND BINDING

3 CHARACTERIZATION OF G586S $nNOS_{oxy}$ THROUGH UV/ VISIBLE SPECTROSCOPY AND LIGAND BINDING

Amino acid residues in the distal portion of NOS heme domain are involved in the stabilisation and activation of the oxygen-heme complexes formed during NO production. The interactions they form with the transforming species have the task to promote oxygen binding, prevent uncoupled reactions and assist punctual O-O bonding breakage. Inspection of the distal side of catalytic domain reveals a striking hydrophobic character of the residues which are placed to allow interactions during the reaction: surprisingly there are no residues capable of hydrogen-bonding which presence is expected in a reaction of this kind. The reaction performed by NOS is indeed similar to that performed by cytochrome P450, where hydrophilic residues play a key role during the activation of oxygen. An amino acid residue with the ability of forming hydrogen-bonds at a suitable distance from the space where substrate and oxygen-heme complexes interact may introduce species stabilization during the course of oxygen activation. With this in mind a mutant where the glycine 586 was replaced by a serine residue ($nNOS_{oxy}$ G586S) was generated. The generation of a residue mutation in the heme proximity may alter the UV-Vis spectroscopic features of the mutant in a comparison with the wild type. Hence all the stabilized states in respect of their UV-Vis spectra were characterized, even in consideration of more complex analysis of the mutant, identifying each redox, substrates, ligands and cofactors-binding state of the enzyme. The way the mutation affects the binding of a variety of compounds, such as substrates, substrate-analogues and diatomic ligands, was tested and compared with that characterizing the wild type.

3.1 UV/Visible spectra

As isolated, G586S $nNOS_{oxy}$ is in the oxidised (ferric) form and the visible spectrum has a broad Soret peak at 397 nm like the wild type enzyme (figure 3.1). The position and the broadness of the Soret peak were interpreted as indicating a mixture of high and low spin states in the sample. This was confirmed when the peak narrowed and moved to the left upon addition of L-Arginine, by indicating a shift to high-spin state. The Soret peak of G586S $nNOS_{oxy}$ in this state is at 395 nm, as for the wild type enzyme (107).

When L-Arginine-bound G586S was chemically reduced by Sodium Dithionite the Soret peak shifted to 413 nm, similar to the ferrous wild type enzyme (figure 3.1).

The enzyme obtained from purification was showed evidence of partial substrate binding, i.e. it was more high-spin than the wild type enzyme. In order to remove bound substrate the enzyme was dialysed overnight against a high concentration imidazole to displace the L-Arginine, and then several times in imidazole-free buffers to remove the imidazole: the imidazole-removing dialysis steps were repeated until no further changes were detected in the spectrum of the enzyme. Substrate-free G586S $nNOS_{oxy}$ had a Soret peak at 400 nm. This compares to 398 nm for wild type $nNOS_{oxy}$. When chemical reduction was performed on substrate-free G586S $nNOS_{oxy}$ the Soret peak shifted from 400 to 410 nm as for the wild type $nNOS_{oxy}$ (figure 3.1) (107).

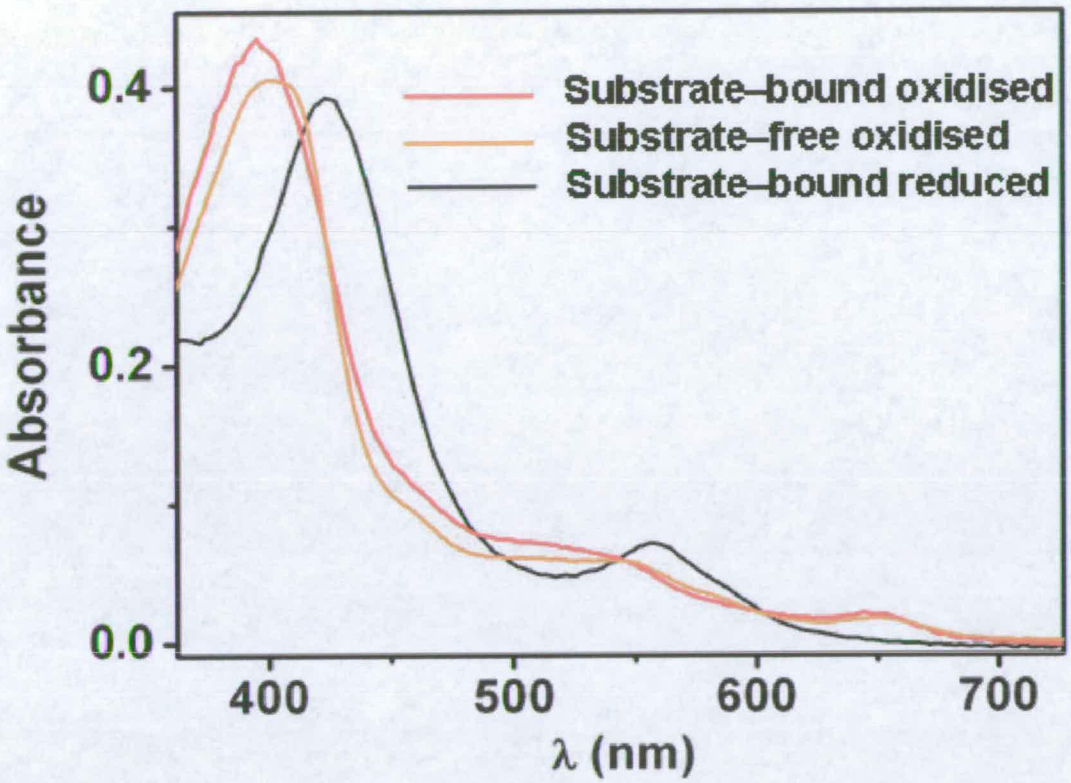

Figure 3.1 UV-Visible spectra of G586S $nNOS_{oxy}$ in different conditions of substrate binding and redox state.

Imidazole binds to the NOS catalytic site (107, 108) by forming a complex directly with the heme, converting it to a low-spin form by competitively replacing the substrate and acting as sixth axial heme-ligand (figure 3.4). The binding of imidazole induces a shift in the Soret peak to 428 nm in wild type nNOS and for G586S $nNOS_{oxy}$ to 426 nm indicating the same binding interaction. When ferrous G586S $nNOS_{oxy}$ was bubbled with CO it formed a characteristic heme protein-CO complex with a Soret peak at 444 nm, as in wild type $nNOS_{oxy}$ (figure 3.5). This was used to measure the enzyme concentration (see mat. & methods).

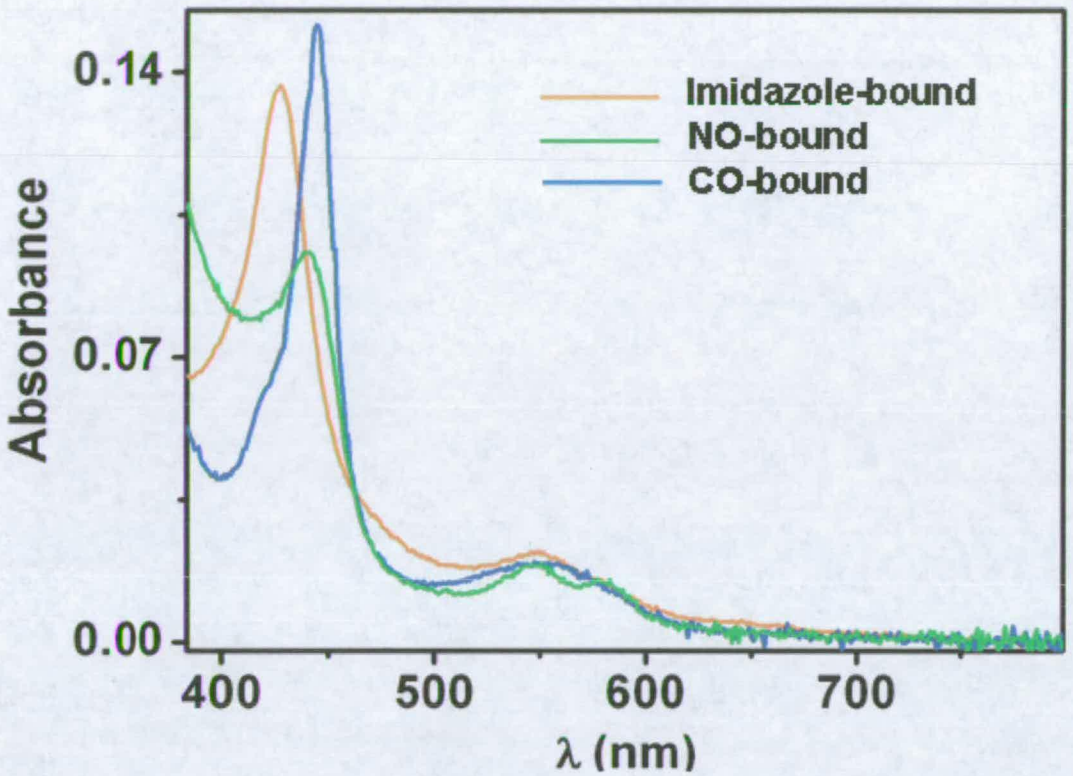

Figure 3.4 UV-Visible spectra of G586S $nNOS_{oxy}$ imidazole-bound (orange), NO-bound (green) and CO-bound (blue).

In summary all the optical spectroscopic features of G586S $nNOS_{oxy}$ closely resemble those of the wild type enzyme, this indicates the absence of major structural rearrangement due to the mutation.

3.2 Affinity titrations

The substitution of glycine 586 to a serine introduces a hydroxyl group directly into the active site. This may affect oxygen binding to the heme and its activation process during the reaction due to possible hydrogen bonding newly formed with the intermediates. Substrate binding also can be affected: the interactions with the amino acid residues into the wild type catalytic site are optimized in a way that both substrates have a similar affinity for the enzyme. The presence of a new hydroxyl group can introduce stabilizing hydrogen bonding but also create a different space limitation by the bulkier steric occupancy. Consequently there could be a newly introduced discrimination between L-arginine and NOHA way of binding. The same can be referred to the way the G586S $nNOS_{oxy}$ binds substrate-analogues and small diatomic ligands. Thus a series of affinities were measured and compared with those characterizing the wild type nNOS.

3.2.1 Substrate affinity

The space where the guanidinium group is located in the catalytic site could be described as being formed by two pockets, each hosting one amino group (figure 3.6): the left pocket, viewing the ligand and the heme from above, is very tight and does not tolerate even the smallest substituent groups. The right-side pocket is slightly more spacious and is defined by the three residues Pro 565, Val 567 and Phe 584. As the x-ray structures of NOSs catalytic site with substrate-analogues show, the right-side

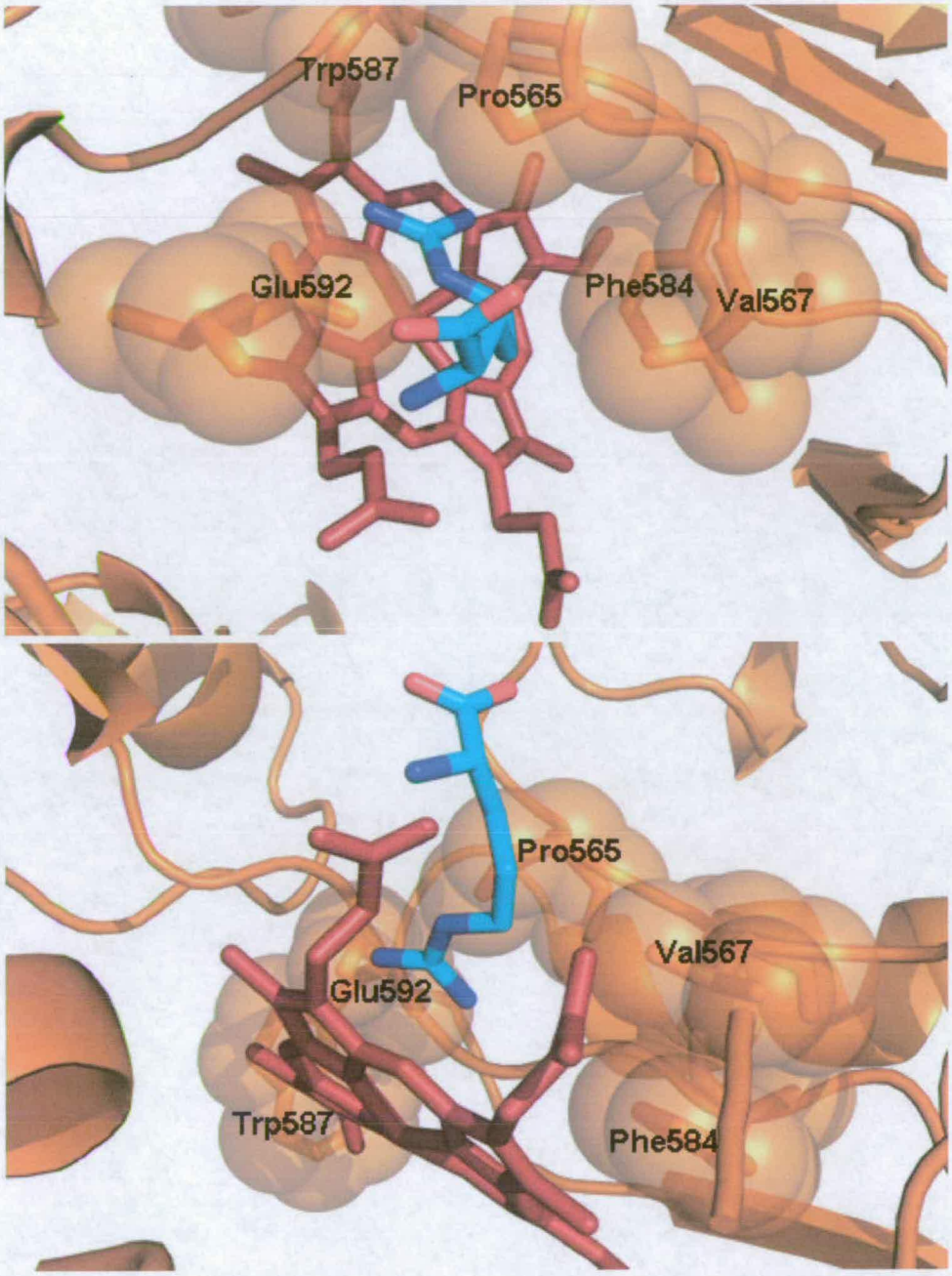

Figure 3.6 Catalytic site of L-arginine bound nNOS: the pictures are taken from above the heme plane and from behind the α–carbon portion of the substrate (rotating the position of 90° around the x axis). The two corners hosting the two guanidinium amino groups are highlighted: on the left side of the allocation site the two residues Glu 587 and Trp 592 define a narrow space. On the right side Pro 565, Val 567 and Phe 584 limit a wider space that can tolerate bulkier groups (PDB file: 1OM4).

pocket always hosts the bulkier side of the guanidinium group (or of its substituted form) (figure 3.7). This is possible in all the cases where the analogues have at least a sp_3 bond along the lateral chain (or what resembles it) of the arginine analogue: the free rotation around the axis of this bond allows the most comfortable position to be assumed.

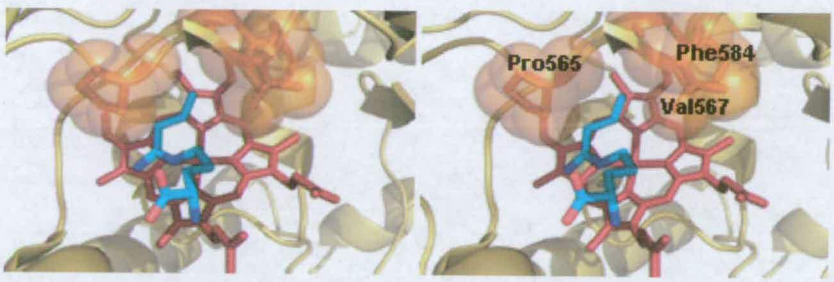

Figure 3.7 Stereoview of nNOS catalytic site binding vinyl-L-NIO. It is highlighted the corner formed by Pro 565, Val 567 and Phe 584 residues, hosting the intrusive vinyl group on the ligand (PDB file: 1MMW).

The original 586 glycine residue is positioned in the right-side corner of the guanidinium group allocation (figure 3.8), and its mutation to a serine is highly probable to affect the spatial definition of this pocket. Although crystallographic evidence would be needed for a complete analysis, the affinity data collected were interpreted in consideration of the new shape assumed by this corner of the catalytic site.

Difference spectrophotometry measurements were conducted to quantify substrates affinities. UV/Vis spectra of the enzymes were recorded prior and after each addition of high concentration substrate stock. From each spectrum corresponding to the enzyme partially bound to the substrate, the substrate-free enzyme spectrum was subtracted. In the resulting spectrum the difference absorbance between two evident peaks was determined, and the series of differences ($\Delta\Delta$Abs) plotted against substrate

concentration. The points were fitted to a Michaelis-Menten-like rectangular hyperbola,

$y = (\Delta Abs\ Max*x)/(K_d+x)$,

where y and x are the change of absorbance and substrate concentration respectively; values of K_d were extrapolated (concentration of substrate at which half of the maximum concentration of the complex enzyme-substrate is observed) using Microcal Origin 7.0 software. The method used to determine the binding affinity of $nNOS_{oxy}$ for its ligands is graphically represented in figure 3.9. Even at a first glance it was clear that the G586S mutation had increased the affinity of the enzyme for L-Arginine: as isolated from the purification, G586S was in a mixed high-low spin state with a high-spin predominance in comparison to the isolated wild type enzyme. This most likely indicated a higher percentage of the enzyme being complexed with substrate due to the sequestering of L-Arginine from the cells and retained during purification. A first attempt to titrate the affinity of G586S for L-Arginine was made using the enzyme as isolated from the purification, exploiting the small shift to complete high-spin state upon substrate addition, as previously done with the wild type heme domain (107). The K_d values obtained were lower than those of wild type $nNOS_{oxy}$.

In order to apply a hyperbolic ligand binding function, the L-Arginine concentration has to be in excess of that of the enzyme throughout the titration. If the K_d value is comparable with that of the enzyme concentration then the K_d would be underestimated. Consequently the enzyme concentration needed to be low. On the other hand enzyme concentration cannot be too low otherwise the absorbance signal is too small to give detectable and reliable shifts upon substrate addition.

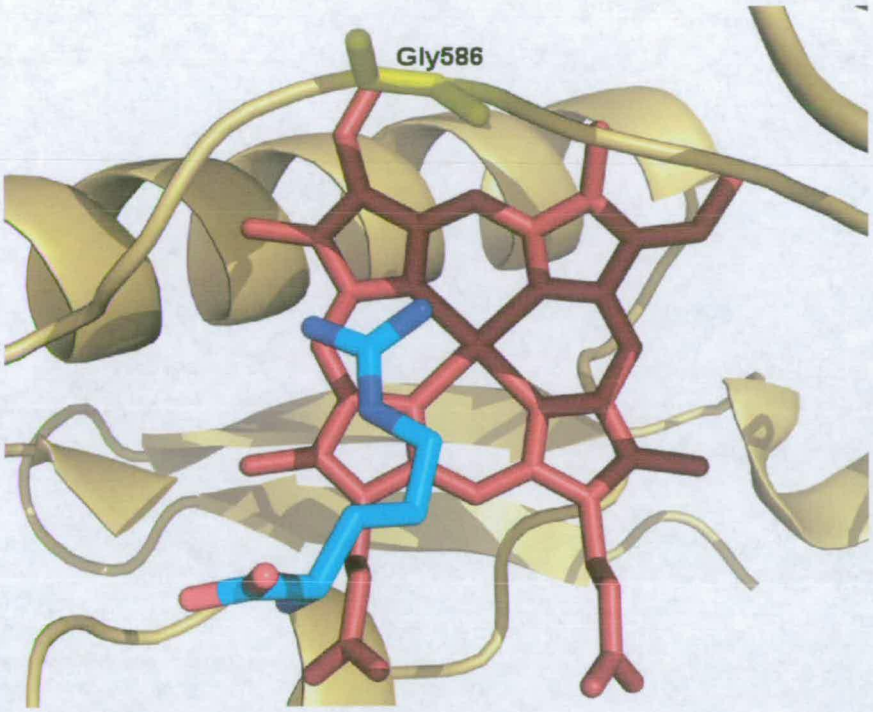

Figure 3.8 Catalytic site of L-arginine binding nNOS: the picture shows the proximity of the 586 glycine residue to the hosting site of the bulkier moiety of the guanidinium group. The mutation of this residue into a serine is highly probable to redefine the this corner of the catalytic site (PDB file: 1LZX).

To overcome this issue the titrations were conducted in the presence of imidazole which behaves as a competitive inhibitor for the active site binding with L-Arginine (116). The absorbance shift from the low spin-state of partial imidazole-occupied enzyme to that of high spin of substrate-binding enzyme was much more appreciable. The affinity of imidazole for G586S previously calculated by similar methods was then used to determine the K_d according to the formula

$$K_{d\ apparent} = K_s\ (1+[imidazole]/K_i)$$

where K_s is K_d for substrate binding and K_i is K_d for imidazole binding. Titrations

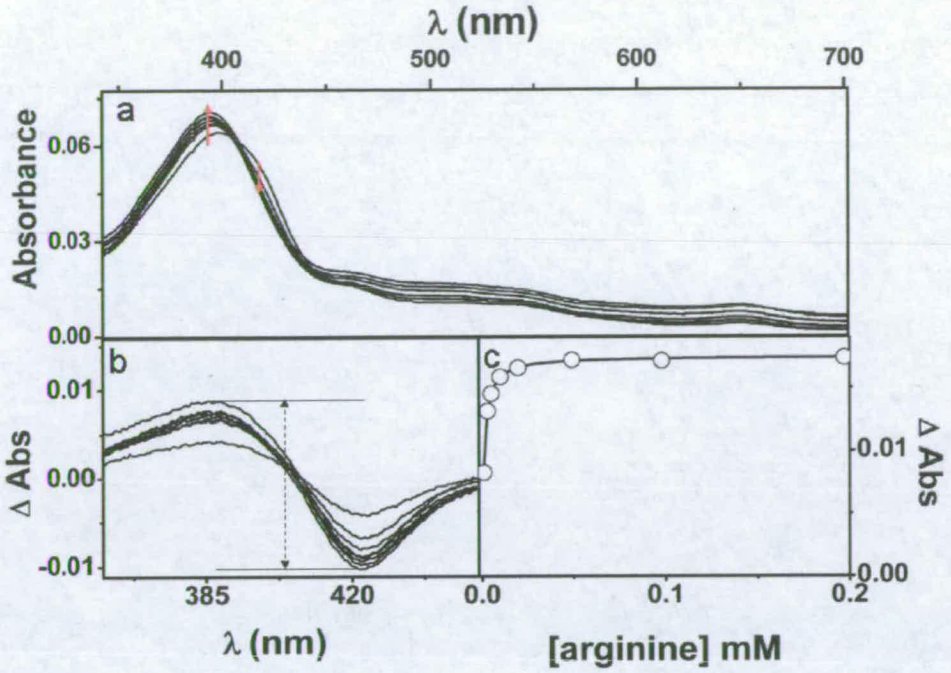

Figure 3.9 Graphical representation of the method exploited to evaluate ligands binding constants to nNOSs: to a solution of the enzyme successive aliquots of the ligand were added and after an equilibration time a spectrum was recorded (panel a). From each spectrum was subtracted the ligand-free corresponding one: in the resulting difference-spectra (panel b) two clear peaks were identified and the absorbance difference between them measured. Each of these differences was plotted against the corresponding ligand-concentration and fitted to a rectangular hyperbole (panel c) and the K_d was calculated based directly on Michaelis–Menten equation

were conducted in the presence of different concentrations of imidazole and the K_ds averaged.

Data are graphically presented in figure 3.11. To confirm that imidazole behaves as a competitive inhibitor with L-arginine for the NOS active site, data corresponding to different concentrations of imidazole were manipulated and plotted according to the Lineweaver-Burk graphical representation (figure 3.10): the different x axis intercepts (indicating different apparent K_d) joined to identical y axis intercepts of the plot indicate a competitive type of inhibition..

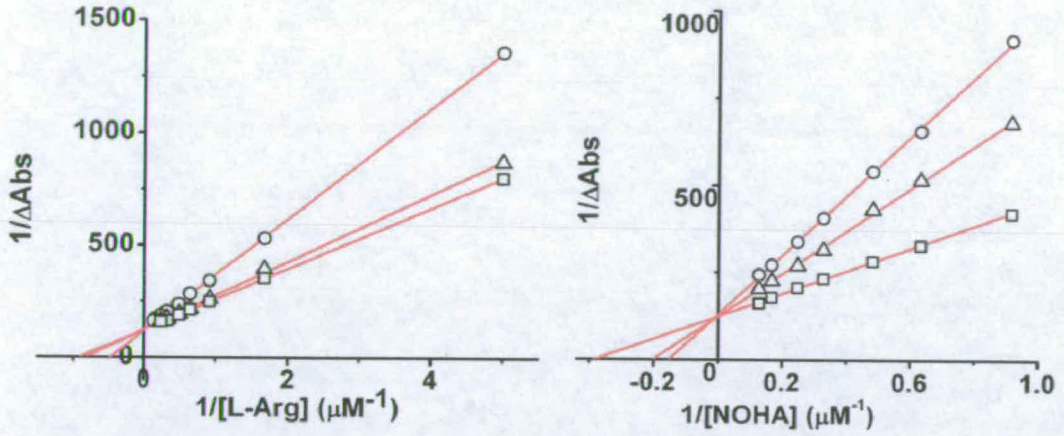

Figure 3.10: Lineweaver-Burk graphs for imidazole competitive inhibition of G586S nNOSoxy in the presence of L-arginine (left) and NOHA (right). Circles, triangles and squares indicate imidazole 15, 10 and 5 μM respectively.

In order to make comparison between the affinity constants of the mutant and wild type, those of the wild type were measured using the same method. The dissociation constants characterizing the binding of substrates to both wild type and G586S $nNOS_{oxy}$ are presented in table 3.1.

	G586S K_d (μM)	Wild Type K_d (μM)
L-Arg	0.10±0.05	1.0±0.1
NOHA	0.5±0.1	0.9±0.1
Imidazole	235±4	86±2

Table 3.1 Substrates and imidazole dissociation constants comparison for nNOS wild type and G586S.

The K_d determined for the wild type heme domain for L-Arginine was in good agreement with that published previously (1 μM) (107). The K_d for the binding of L-Arginine to G586S $nNOS_{oxy}$ was found to be 0.1 μM, indicating an increased

effectiveness of L-Arginine binding into the catalytic site. The comparison between the affinities of wild type and G586S $nNOS_{oxy}$ for NOHA showed also an increased affinity induced by the mutation: K_ds were 0.9 μM and 0.5 μM respectively. While, for the wild type enzyme both substrates bind with similar affinity, for the mutant L-arginine binds 5 folds more tightly than NOHA.

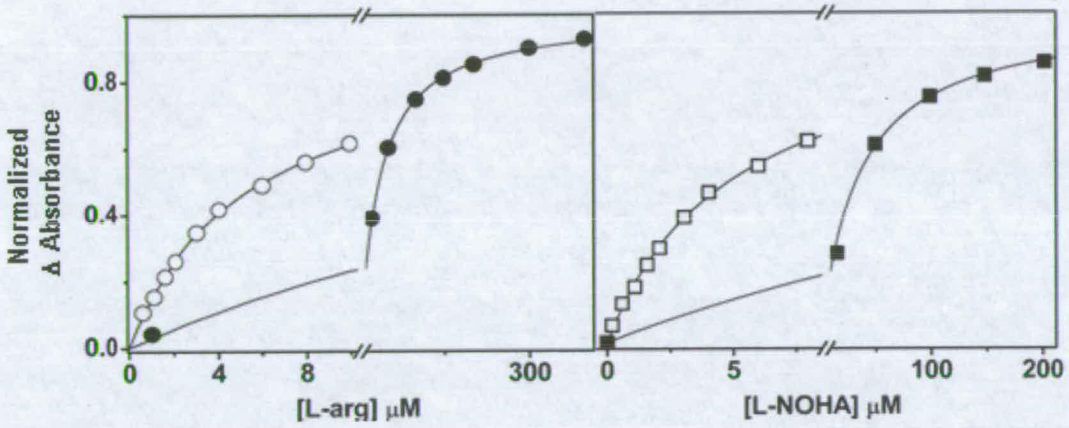

Figure 3.11: Absorbance-difference titrations of substrates affinity. Left panel: wild type (●) and G586S (○) $nNOS_{oxy}$ titrated with L-Arginine. Right panel: wild type (■) and of G586S (□) $nNOS_{oxy}$ titrated with NOHA in the presence of 15 μM imidazole. NOS concentration was 0.5 μM.

A possible explanation for the different action of the newly introduced serine residue should take in consideration not only hydrogen-bonding capacities, but space occupancy as well. In the crystallographic chapter it will be shown what is predictable by interpreting the affinity results: the 586 serine residue with its hydrogen-bonding capability must be positioned pointing towards the substrate. In particular, an interaction with the guanidinium group of the substrate seems likely from the effects of the mutation on substrates affinities. This position assumed by the

serine though, indicates its occupation of more space than in native 586 glycine. The mutation has an exclusively positive effect on L-Arginine binding, increasing its affinity 10-fold. Concerning NOHA, the modest increase in the affinity may derive from the larger size of the NOHA guanidinium group: the hydroxyl substituent group may be impeded by the serine hydroxyl and the negative effect of this interaction would decrease the positive effect of a serine H-bond.

3.2.2 Substrate analogue affinities

To further investigate the effects of the 586 serine introduction in the catalytic site, a series of substrate analogues (figure 3.11) were tested for their affinity to the G586S mutant and to wild type $nNOS_{oxy}$. The method used was the same as in the case of substrates affinity determination: the hyperbolic ligand binding functions corresponding to each titration are shown in figures 3.13 and 3.14. The common structural feature of the compounds tested was the resemblance of the overall L-Arginine structure or the presence of portions of it. The dissociation constants for all the tested analogues with nNOS are presented in table 3.2.

	G586S K_d (μM)	**Wild Type** K_d (μM)
Agmatine	42.8±5.7	130±23.5
Amino Guanidine	546±70	1530±77
L-NAME	31.7±2.0	7.9±3.3
L-NIO	11.4±0.6	2.7±0.7

Table 3.2 Substrate-analogues dissociation constants for $nNOS_{oxy}$ and G586S $nNOS_{oxy}$.

The structure of agmatine is identical to that of L-Arginine but for the absence of the carboxyl group on the α-carbon (figure 3.12). Although sharing a very similar structure with L-Arginine, and particularly having a guanidinium group identical to that of the native substrate, its binding affinity is rather modest. It is in fact a competitive inhibitor of NOS with a K_d of 130 μM for the wild type enzyme. The average effectiveness of agmatine as a NOS inhibitor is possibly due to incorrect orientation. The mispositioning of the α carbon may result in a suboptimal positioning of the guanidinium group in its interactions

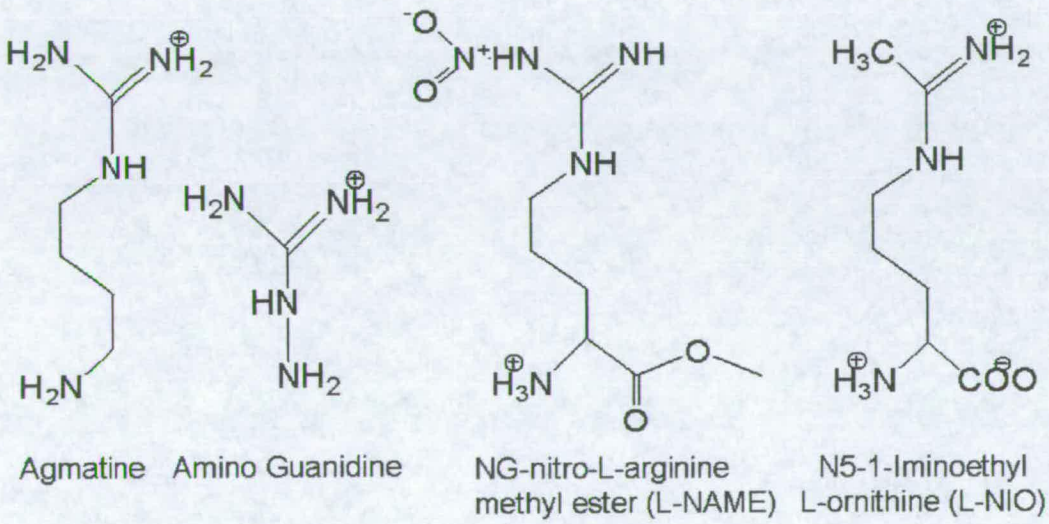

Figure 3.12: Substrate analogues of NO Synthase.

with the key residues in the active site. Nevertheless when titrated with the G586S mutant, the affinity of agmatine was increased by a 3 fold , with a K_i of 42.8 μM. This suggest that the hydrogen-bonding capacity introduced with the serine mutation assists binding of the guanidinium group.

The amino-guanidine structure resembles that of the guanidinium group of L-Arginine: it is composed of a guanidinium group and a terminal amino group. Its inefficiency as a NOS inhibitor indicates how important the α-carbon-portion contacts are to achieving a position that maximizes binding. Its dissociation constant for wild type nNOS was calculated to be 1.53 mM. Even in this case of poor binding though, the affinity is increased again by 3 fold in the mutant. The interactions that are formed in the presence of serine 586 are offset the loss of a large portion of the molecule. In both cases, it appears that interactions formed between the guanidinium nitrogens, probably of an H-bonding nature, are able to increase the affinity of enzyme for analogue, possibly making it shift into a position closer to that of the native substrate.

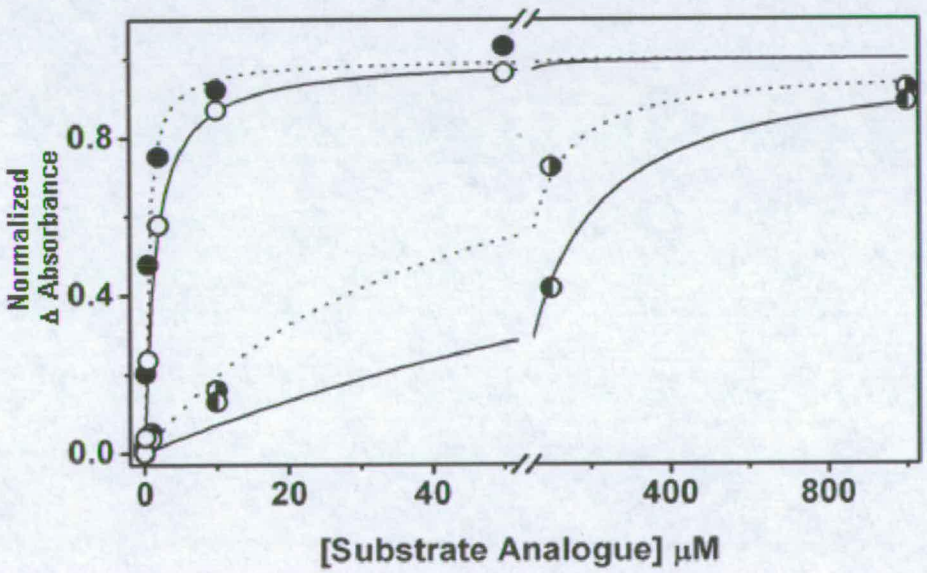

Figure 3.13: Absorbance-difference titrations of substrate-analogues. Wild type (○) and G586S (●) nNOS with agmatine. Wild type (◐) and G586S (◑) with amino guanidine. The function K_d's derived are in table 3.2. NOS concentration was 0.5 μM.

The structure of L-NAME is like that of L-Arginine with a nitro group on one of the guanidinium nitrogens and an ester group on the α-carboxyl group. These substitutions make L-NAME a NOS inhibitor rather than a substrate. The binding constant for wild type nNOS has been calculated to be 7.9 μM. The binding of L-NAME to the G586S mutant was characterized by a K_d of 31.7 μM, 4 fold lower than for the wild type enzyme. This decrease in affinity indicates that the newly introduced serine could clash with the terminal nitro group: this suggests that the serine points toward the nitro group of the modified guandinium group. As a consequence of the steric clashes H-bonding may not be possible between the oxygen of the nitro group and the hydrogen of serine 586. The overall result would be an unstable position for L-NAME in the active site of the mutant.

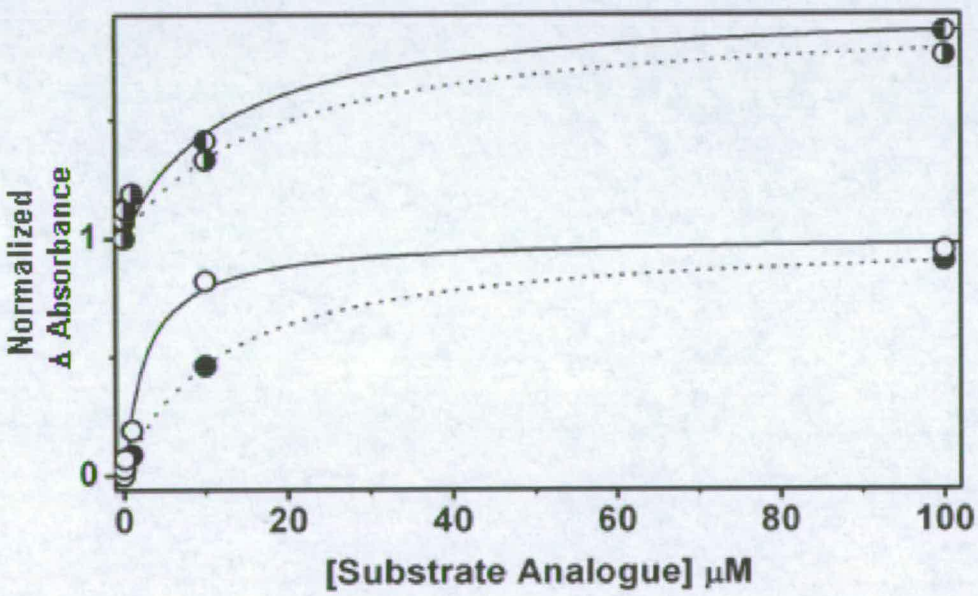

Figure 3.14 Absorbance-difference titrations of L-NAME and L-NIO. Wild type (◐) and G586S (◑) nNOS with L-NAME. Wild type (○) and G586S (●) with L-NIO. The function K_d's derived are in table 3.2. NOS concentration was 0.5 μM.

L-NIO is a powerful NOS inhibitor and it differs from L-Arginine in having a methyl group in place of one of the two guanidinium amino groups. Its efficiency as a wild type NOS inhibitor was characterized by a K_i of 2.7 μM. The affinity of L-NIO for the G586S mutant was characterized by a K_d of 11.4 μM. Therefore the affinity was decreased by the serine mutation by more than 4 fold. As in the case of L-NAME, as the serine 586 is pointing towards the guanidinium group in the active site, it may clash with substituents on it. In this case there is no capability of H-bonding between the serine and the terminal methyl, as the latter is not responsive to this kind of interaction. Overall binding is destabilized.

3.2.3 Diatomic ligands affinity

Small diatomic molecules such as NO and CO bind to the heme as sixth, distal ligands. NO binding to the heme is an important part of the catalytic cycle. Although with different affinities, it has the capability to bind both ferric and ferrous heme (62). Immediately after its production, NO stays bound to the ferric heme with micromolar affinity. NO is then released as part of a productive cycle. If another electron is delivered to the heme, producing ferrous iron, the enzyme is partitioned into a futile cycle, where the affinity of NO towards the reduced heme is very high, with a K_d in the nanomolar range, and from which it can be released only in the presence of oxygen in the form of NO_3^- (62). CO binding to the heme may not have such an important role during the normal functioning of NOS, but its exclusive binding to the ferrous form mimics that of oxygen (109). In fact the characterization

of both NO and CO binding to the heme in different conditions is important as source of information about the binding fashion of oxygen and the elements that regulate the reactivity of the much less stable oxy-heme complexes. We measured the affinities of NO and CO to the wild type and G586S mutant in the absence of substrate, in the presence of L-arginine and of NOHA. The graphic representation of the titrations data and the Michaelis-Menten-like function fittings are shown in figure 3.17 and 3.18.

Prior to each titration, buffer was bubbled with either NO or CO. The concentrations of the gases were measured with a spectrophotometer into the anaerobic box exploiting their high affinity for P450 BM3 and the peculiar peak formed upon heme-binding: the extinction coefficients are ε_{418}=108.000 cm^{-1} for NO/ferric-NOS and ε_{445}=92.000 cm^{-1} for CO/ferrous-NOS. UV/Vis spectra of the enzymes were then recorded prior and after each addition of diatomic ligand containing stock. From each spectrum corresponding to the enzyme partially bound to the ligand, the non-bound enzyme spectrum was subtracted. In the resulting spectrum the difference absorbance between two evident peaks was determined, and the series of differences (ΔΔAbs) plotted against ligand concentration (figures 3.16 and 3.17). The points were fitted to a Michaelis-Menten-like rectangular hyperbola,

$y = (\Delta Abs\ Max * x)/(K_d + x)$,

like for the substrate affinity titrations.

NO binding measurements were possible only with the heme being in its ferric form: the affinity of NO for ferrous heme (nanomolar) (109) is too high to be determined with difference spectrophotometry techniques . The binding constant (K_d) of wild type $nNOS_{oxy}$ in the absence of any substrate was calculated to be 2.5 μM. The

affinity decreased when substrate was present, the K_d being 6.9 and 20.3 μM in the presence of L-Arginine and NOHA respectively. This is in agreement with previous crystallographic results where the presence of L-Arginine and NO together in the active site causes a backshift of the substrate position and the bending of the Fe-N-O angle (109) (figure 3.15).

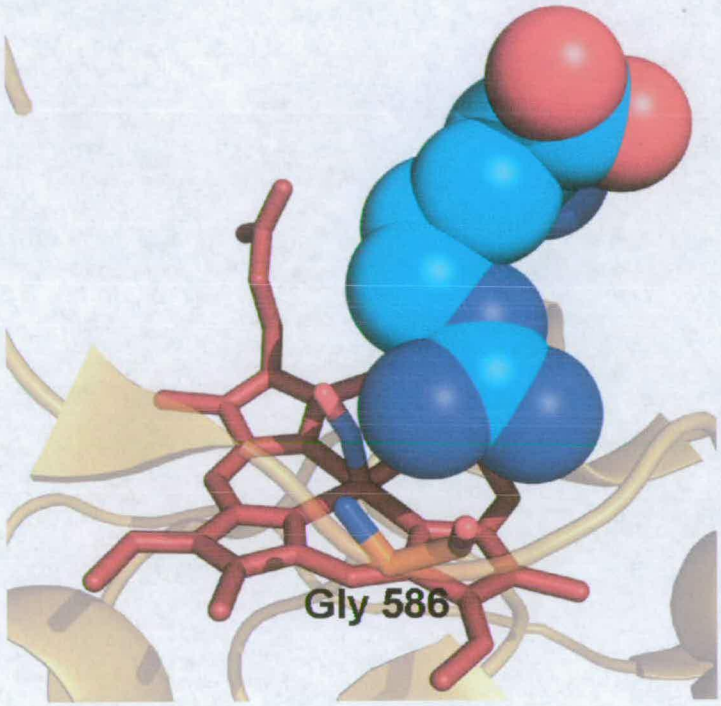

Figure 3.15 Catalytic site of NO-binding nNOS in the presence of L-arginine. In the picture is highlighted the proximity between the guanidinium group of the substrate, NO and the 586 residue (PDB file: 2G6K).

This is due to steric clashes and electrostatic interactions: when binding to the heme, NO can be considered as an electron donor, acquiring a positive charge (110), thus forming a repulsive interaction with the positive guanidinium group of the substrate. On the other hand the affinity constants of NO calculated for the G586S mutant were not significantly affected by the presence of the substrates: K_ds were 1.8, 3.2 and 2.2

μM in the absence of substrate, in the presence of L-Arginine and in the presence of NOHA respectively. When binding, the CO donates one lone pair to the heme, causing it to acquire a slight positive charge. Furthermore the higher bond order between the atoms of the molecule make it bind in an almost linear fashion, with a very small tilt angle to the heme plane (109) (figure 3.16).

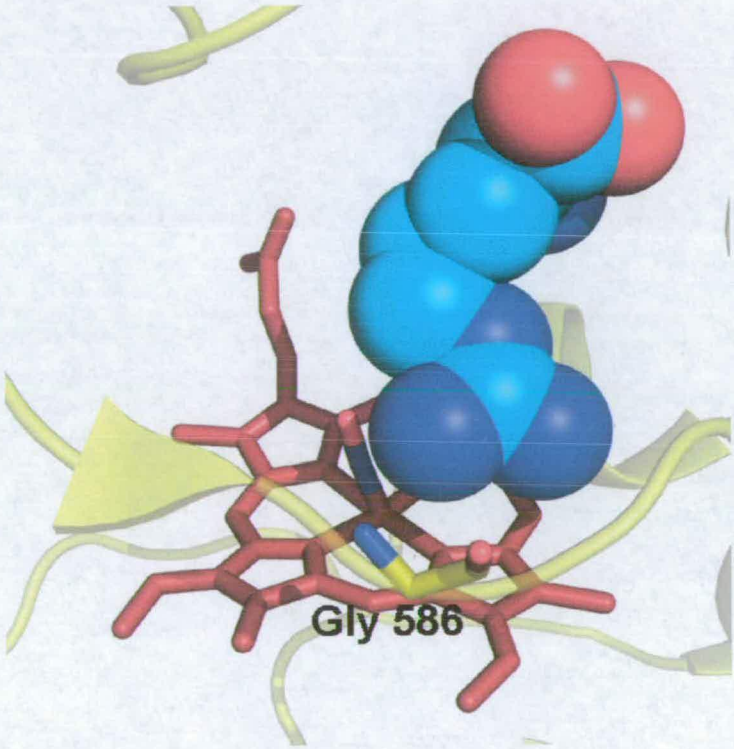

Figure 3.16 Catalytic site of CO-binding nNOS in the presence of L-arginine. In the picture is clear how the guanidinium group of the substrate, CO and the 586 residue are at an interacting distance (PDB file: 2G6M).

Not surprisingly, in wild type $nNOS_{oxy}$ the binding of CO follows the same pattern of NO, being negatively affected by the presence of substrates. The anticooperative binding of CO and L-arginine due to the overlap between the nitrogen of the substrate guanidinium group and the diatomic ligand has been evidenced previously

(131, 132): this determines constraints that stretch the key enzyme-substrate interactions (e.g. the bidentate binding from the conserved glutamate). In the titrations conducted with the WT enzyme this effect was evident, although at a lower grade than expected. The K_d of CO for the substrate-free enzyme is 10.4 μM, while in the presence of L-Arginine and NOHA the K_ds are 21.4 and 30.8 μM respectively. It is remarkable that the binding of CO in the active site of G586S is promoted by the presence of both substrates. The K_d for the substrate-free mutant is 11.5 μM, while in the presence of L-Arginine and NOHA it is 2.9 and 2.6 μM respectively. These results (table 3.3), taken altogether indicate that the G586S mutation does not significantly alter the values of the constant binding for both NO and CO determined in the absence of substrate. There are, however differences between wt and mutant when the enzymes are complexed with substrate: generally the mutation increases the affinity for the ligand by factors

	Ferric $nNOS_{oxy}$			**Ferrous $nNOS_{oxy}$**		
	NO	**NO**	**NO**	**CO**	**CO**	**CO**
	No subs.	**L-Arg**	**NOHA**	**No subs.**	**L-Arg**	**NOHA**
G586S						
K_d (μM)	1.8±0.1	3.2±0.2	2.2±0.2	11.5±1.5	2.9±0.3	2.6±0.2
wt						
K_d (μM)	2.5±0.2	6.9±0.4	20.3±1.8	10.4±1.0	21.4±2.3	30.8±1.9

Table 3.3 Affinities of NO and CO for both G586S and wild type nNOS in the substrate-free, L-arginine-binding and L-NOHA-binding enzyme.

ranging from 2-fold to 12-fold, indicating that a new interaction is formed by serine 586 that requires the presence of the substrate in order to be formed.

This stabilizing interaction may be due to a repositioning of the substrate caused by its interaction with 586 serine: as a consequence this may determine the formation of new positive interactions between heme binding molecules and the guanidinium-terminal of the substrate. It can be consequently speculated that, in the presence of

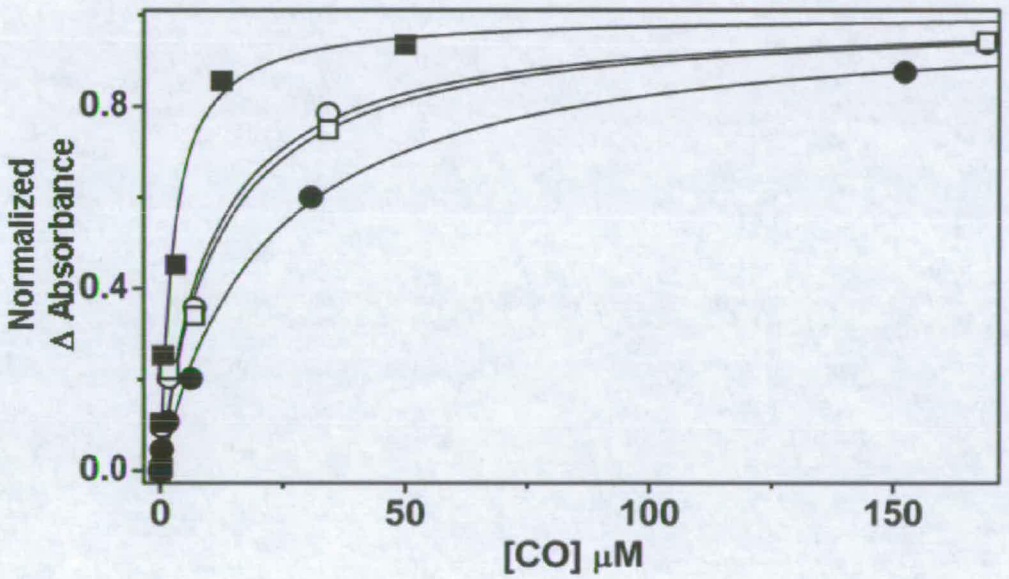

Figure 3.17: Difference-absorbance titrations of carbon monoxide binding to nNOS wild type in the absence (○) and presence of L-Arginine (●) and G586S in the absence (□) and presence of L-Arginine (■).NOS concentration was 0.5 μM.

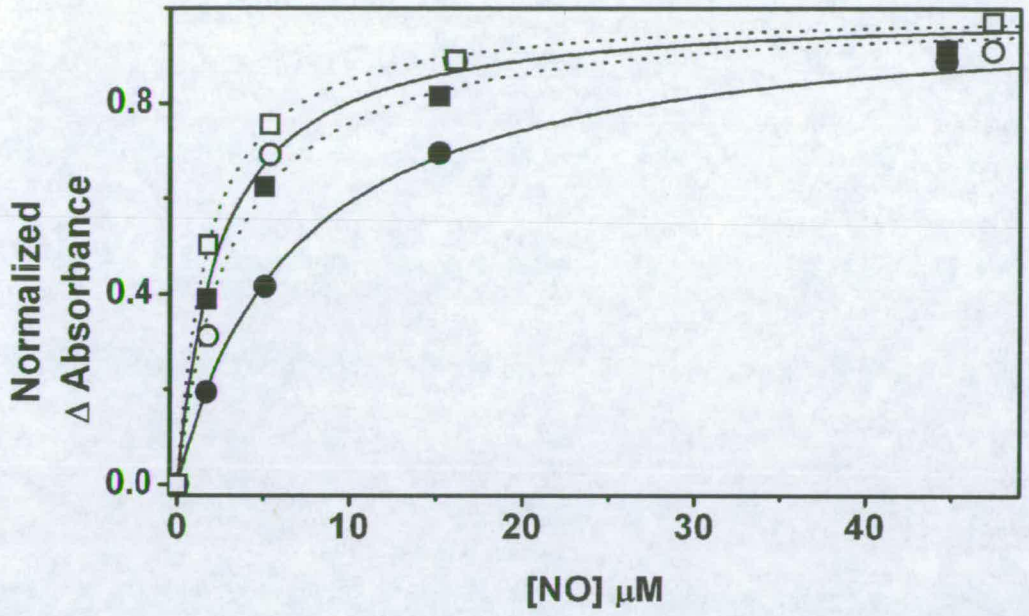

Figure 3.18: Difference-absorbance titrations of nitric oxide binding to nNOS wild type in the absence (○) and presence of L-Arginine (●) and G586S in the absence (□) and presence of L-Arginine (■). NOS concentration was 0.5 μM.

substrate, the heme binding of oxygen during NOS reaction may be influenced in a similar manner: a faster formation of the oxyferrous compound during the reaction, and its stabilization once is formed may be detected when the enzyme reacts in the presence of substrate.

Chapter 4

PRE-STADY-STATE KINETIC ANALYSIS

4 PRE-STADY-STATE KINETIC ANALYSIS

4.1 Stopped flow experiments

Stopped flow spectroscopy was used to study the heme redox-state transitions during reaction of both wild type and G586S $nNOS_{oxy}$ with dioxygen in single turnover reactions. $nNOS_{oxy}$ was chemically reduced through the addition of Sodium Dithionite, and excess of reductant was removed through gel filtration in order to avoid interference in successive steps of the reaction. The ferrous enzyme was then mixed with O_2-containing buffer in a stopped-flow experiment. The reaction was monitored by identifying the different intermediates through their UV-Vis spectra, with both rapid-scanning multiwavelength diode array and single wavelength detectors. The collected spectral data were then analyzed through software performing global analysis. The main intermediate observed in this reaction is usually the oxy-ferrous compound (Fe^{II}-O_2); the experiment follows its formation and its disappearance (figure 4.1), and the rates of both are determined.

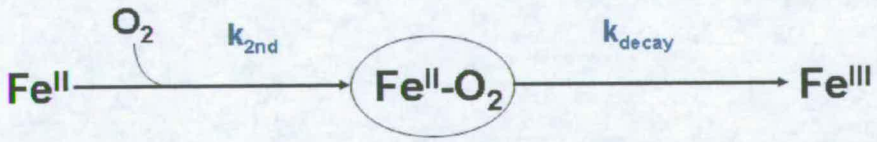

Figure 4.1

For every step of the reaction the dependence on oxygen concentration was tested: when applicable, second order rate constants were derived by monitoring the reaction at

different oxygen concentrations. As the enzyme is active in a dimeric form, all the reactions were performed in the presence of pterin, either H_4B or 4-amino-H_4B (aH_4B), which stabilize and promote the dimerization of the enzyme. The rate constants determined for the formation and decay of enzyme oxy-ferrous complexes in a variety of conditions are in table 4.1. Although most of the stopped flow experiments in different conditions with wild type $nNOS_{oxy}$ were performed during the project, some data from a previous work has also been included as referenced (63).

	Oxy-ferrous formation k_{2nd} (μM^{-1} s^{-1})	**Oxy-ferrous decay k_{decay} (s^{-1})**	
G586S/H_4B/Arginine	2.8±0.2	16±2	1.2±0.1
wt/H_4B/Arginine	1.1±0.1	17±2.0	
G586S/H_4B/NOHA	3.1±0.2	15±2	1.0±0.1
wt/H_4B/NOHA	1.1±0.1	4.9±0.5 (63)	
G586S/aH_4B/Arginine	1.4±0.1	0.20±0.02	
wt/aH_4B/Arginine	1.2±0.1	0.06±0.01 (63)	
G586S/H_4B	0.10±0.01	-	
wt/H_4B	0.46±0.10	>160±13 (63)	
G586S/aH_4B	0.14±0.01	-	
wt/aH_4B	0.47±0.04	8.3±0.9 (63)	

Table 4.1 Rate constants for the oxy-ferrous formation (left) and decay (right, either in one or two steps) determined in a variety of conditions.

4.2 Substrate-free $nNOS_{oxy}$

When the ferrous wild type $nNOS_{oxy}$ complexed with H_4B and with no substrate was mixed with the oxygen, the starting Soret peak at 410 simply broadened towards shorter wavelengths (63); contemporarily, the ferrous-heme characteristic peak in the α–β region was replaced by the two ferric-type peaks. There was no sign of oxyferrous species formation, but a direct increase of the ferric-form population of the enzyme. The decays were fitted to single exponential functions and the rates observed showed a linear dependence on the oxygen concentrations tested. These results were interpreted as an extremely fast decay of the newly formed oxyferrous species occurring: its rate differs so much from that of the formation (being faster) that there is no detectable accumulation of the oxyferrous compound (figure 4.2). The rates observed through the fitting of the traces are then those of the formation step, which being much slower than the decay is the limiting step. Plotting them against the oxygen concentrations, the authors determined a second order rate constant for the formation process of 0.46 $\mu M^{-1} s^{-1}$ (63).

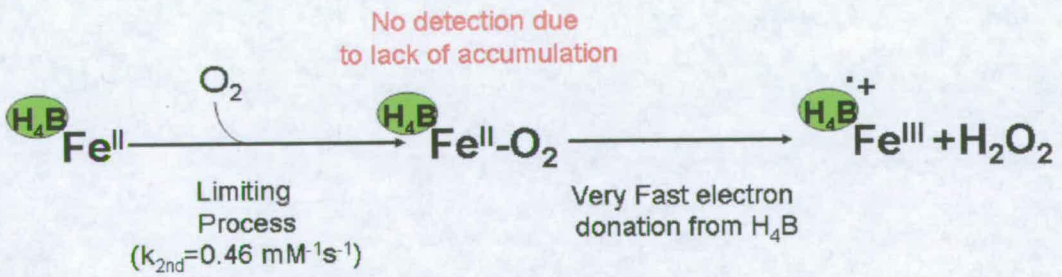

Figure 4.2

When the stopped flow experiment was repeated with enzyme purified in the presence of amino-H4B in the absence of any substrate, the detected path of the reaction was different.

Amino-(6R)-5,6,7,8-tetrahydro-L-biopterin (amino-H_4B) (figure 4.3) is a useful tool in the analysis of the NOS catalytic cycle. It is an analogue of H_4B, with an amino group substituted for a double-bound oxygen. Amino-H_4B is a strong inhibitor of NOS activity.

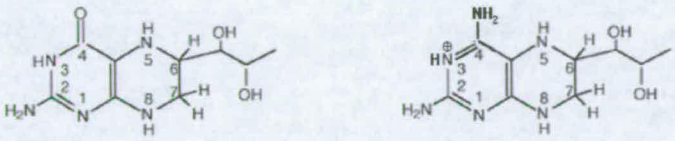

H_4B Amino-H_4B

Figure 4.3: H_4B and amino-H_4B pictured in the forms with which they bind into the catalytic site of the enzyme.

It binds to the enzyme with a 20-fold higher affinity compared with H_4B (111), and the position assumed in its binding site is virtually undistinguishable from that of the physiological pterin (fig. 4.4).

The widely accepted reason for amino-H_4B inhibiting NOS is its inability to perform the second electron donation. The redox properties of amino-H_4B tested in solution are similar to those of H_4B, being the potential of the latter is only 60 mV more negative: this difference is too small to justify the inability to donate an electron. An important

aspect to be considered analyzing the different behaviour of the two pterins is the tautomeric form with which they bind the enzyme: H_4B is found exclusively in the form where the oxygen on the C4 is bound with a double bond (4.4). This form corresponds to that of the imino tautomer of amino-H_4B, which, on the other hand, binds preferentially to the enzyme in its amino tautomer. As a consequence, in amino-H_4B the N3, to keep on forming the hydrogen bond with the heme propionate needs to be protonated (such is that of H_4B), and as a result is positively charged. The charge on amino-H_4B is thought to stabilize the tetrahydro form, disfavouring the formation of the radical upon one electron donation (111).

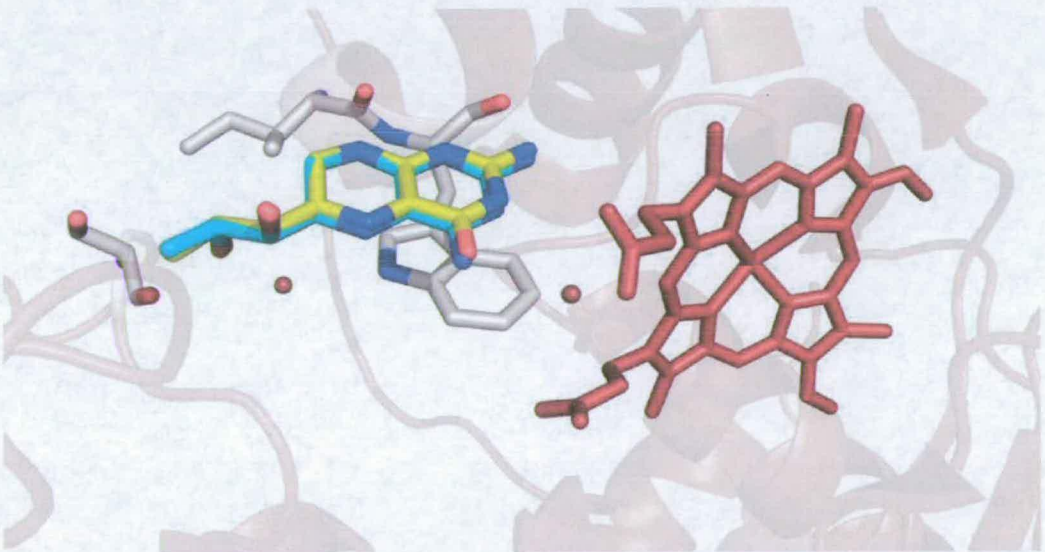

Figure 4.4: Overlaid structures of H_4B (mainly yellow) and amino-H_4B (mainly light blue). The two pterins assume position virtually identical into the catalytic site.

However it has also been proposed that the inhibition of NOS by amino-H_4B is due to its inability to donate a proton, rather than an electron (115): this hypothesis was based on the EPR detection of the radical form of amino-H_4B during NOS turnover in the presence of L-arginine, very similar to that formed by H_4B. The lack of NO production was then justified by proposing that the amino group substituent stabilizes the pterin structure in a way that impedes the proton donation to the electron activated (by amino-H_4B itself) oxyferrous compound. Given that amino-H_4B binds in a cationic form, this is unlikely.

As said, when the stopped flow experiment was performed with wild type enzyme purified in the presence of amino-H_4B in the absence of substrate, the detected path of the reaction was different from that in the presence of H_4B (figure 4.5).

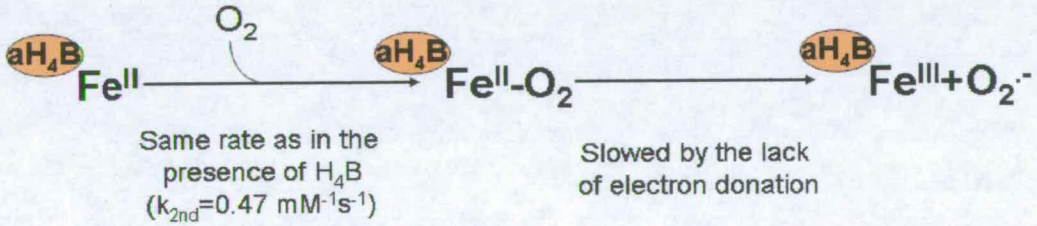

Figure 4.5

Upon mixing with oxygen the ferrous Soret peak shifted to 419 nm, demonstrating the formation and accumulation of an oxyferrous compound. This step was linearly dependent on the oxygen concentration and the second order rate constant was virtually identical to that of the process in the presence of H_4B: 0.47 μM^{-1} s^{-1}. The peak then

shifted to that characteristic of the ferric enzyme at 395 nm, in a slow and oxygen independent manner. The traces were fitted to single exponential equations and the rate determined to be 8.3 s^{-1}. The comparison between the two stopped flow experiments conducted in the presence of the different pterins, confirmed the role of H_4B as an activator of the oxyferrous compound by donation of one electron. Amino-H_4B on the other hand, doesn't influence the 2nd order rate constant for formation of the oxyferrous species, but delays its decay by not donating the activating second electron. The decay proceeds more slowly by release of superoxide (O_2^-).

When the stopped flow experiment was performed with the G586S mutant in the absence of any substrate complexed with either H_4B or amino-H_4B the spectrophotometric pattern followed by the reaction was the same (figure 4.6).

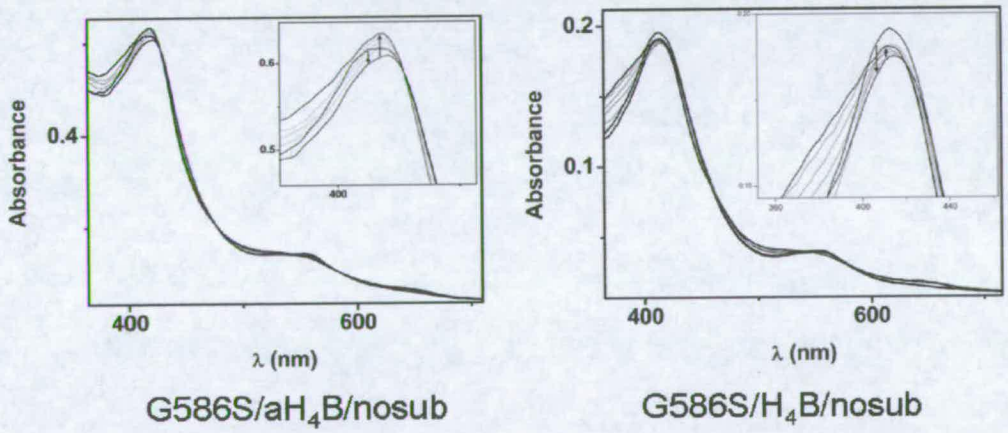

Figure 4.6: The spectrophotometric pattern of the substrate-free mutant reaction, either in the presence of H_4B or amino-H_4B is very similar: it evidences a hint of the oxyferrous species formation and a successive decay not simple to interpret.

Two phases were distinguishable: in the first milliseconds there was a quick shift of the Soret peak from 410 to 416 nm, accounting for a subpopulation of the ferrous enzyme forming the oxy-ferrous compound. Subsequently the peak broadens, and slightly shifts to lower wavelength on a time scale of seconds The Soret peak never reaches at 395 nm that characterizes the high spin ferric enzyme, but stops at 405 nm indicating low spin ferric $nNOS_{oxy}$ (formed in the absence of substrate). This transition, reflecting the decay of the oxy-ferrous compound (figure 4.7) is oxygen concentration dependent and shows no evidence of

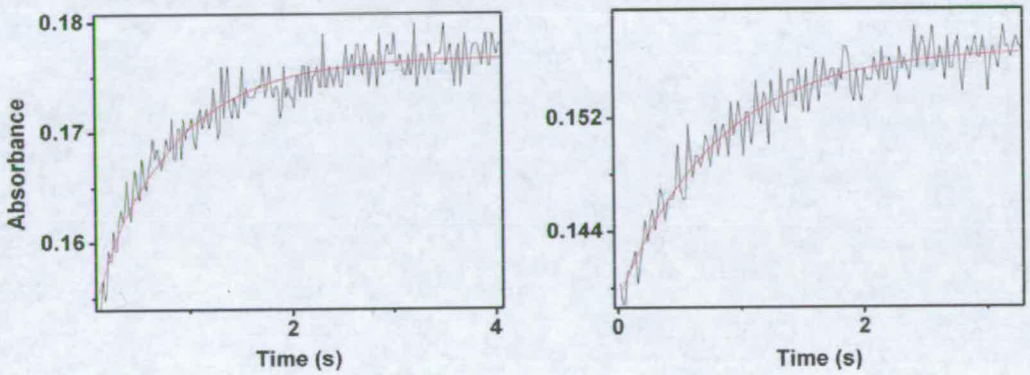

Figure 4.7: Decay traces for the substrate-free G586S $nNOS_{oxy}$ in the presence of amino-H_4B (left) and H_4B (right).

saturation in our range of concentrations.

The interpretation of the reaction is not simple, for the spectral transition is not completely defined. As in the wild type enzyme in the absence of substrate and H_4B-bound, in the cases here discussed it is possible to calculate the second order rate constant for the oxyferrous species formation by plotting the rates of decay observed against the corresponding oxygen concentrations: very similar values were obtained, the

rate constant for the oxyferrous formation in the presence of H_4B 0.10 $\mu M^{-1} s^{-1}$, and that in the presence of amino-H_4B 0.14 $\mu M^{-1} s^{-1}$. A possible explanation of the transformations occurring in both cases involves a very slow formation of the oxyferrous compound such that the accumulation (if any) is just partial, due to the much higher rate of decay of the oxyferrous species. The comparison between the second order rate constants for oxyferrous formation in both wild type and G586S $nNOS_{oxy}$ in the presence of either H_4B and amino-H_4B is shown in table 4.2: the values indicate a slow oxyferrous formation step in the absence of substrate, and consequently an overall poor oxygen affinity. In the mutant the affinity for oxygen is lower than that of the wild type with no substrate present. The diatomic ligand binding stabilizing effect detected in the titrations (chapter 3) is not present due to the absence of substrate.

	Oxy-ferrous formation k_{2nd} ($\mu M^{-1} s^{-1}$)	**Oxy-ferrous decay k_{decay} (s^{-1})**
G586S/H_4B	0.10±0.01	-
wt/H_4B	0.46±0.10	>160±13
G586S/aH_4B	0.14±0.01	-
wt/aH_4B	0.47±0.04	8.3±0.9

Table 4.2 Rate constants for the oxy-ferrous formation (left) and decay (right) determined in the absence of substrate and in the presence of either H_4B or aH_4B in the G586S and WT $nNOS_{oxy}$.

It can be inferred then that the stabilizing effect introduced by the serine 586 mutation is exerted through the substrate, rather than through a direct interaction with the bound oxygen; it is also possible that a negative effect on ligand binding in the mutant may be due to the bulkier space occupied by the hydroxyl group pointing to the heme, or the ordering of water molecules in the active-site pocket.

4.3 Wild type $nNOS_{oxy}$ in the presence of substrate and H_4B

When wild type $nNOS_{oxy}$ in its ferrous form was mixed with oxygen-containing buffer in the presence of L-arginine and H_4B, the UV-Vis Soret peak at 410 nm shifted to 429 nm, the characteristic position of the oxyferrous compound spectrum (figure 4.8), as in 63.

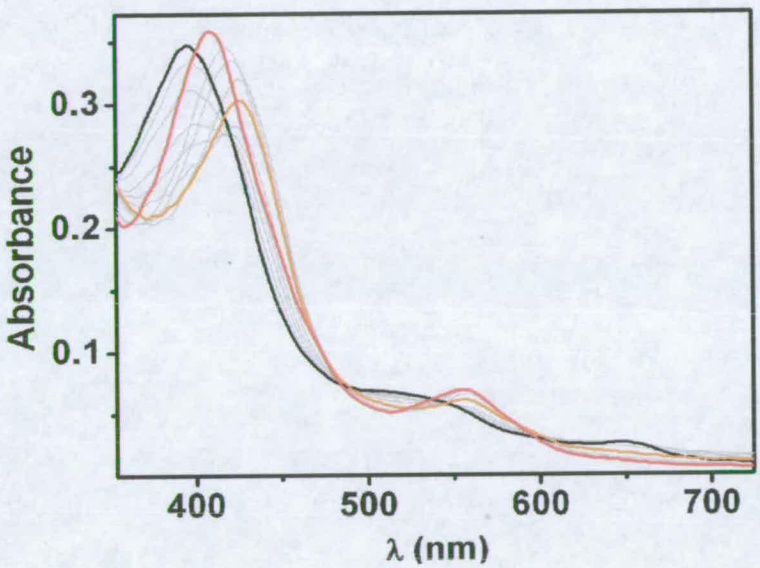

Figure 4.8: Diode array spectra for stopped flow reaction of wild type $nNOS_{oxy}$ with O_2 in the presence of L-arginine and H_4B. Absorbance spectra of the enzyme species are ferrous (red), oxyferrous (orange) and ferric (black).

The Soret peak of the enzyme then shifted to 395 nm, the position of the high spin ferric heme. In order to understand the overall process, the spectral data were analyzed through the global analysis software provided with the stopped flow apparatus. A two-step model corresponding to oxyferrous complex formation and decay was used:

$A \rightarrow B \rightarrow C$

Also, the three accumulating species spectra characterizing the reaction were extrapolated by the software: these were identified to be the starting ferrous enzyme (A),

the oxyferrous species (B) and the eventually formed resting ferric enzyme (C) (figure 4.9).

The overall process was in good accordance with what was observed previously in a study focusing on wild type $nNOS_{oxy}$ (63): the oxyferrous compound is the last species identified during the reaction, before the ferric resting state complexed with the newly formed product, NOHA is observed. Although the global analysis provided the rates for each step, for greater accuracy both formation and decay of the oxyferrous compound were followed at single wavelength: at 419 and 398 nm respectively, it was possible to fit the traces to single exponential functions (figures 4.10 and 4.11). It was also possible,

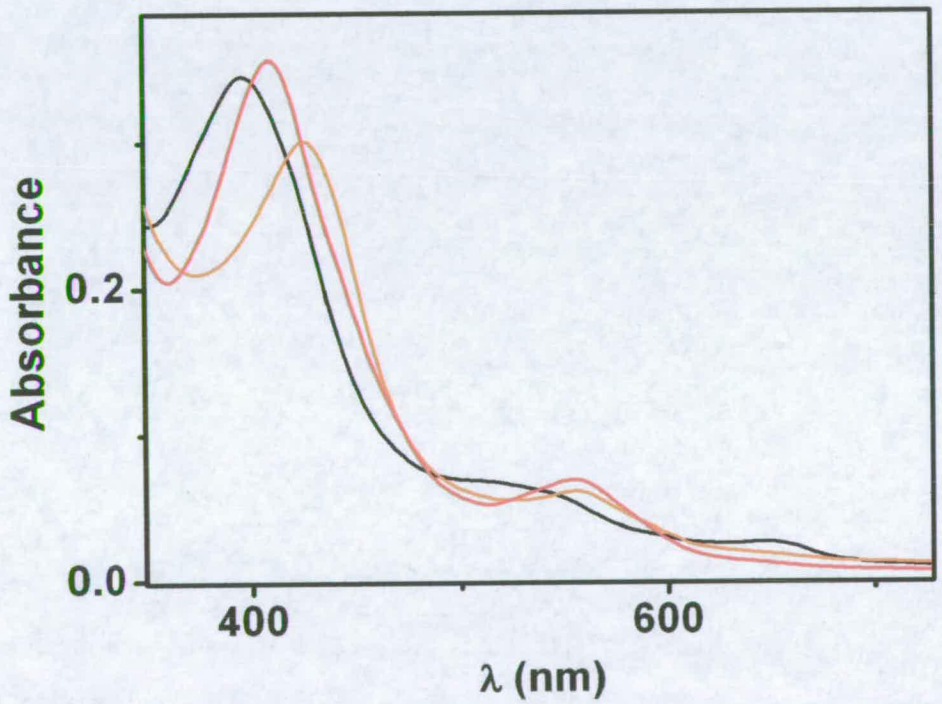

Figure 4.9: UV-Visible spectra of accumulating species determined by global analysis of WT+substrate vs. O_2 data: ferrous enzyme (red), oxyferrous species (orange) and ferric enzyme (black).

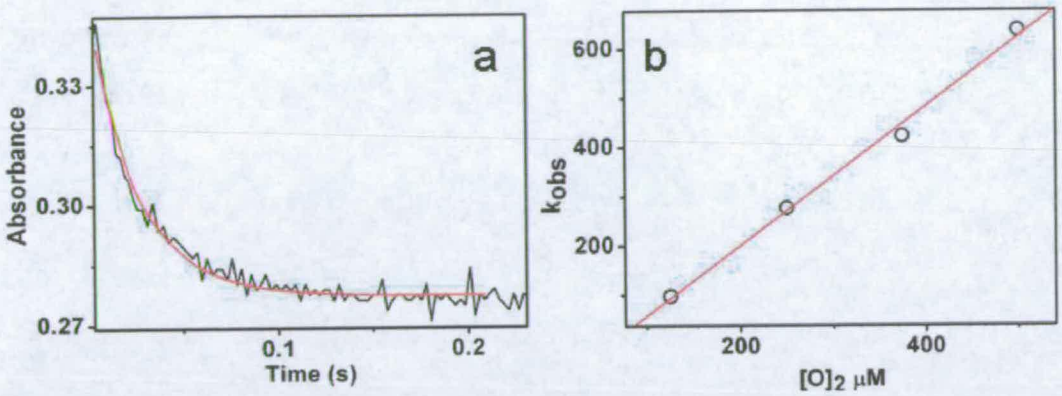

Figure 4.10: Oxyferrous species formation in the wild type enzyme with L-arginine. Traces were followed at 419 nm (a) and k_{obs} plotted against oxygen concentrations to calculate graphically the second order rate constant of oxyferrous formation (b).

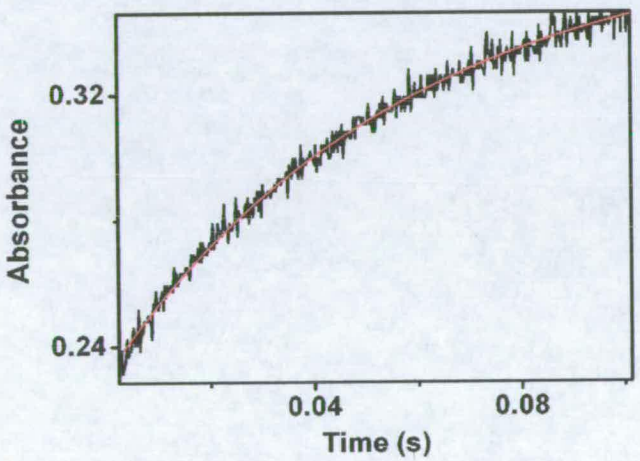

Figure 4.11: Oxyferrous species decay followed at 398 nm.

using the single wavelength spectral change recorded at 390 nm, to fit the trace to a double exponential equation that summarizes the reaction (figure 4.12). The formation of the oxyferrous compound showed a dependence on oxygen concentration: when the k_{obs} were plotted against the oxygen concentration, the second order rate constant was

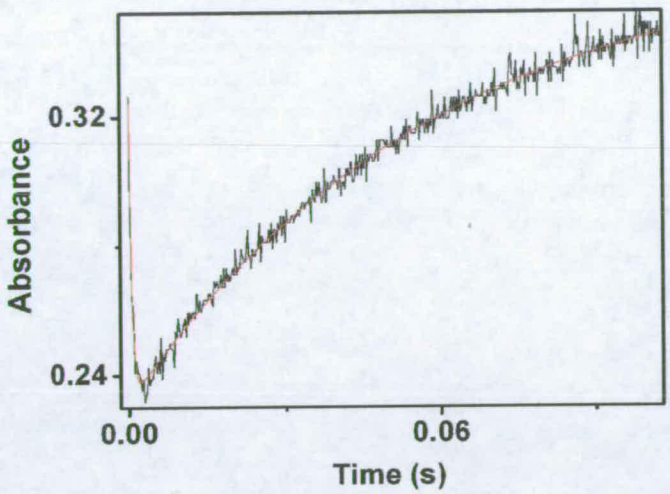

Figure 4.12: Absorbance change at 390 nm during wild type reaction representing both quick oxyferrous formation and slow decay. Fitted to a double exponential equation.

calculated to be 1.1 $\mu M^{-1}s^{-1}$. The decay transition occurred in an oxygen concentration independent manner, with a rate constant of 17 s^{-1}.

Global analysis of the spectral data allowed also the plotting of the timecourse of the overall reaction concerning the concentration of the species (figure 4.13).

When the NOS reaction was triggered by mixing with oxygenated buffer in the presence of NOHA as substrate, the UV-Vis spectrum changed in a similar way. Oxyferrous compound formation was detected by the Soret peak shifting from 410 to 429 nm. Also in this case the formation showed dependence on oxygen concentration, and the second order rate constant for this process was virtually identical to that in the presence of L-Arginine: 1.1 μM^{-1} s^{-1}. The decay of the oxyferrous species was in these conditions somewhat slower, the rate constant being 4.5 s^{-1}. Also in this case the traces recorded at single wavelength were fitted to single exponential functions: hence at least one of the

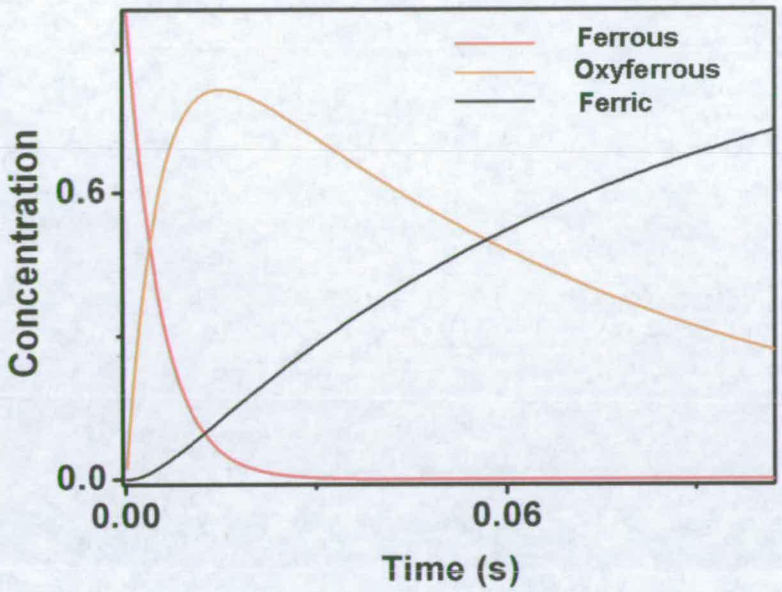

Figure 4.13: Concentration timecourses of the intermediates during the reaction of the wild type $nNOS_{oxy}$ with O_2 in the presence of L-Arg and H_4B. The plot was elaborated by global analysis of raw data shown on figure 4.6.

steps of the unknown part of the reaction slows down the overall process of decay of the oxyferrous species. There is no spectral evidence of NO-bound enzyme or of NO release from the heme: presumably this step is too fast to be observed (62).

4.4 G586S $nNOS_{oxy}$ in the presence of L-arginine and H_4B

When reduced G586S mutant with L-arginine and H_4B bound was mixed with oxygen, formation of the oxyferrous compound was evident by the shift of the Soret peak from 413 to 434 nm (4.14).

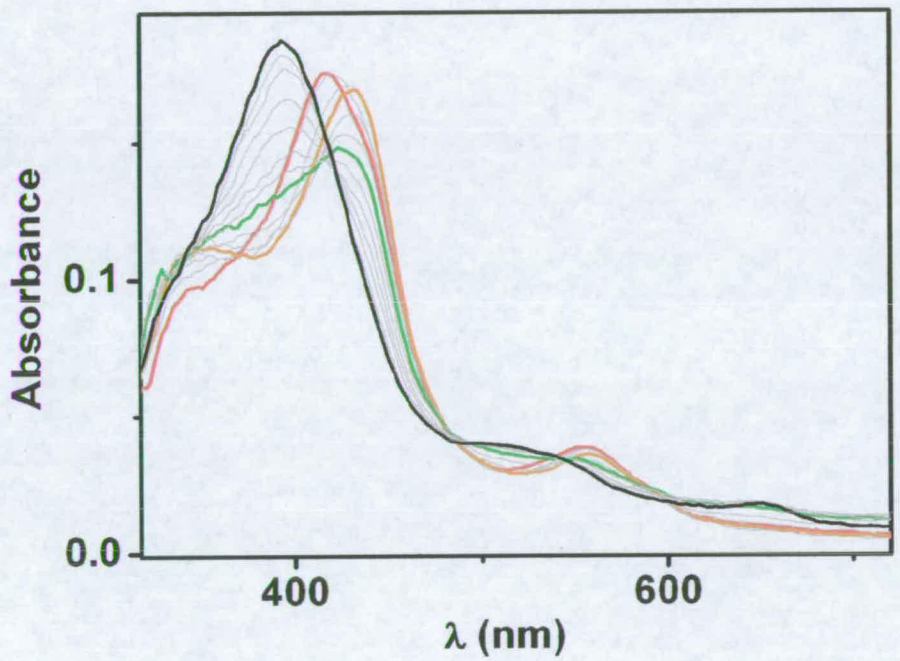

Figure 4.14 : Diode array spectra showing stopped flow reaction of G586S $nNOS_{oxy}$ with O_2 in the presence of L-arginine and H_4B: the ferrous enzyme (red) binds oxygen forming the oxyferrous species (orange), which decays in two phases through accumulation of a new intermediate (green), and to ferric enzyme (black).

Once formed in the mutant, the oxyferrous species faced a different fate compared with the wild type species: the main difference at a first glance was a slower overall decay to ferric form than in the same conditions in the wild type enzyme. Also, a difference in the sequence spectra detected was noticeable. To make sense of the overall reaction, global

analysis was conducted on the spectral data. The two-steps model used for the wild type enzyme did not fit the spectral changes. A three-steps model,

$A \rightarrow B \rightarrow C \rightarrow D$

fitted the process successfully. This elaboration allowed the identification of four spectral species transforming one into the other (figure 4.15): the ferrous enzyme (A), as already said, reacts with oxygen to form the oxyferrous compound (B). The latter then, during the first phase of its decay, forms a species (C) not easily identifiable by its spectrum, the maximum peak at 423 nm being extremely broad and lower. Furthermore on the α–β region there is no sign of the bumps characterizing the ferric heme, nor of

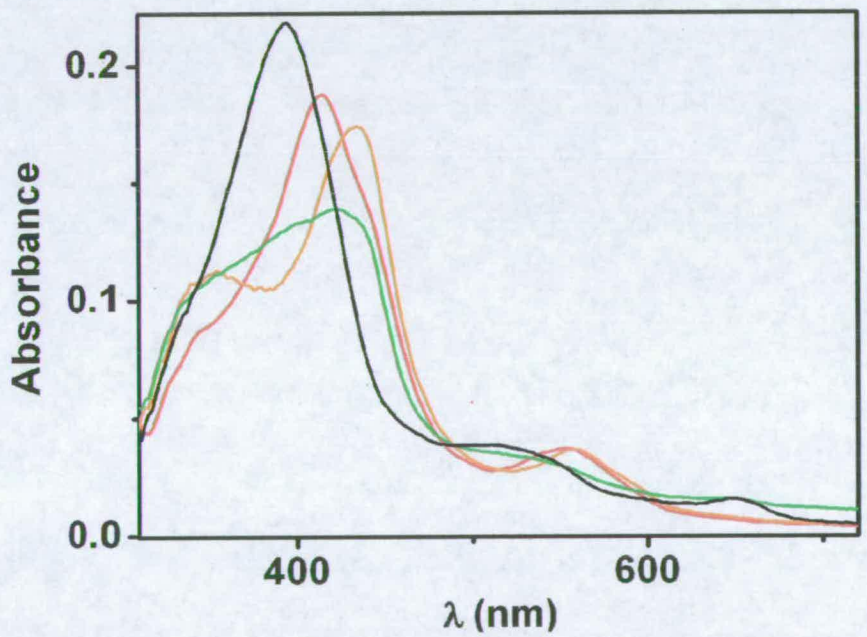

Figure 4.15: Accumulating species sequence elaborated by global analysis in the G586S reaction with L-arginine and H_4B: ferrous enzyme (red), oxyferrous species (orange) new intermediate (green) and ferric enzyme (black).

the bump peculiar of the ferrous state of the enzyme: the signal is somewhat evenly flattened.

The newly detected intermediate decayed then in a second phase to the ferric form in a slow manner. The rates of each step of the process were provided by the fitting of the spectral data to a A→B→C→D model, but for greater accuracy they were determined through single wavelength trace fitting. As with wild type enzyme the oxyferrous formation process showed dependence on the oxygen concentration and its second order rate constant was calculated to be 2.8 $\mu M^{-1} s^{-1}$(fig. 4.16): the mutation of the 586 glycine into a serine caused an increased effect on the rate of oxygen binding to

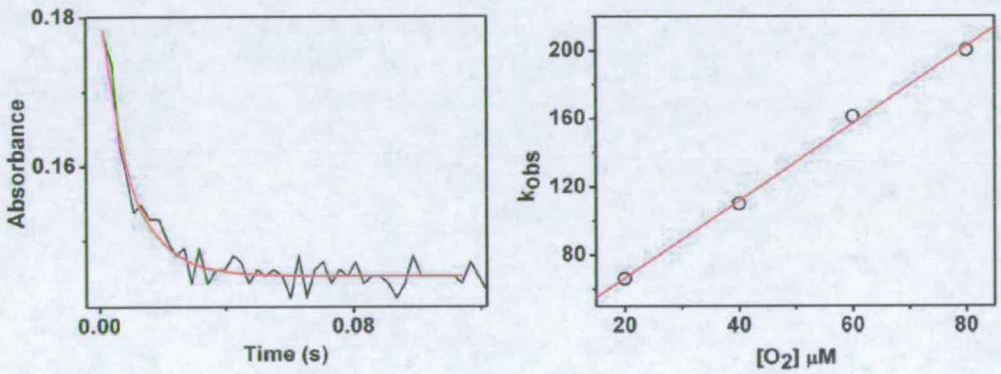

Figure 4.16 : Oxyferrous species formation in the G586S enzyme. Traces were followed at 417 nm (a) and k_{obs}s plotted against oxygen concentrations to calculate graphically the second order rate constant of the oxyferrous formation (b).

the ferrous heme in comparison with the wild type enzyme. The first phase of decay showed no dependence on oxygen concentration and its rate constant was measured to be 16.0 s^{-1} (fig. 4.17). The newly detected intermediate decayed to the ferric form at 1.2 s^{-1} and was also independent of oxygen concentration (fig. 4.18).

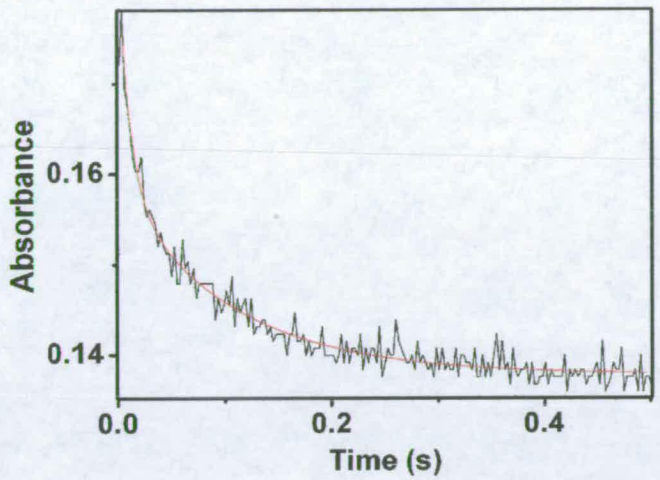

Figure 4.17: Oxyferrous species first phase of decay followed at 427 nm. Fitted to a single exponential equation.

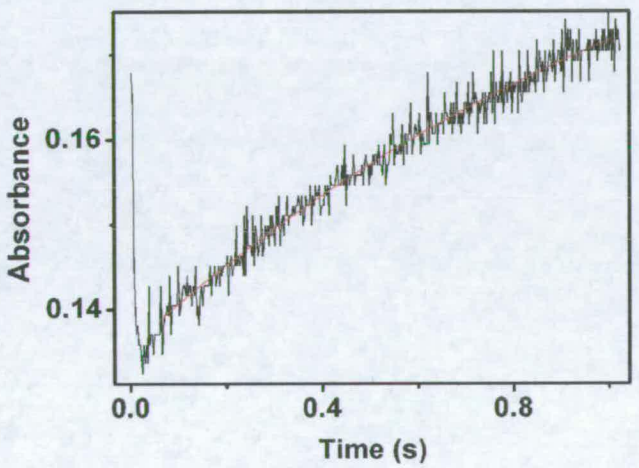

Figure 4.18: Eventual decay to ferric enzyme of the newly stabilized intermediate followed at 408 nm (fitted to a single exponential equation). In the trace is also evident the oxyferrous formation phase.

The normalized concentration timecourse of the intermediates forming during the overall reaction are shown in figure 4.19.

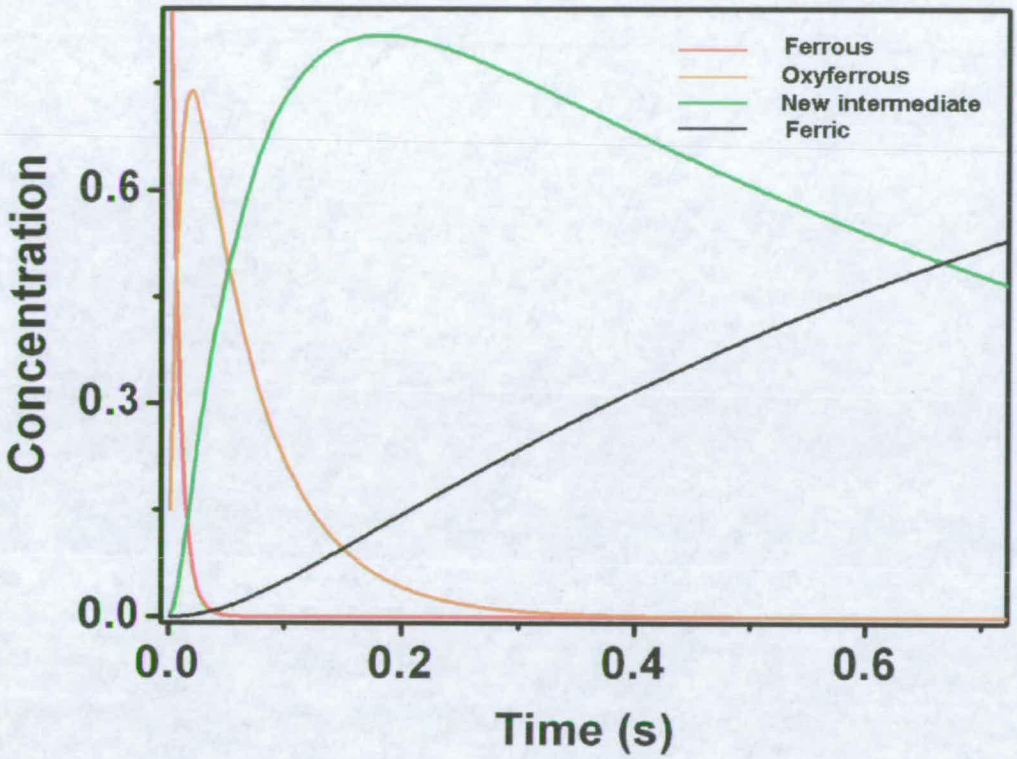

Figure 4.19: Concentration timecourses of the intermediates during the reaction of the G586S mutant with O_2 in the presence of L-Arg and H_4B. The plot was elaborated by global analysis of raw data shown on figure 4.4.

When the mutant complexed with H_4B was provided with NOHA as substrate in place of arginine, the overall pathway of the reaction didn't change. The oxyferrous compound formation had a second order rate constant of 3.1 $\mu M^{-1} s^{-1}$. The first phase of decay rate constant was measured to be 15.0 s^{-1}. The second and final decay to ferric enzyme had a rate of 1.0 s^{-1}.

From the results presented (the rates of the reactions with both enzymes in the presence of substrate are in table 4.3) it is clear that the newly introduced serine influences the reaction in the presence of H_4B and substrate.

	Oxy-ferrous formation k_{2nd} ($\mu M^{-1} s^{-1}$)	Oxy-ferrous decay k_{decay} (s^{-1})	
wt/H_4B/Arginine	1.1±0.1	17±2.0	
G586S/H_4B/Arginine	2.8±0.2	16±2	1.2±0.1
wt/H_4B/NOHA	1.1±0.1	4.9±0.5	
G586S/H_4B/NOHA	3.1±0.2	15±2	1.0±0.1

Table 4.3 Rate constants for the oxy-ferrous formation (left) and decay (right, either in one or two steps) determined in the presence of substrate and in the presence of H_4B in the WT and G586S $nNOS_{oxy}$.

The contribution is likely to be based on a newly formed hydrogen-bond interaction. As shown by the affinity comparisons between the wild type and the G586S mutant (chapter 3) the mutated serine must be directed towards the space where the substrate is located over the heme plane. This will be confirmed by the structure of the G586S mutant in the presence of L-arginine (chapter 6). Particularly, it can be inferred that the interactions modifying the affinity of the substrates and substrate-analogues must involve the guanidinium group of the ligand (or its modified form) and the lateral chain of the serine 586. The interaction of this residue with the heme-substrate-oxygen species occurs during the course of the reaction. A comparison between the catalytic results obtained with both enzymes in the presence and absence of substrate, supports the theory that the new stabilizing interaction in the catalytic site is exerted through a direct interaction between the substrate and the mutated residue.

4.5 Analysis of the nature of the newly stabilized intermediate

Stopped-flow analysis of the G586S mutant complexed with amino-H_4B in the presence of L-arginine is shown in figures 4.20 and 4.21. The reaction follows a pattern similar to amino-H_4B bound wild type $nNOS_{oxy}$ in the same conditions (63): it shows a first step of oxyferrous formation which is oxygen-concentration dependent and characterized by a second order rate constant of 1.4 $\mu M^{-1}s^{-1}$. The decay to the ferric heme occurs via a single step in an oxygen-independent manner, but is much slower than that occurring in the H_4B and arginine bound enzyme, at 0.2 s^{-1}. In the same conditions, the wild-type enzyme's oxyferrous formation is characterized by a second order rate constant of 1.2 $\mu M^{-1}s^{-1}$ which doesn't differ significantly from that of the mutant; the decay

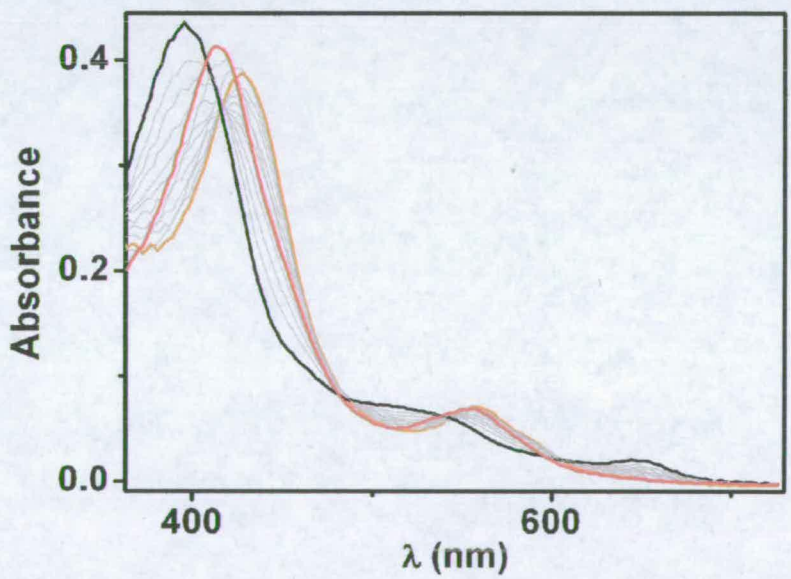

Figure 4.20: Stopped flow reaction of G586S $nNOS_{oxy}$ with O_2 in the presence of L-arginine and amino-H_4B: the enzyme species are ferrous (red), oxyferrous (orange) and ferric (black).

transition also occurs in a single slow step with a first order rate constant of 0.06 s^{-1}, i.e. slightly slower than that of the mutant.

The fact that the new intermediate is not detected when substrate-bound G586S $nNOS_{oxy}$ reacts in the presence of amino-H_4B, points to how its formation relies on the second electron being donated to the oxy-ferrous compound (from H_4B).

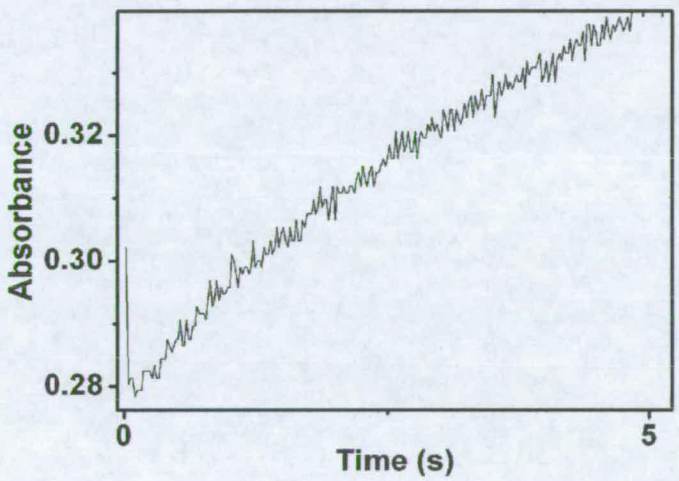

Figure 4.21: Absorbance change trace at 398 nm during G586S $nNOS_{oxy}$ reaction in the presence of L-arginine and amino-H_4B. The fast formation and slow decay processes are evident.

Thus the newly stabilized intermediate is possibly a species involved normally in the catalytic cycle and must be an intermediate formed after the oxyferrous complex. In the attempt to define the identity of the new intermediate, similar features in the spectra of reaction intermediates of heme proteins which perform oxygenase reactions were researched. Similarities were found with the spectrum of the second intermediate

deriving from the reaction of low spin ferric P450cam with m-chloroperbenzoic acid (112). Characteristics of this species include the presence of a broad Soret band at 370 nm and a weak band at 695 nm. *Egawa et al.* achieved a clean spectrum of chloroperoxidase Compound I through mathematical elaboration, which was previously isolated and recognized in the peroxidase reaction. Successive studies confirmed the identity of this spectrum (113, 114) (figure 4.22). Although the intermediate identified in the reaction performed by

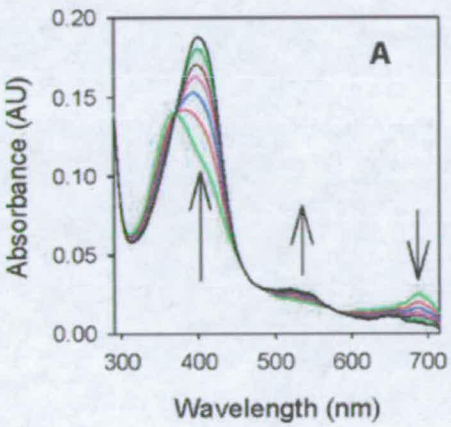

Figure 4.22: Time-resolved UV-vis spectrum for reaction of chloroperoxidase Compound I (lower green spectrum) with the substrate (styrene) (113).

the glycine 586 mutant is not identical, there are some features that suggest that it could represent a mixture of the oxyferryl compound and other transients: first, there is a lowering and broadening of the peak during the step that leads from the oxyferrous compound to this new transient; second, the big shoulder at around 370 nm is evidence of the strong presence of a species with an absorption peak at that wavelength; third, during this step some flattening in the α/β region occurs, which tells us about the

presence of a species which is neither ferrous nor ferric. The characteristic small peak of compound I at around 695 nm is also in evidence by an increase in absorbance in this region.

Chapter 5

ELECTROCHEMISTRY

5 ELECTROCHEMISTRY

5.1 $nNOS_{oxy}$ G586S reduction potentials

In order to assess whether the mutation affects the reduction potential of the G586S mutant, potentiometric titrations were conducted in the presence and absence of the substrate. The ferric enzyme kept in its dimeric form by the presence of H_4B, was reduced and then oxidised stepwise in an anaerobic OTTLE cell by modulating the potential of the working electrode; after each potential change the enzyme solution was allowed to equilibrate and the UV-Visible absorption spectrum was recorded. At each applied potential, positions of the Soret peak shifting from those of the ferric and ferrous states (figure 5.1) were interpreted as the statistical distribution of the enzyme into the two reduction states.

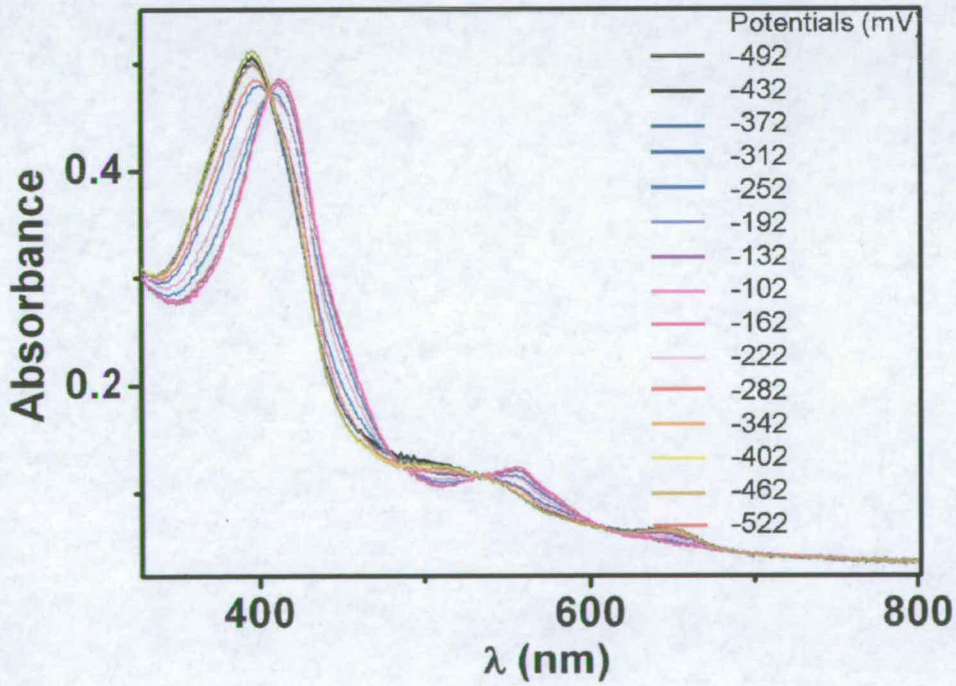

Figure 5.1: Spectra of the G586S enzyme in the presence of L-arginine shifting between a fully oxidised and a fully reduced population upon applied electric potentials.

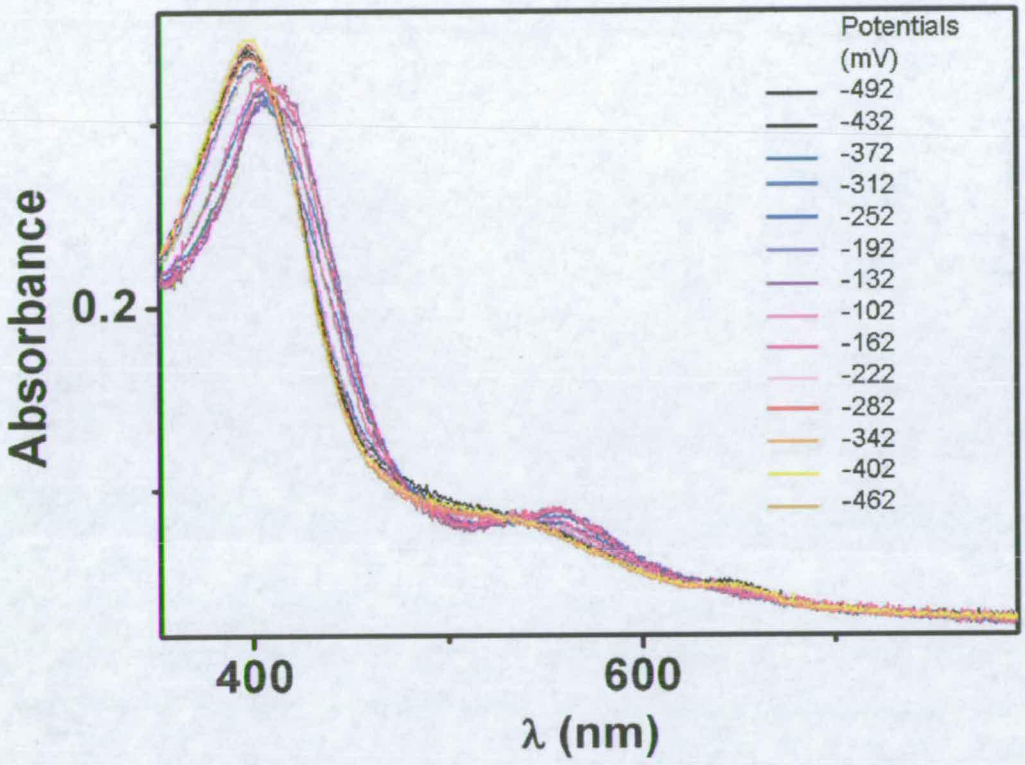

Figure 5.2: Spectra of the G586S enzyme in the absence of L-arginine shifting between a fully oxidised and a fully reduced population upon applied electric potentials.

The absorbance change (figure 5.2), after being normalized was then plotted against the applied potential and the curve fitted to the Nernst equation,

$$E = E^0 - \frac{59.1\ \mathrm{mV}}{z} \log_{10} \frac{a_{\mathrm{Red}}}{a_{\mathrm{Ox}}}$$

The plots are showed in figure 5.3: the value of the applied potential at the midpoint, accounting for the enzyme being half ferric and half ferrous, is the heme reduction potential.

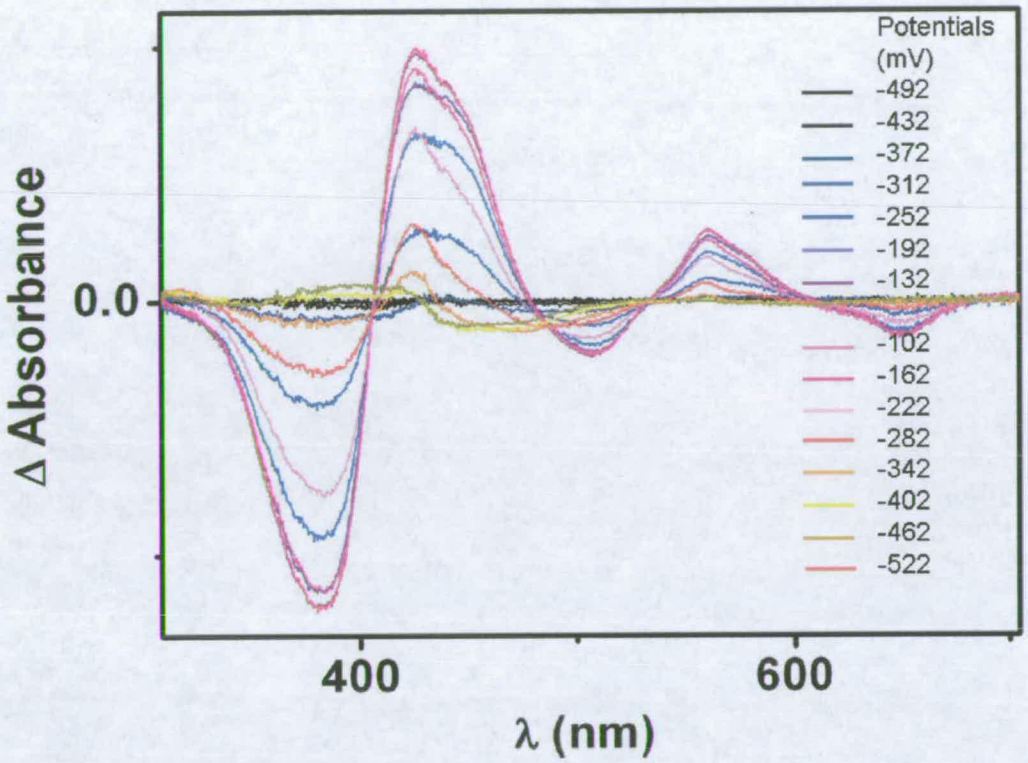

Figure 5.3: Series of difference spectra corresponding to each applied potential in the presence of L-arginine-complexed enzyme.

During the determination of the heme potential of substrate-free NOS_{oxy}, hysteresis was observed, in that the curves obtained going from ferric to ferrous states and back don't overlap exactly. More precisely a portion of the enzyme retains its reduction state regardless of the change in the electric field applied: consequently the distribution of the enzyme population into the two different oxidation states doesn't rely exclusively on the absolute value of the electric field applied, but on the direction of the changes as well. This effect may be connected with the lack of structural stability caused by the absence of L-arginine in the catalytic site. Nevertheless a Nernst equation fitting was obtained for the substrate bound mutant (table 5.1).

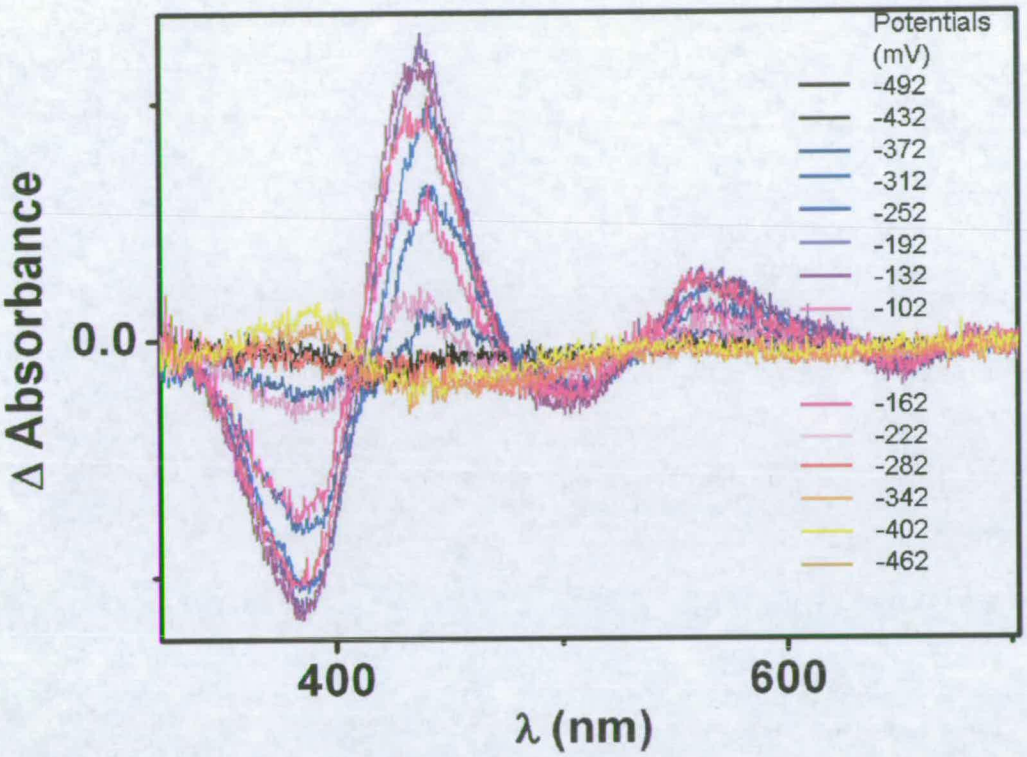

Figure 5.4: Series of difference spectra corresponding to each applied potential in the presence of L-arginine-free enzyme.

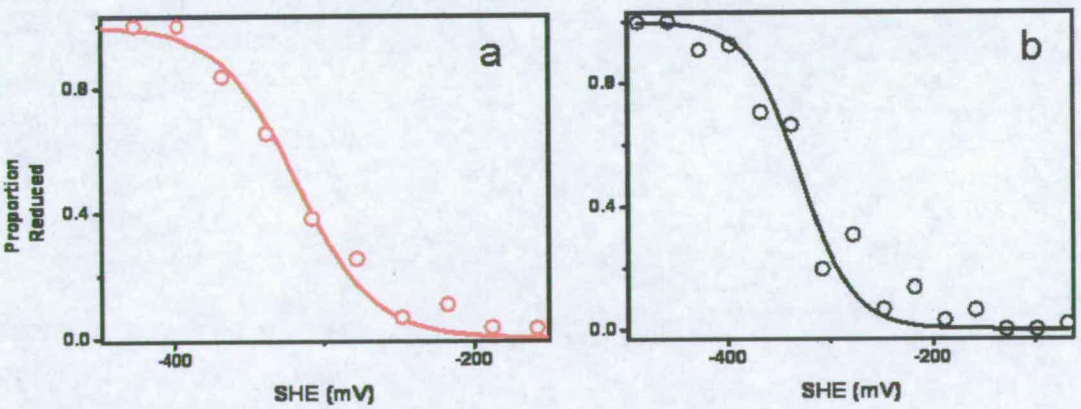

Figure 5.5: Nernst curves for the potentiometric titration of the G586S enzyme in the presence (a) and in the absence (b) of L-arginine.

In the first step of the P450 reaction, the binding of substrate commonly displaces a loosely bound molecule of water acting as the sixth iron ligand (52, 88, 89).

	No substrate	L-Arg
G586S (mV)	-329±8	-318±4
wt (mV)	-316±5 (63)	-306±4 (63)

Table 5.1: $nNOS_{oxy}$ wild type and G586S reduction potentials in the presence and absence of L-Arginine.

This has a destabilizing effect on the ferric form of the enzyme. Substrate binding has been measured to cause a heme reduction potential shift of about +100mV (i.e. P450 BM3) (117), directing the enzyme into a state where the first electron transfer that triggers the entire reaction is considerably more favourable. This mechanism helps to prevent uncoupled hydride consumption in the substrate-free enzyme. The heme reduction-potential shift induced by substrate binding in wild type $nNOS_{oxy}$ doesn't result in a similar uncoupling-preventing mechanism (63): the preferential binding of L-arginine to the ferrous form of nNOS has been causes a potential shift of about 10 mV. This is a relatively small difference.

The midpotential measured for the G586S $nNOS_{oxy}$ mutant in the absence of any substrate is -329 mV, while the potential measured in the presence of L-arginine is -318 mV. The positive 11 mV shift in the heme potential is due to the preferential binding of the substrate to the reduced form of the enzyme. Although the corresponding midpotential values of the G586S NOS_{oxy} are some 10 mV more negative than those of the wild type, the potential shift determined in the latter by the presence of L-arginine (10 mV) is virtually the same (63). This is consistent with the G586S mutant enzyme retaining the heme native electrical properties.

Chapter 6

CRYSTALLOGRAPHIC STUDIES ON RAT G586S $nNOS_{oxy}$

6 CRYSTALLOGRAPHIC STUDIES ON RAT G586S $nNOS_{oxy}$ (in collaboration with Chiara Bruckmann)

In order to interpret the spectroscopic, catalytic and electrochemical studies of G586S $nNOS_{oxy}$ in terms of structural information, the enzyme was crystallised in the presence of L-arginine and H_4B. Its structure was determined using X-ray crystallography by C. Bruckmann.

6.1 Purification

The G586S mutant of $nNOS_{oxy}$ was successively expressed and purified as previously described (63). In order to obtain a purer enzyme, necessary for crystallographic studies, the purification protocol followed previously was modified according to that followed by *Li et al.* (109).

Cell homogenate containing over expressed $nNOS_{oxy}$ G586S mutant was loaded into a HisTrap HP column (GE Healthcare), previously equilibrated with 50 mM sodium phosphate buffer at pH 7.8 containing 10% glycerol, 1 mM dithiothreitol (DTT), 20 μM H_4B, 0.1 mM L-arginine, 0.3 M NaCl, and 20 mM imidazole (equilibration buffer). After a thorough washing step with equilibration buffer (5 column volumes) the protein was eluted from the HisTrap HP column using a 100-150 mM imidazole step gradient (figure 6.1) generated mixing volumes of two equilibration buffer batches, one of which containing a higher imidazole concentration (500mM).

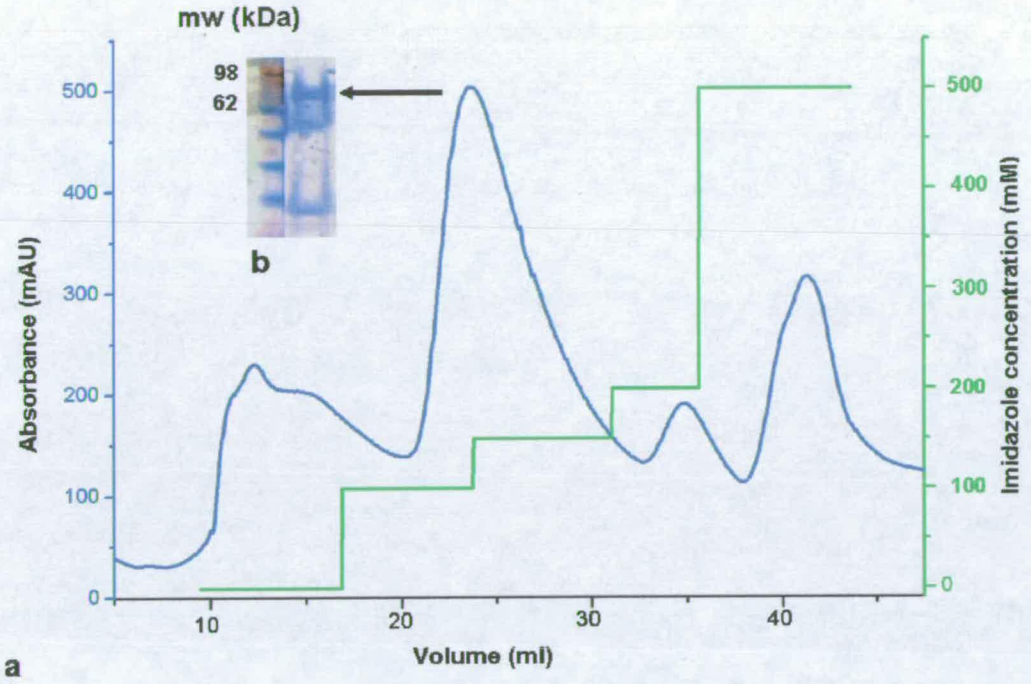

Figure 6.1: Abs_{280} trace (blue) from HisTrap HP purification and elution gradient trace (green) (a). The corresponding fractions of the peak were analysed by SDS-PAGE (b).

The colored elution peak fractions were pooled together and dialyzed overnight at 4°C against buffer 1 (HEPES 50 mM pH 7.5, 10% glycerol, 1 mM DTT, 20 μM H_4B, 0.1 mM L-Arg and 0.25 mM PMSF).

Post-dialysis fractions from HisTrap HP were loaded onto a buffer 1 pre-equilibrated (5 column volumes) HITrapQ FF anion-exchange column. The column was then washed with 2 column volumes of buffer 1 containing 100 mM NaCl. The protein was eventually eluted with a 100– 300 mM NaCl gradient using 10 column volumes (figure 6.2).

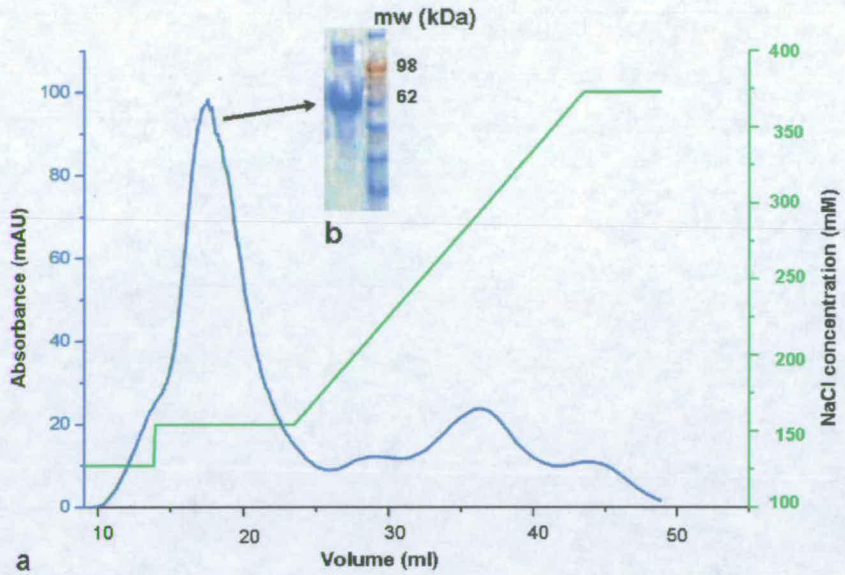

Figure 6.2: The elution profile from ion exchange chromatography using a HITrapQ FF column (a). Abs_{280} trace is represented in blue and elution gradient trace in green. The target enzyme peak can be seen on the elution profile and the corresponding fractions were analysed by SDS-PAGE (b)

Neuronal NOS_{oxy} has an N-terminal PDZ domain, which is a portion essential for the interaction with other proteins (mainly for localization): this is composed of a 6-stranded anti-parallel β-barrel and 2 α-helices (11) (figure 6.3a). Due to its high mobility the PDZ-domain hinders the crystallization of the protein and no structure of nNOS PDZ-domain including sequence has been solved so far. The cleavage of the mobile domain was achieved by a limited trypsin digestion of the protein collected after the Q-Trap column step.

The reaction was carried out by incubating the protein solution on ice overnight with a nNOS:trypsin (weight) ratio of 100:1 under continuous mild stirring.

The results of partial trypsin proteolysis were analyzed by SDS-PAGE and if necessary the digestion was continued. Undigested enzyme was used as a control (figure 6.3b): the successful cleavage was detected by molecular weights

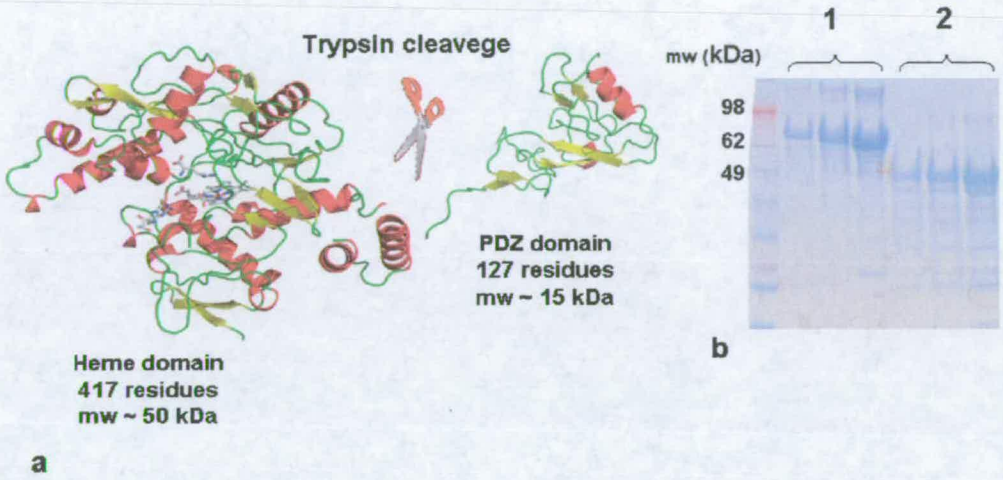

Figure 6.3: a) Illustration of the trypsin digestion of $nNOS_{oxy}$, where the PDZ domain is cleaved from the heme domain. b) SDS-PAGE comparative analysis of the trypsin digestion product (2) with the undigested protein (1).

comparison between the digested and undigested enzyme, considering that the PDZ domain has a mass of 15 kDa.

In order to remove undigested enzyme, the trypsin-treated NOS_{oxy} solution was further purified through a Superdex 200 column equilibrated with 50 mM TrisHCl, pH 7.8, containing 10% glycerol, 10 mM DTT, 20 μM H_4B, 0.1 mM L-Arg, and 200 mM NaCl (figure 6.4). The protein eluted at a volume corresponding to ~ 50 kDa molecular weight.

Protein concentration was determined spectrophotometrically exploiting the absorbance difference between the ferrous and the ferrous CO-bound forms (extinction coefficient $\Delta\varepsilon_{444\text{-}467} = 55,000\ M^{-1}cm^{-1}$) (118).

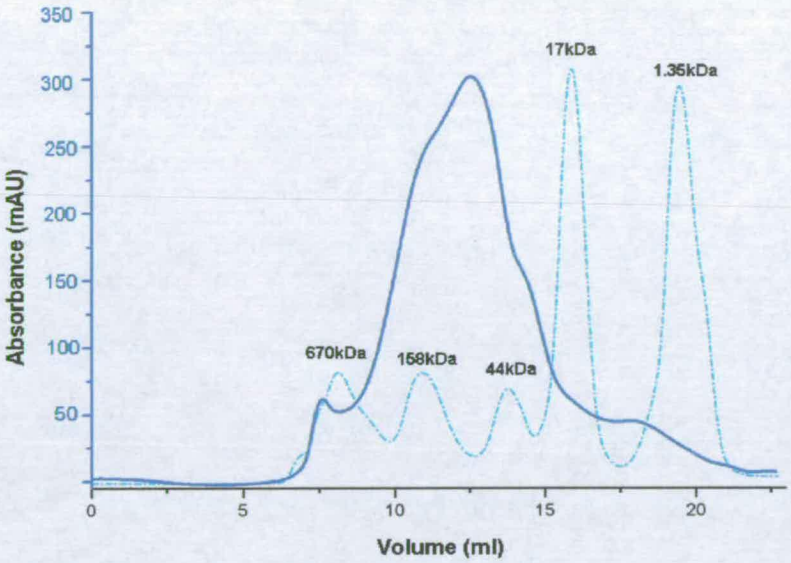

Figure 6.4: The elution profile from gel-filtration chromatography using a Superdex-200 10/30 column for $nNOS_{oxy}$ G586S mutant (blue) overlaid with the elution profile of the molecular weight markers (cyan).

6.2 Crystallization (by D.Papale and C. Bruckmann)

Crystals of the G586S mutant of nNOS heme domain were produced by the hanging-drop or sitting-drop vapour diffusion methods at 18°C, by mixing 2 µl of 7-9 mg/ml protein (in 50 mM TrisHCl, pH 7.8, 10% glycerol, 10 mM DTT, 20 µM H_4B, 0.1 mM L-Arg, and 200 mM NaCl) with 2 µl of reservoir solution (0.1 M pH 5.8/6.0 MES, 22-24% PEG 3350, 0.2 M ammonium acetate, 25 mM L-Arg, 35 µM sodium dodecyl sulfate (SDS), 5 mM glutathione (GSH), 2% isopropanol).

Small crystals appear after 24 h (rod shape) and reached maximum size in 1 week (figure 6.5).

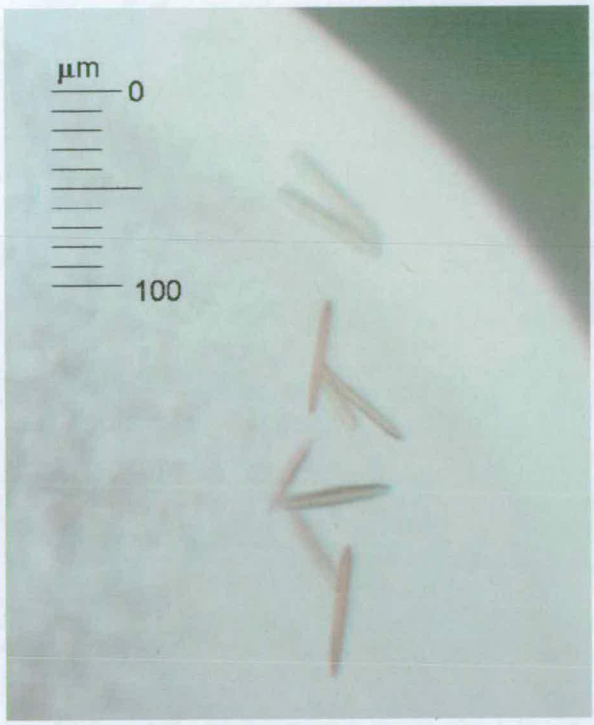

Figure 6.5: Crystals of G586S $nNOS_{oxy}$ grown in a 4 µl volume sitting drop

6.3 Freezing procedure (by C. Bruckmann)

Crystals of G586S $nNOS_{oxy}$ were washed with reservoir solution and then exposed to increasing amounts of cryoprotectant in a step-wise fashion. The final cryoprotectant solution consisted of 25% (w/v) PEG 3350, 0.1 M MES, pH 5.8/6.0, 0.1 M ammonium acetate, 10% (v/v) glycerol, 10% (w/v) trehalose, 5% (w/v) sucrose, 5% (w/v) mannitol and 1 mM L-Arg (119). Crystals were flash-cooled in liquid propane.

6.4 Data collection (by C. Bruckmann)

The best dataset was collected to 2.59 Å resolution at 100 K at the ERSF (Grenoble, France) on beam line BM14 (wavelength $\lambda = 0.9737$ Å) using a Mar Research CCD detector.

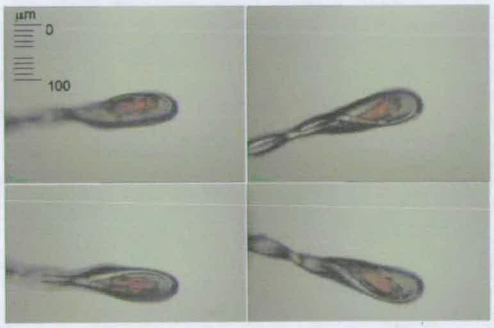

a

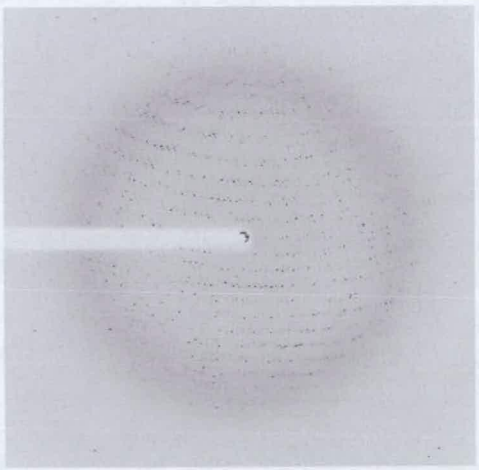

b

Figure 6.6: a) Crystal snapshots on beam line BM14, ESRF. b) Diffraction pattern of NOS G586S mutant crystal. Oscillation range 1.0°, Exposure time 30.0 s; detector distance 269.4 mm; resolution at corner 2.5 Å; resolution at edge 3.54 Å.

The crystals were found to belong to space group $P2_12_12_1$ with cell dimensions a = 51.9630 b = 110.8470 c = 164.6270 $\alpha=\beta=\gamma=$ 90.

Data processing was carried out using MOSFLM (120) and SCALA (121). The structure was solved by molecular replacement using PHASER (122) and the wild-type $nNOS_{oxy}$ structure (PDB entry 1OM4), stripped of water, was used as a starting model. Electron density fitting was carried out using the programs TURBO-FRODO (123) and COOT (124) and structure refinement was carried out using PHENIX (125).

6.5 The crystal structure of G586S nNOS (by C. Bruckmann)

The dataset corresponding to the structure of G586S $nNOS_{oxy}$ was refined to a final R-factor of 19.8% (R_{free} = 25.3 %; table 6.1) achieving a maximum resolution of 2.59 Å.

The refined model is composed of two protein molecules each including residues from 299 to 716 and one b-type heme. Each subunit contains also one H_4B molecule bound in its binding pocket (figure 6.7) and one L-arginine molecule bound in the active site.

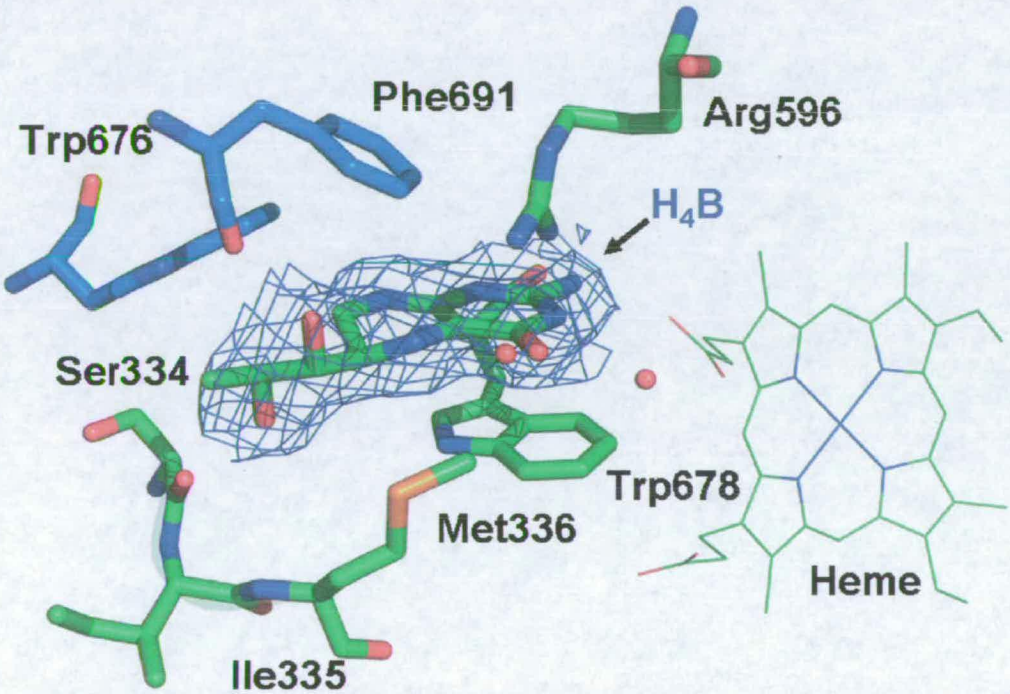

Figure 6.7: the $2F_0 - F_c$ electron density map around the H_4B. The map is contoured at 1 σ. In this figure are also shown some relevant residues binding the cofactor. Residues in green belong to the same monomer, while residues in blue belong to the other monomer of the dimer.

Protein	nNOSoxy (G586S)
Ligand	L-Arg
PDB entry	T.B.A.
Space group	$P2_12_12_1$
cell dimensions	$a = 51.9630$ $b = 110.8470$ $c =$
resolution (Å)	35.00-2.60 (2.69-2.60)*
total no. of reflections	408362
no. of unique reflections	27819
completeness (%)	92.7 (70.8)*
$I/[\sigma(I)]$	13.9 (2.7)*
R_{merge} (%)[a]	10.0 (24.0)*
R_{work} (%)[b]	19.87
R_{free} (%)[c]	25.39
rmsd from ideal values	
bond lengths (Å)	0.006
bond angles (deg)	1.047
Ramachandran analysis	
most favoured (%)	88.0
additionally allowed (%)	11.6
no. of waters included in refinement	196

Table 6.1: Data collection and refinement statistics * Values in parentheses represent statistics for the highest resolution shell [a] $R_{merge} = \Sigma_h\Sigma_i|I(h) - I_I(h)|/ \Sigma_h\Sigma_iI_I(h)$, where $I_I(h)$ and $I(h)$ are the ith and mean measurement of reflection h, respectively. [b] $R_{work} = \Sigma_h|F_o - F_c|/ \Sigma_hF_o$, where F_o and F_c are the observed and calculated structure factor amplitudes of reflection h, respectively. [c] R_{free} is the test reflection data set, 5 % selected randomly for cross validation during crystallographic refinement.

The electron density around residue 586 (figure 6.8), different from that in the wild type enzyme, confirms the presence of the amino acid substitution (G586S).

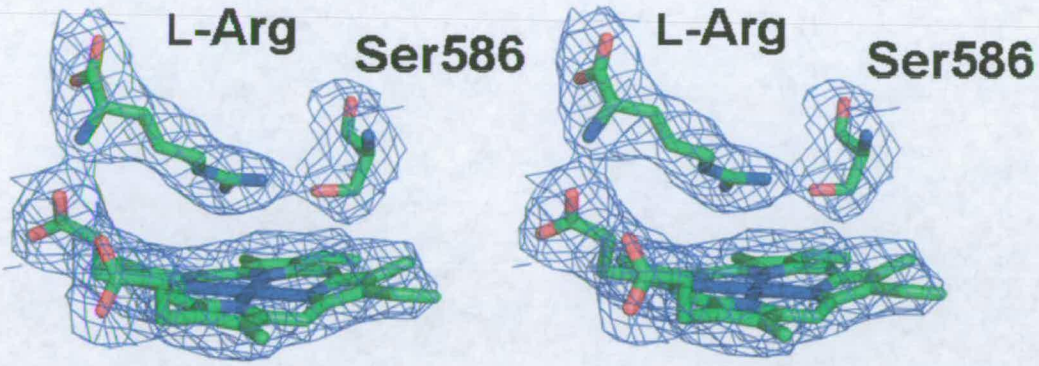

Figure 6.8: Stereoview of electron density around the heme, serine 586, and L-Arg at the active site of G586S nNOS (monomer A). The electron density map was calculated using Fourier coefficients 2 $F_o - F_c$, where F_o and F_c are the observed and calculated structure factors, respectively, the latter based on the final model. The contour level is 1.0 σ, where σ is the rms electron density

As evidenced in the overlay of the monomer of G586S mutant with the wild-type (figure 6.9) the residue substitution in the active site does not have a significant effect on the overall structure of the protein. This is confirmed by the rms parameter (root-mean-square) which indicates the deviation between the α-carbon backbone of each monomer of either G586S and wild type $nNOS_{oxy}$ (PDB code 1OM4): this is only 0.3 Å.

As shown in figure 6.14, L-arginine maintains the same interactions with the G586S enzyme that it has with the wild-type enzyme. However, the distance between the guanidinium nitrogen of L-arginine and the side chain oxygen of the 586 serine is 2.9 Å, consistent with the formation of a hydrogen bond.

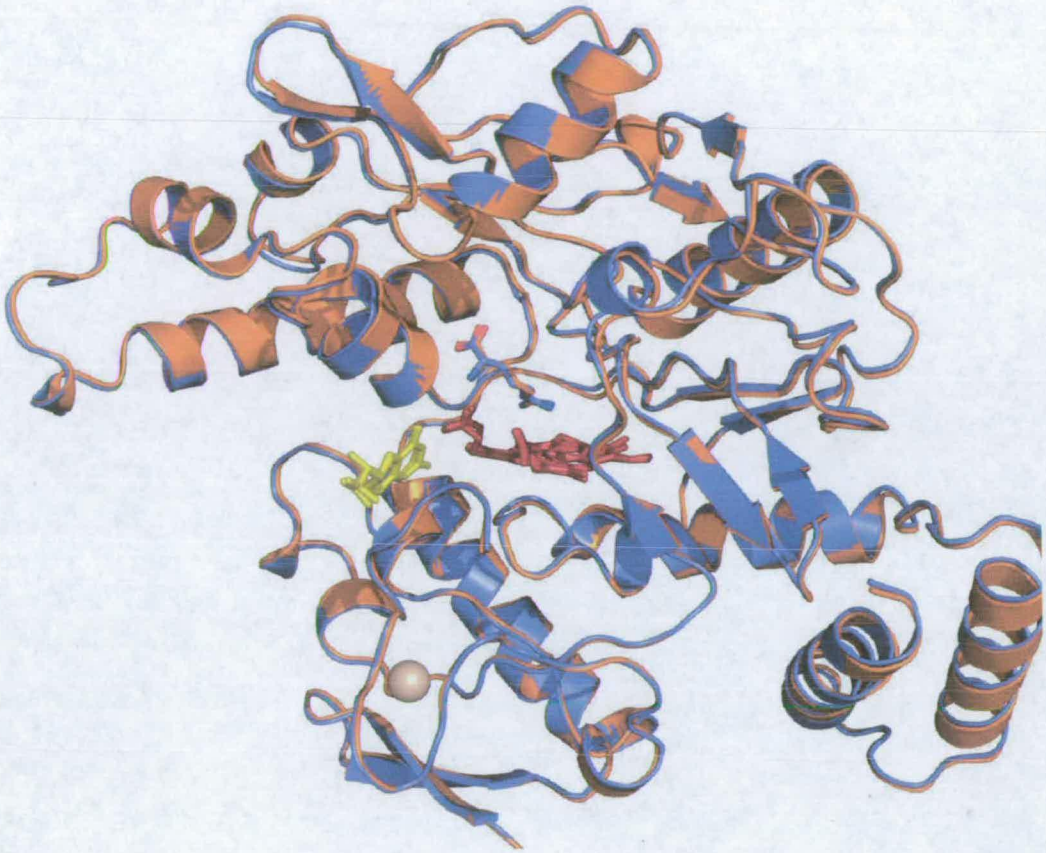

Figure 6.9: Overlay of $nNOS_{oxy}$ wild-type (orange, PDB entry 1OM4) and G586S mutant (blue). The hemes and the H_4B are represented as sticks and coloured respectively dark red and yellow. The Zn atom at the dimer interface is represented as a sphere. The substrates bound at the active site are coloured according to the chain colour.

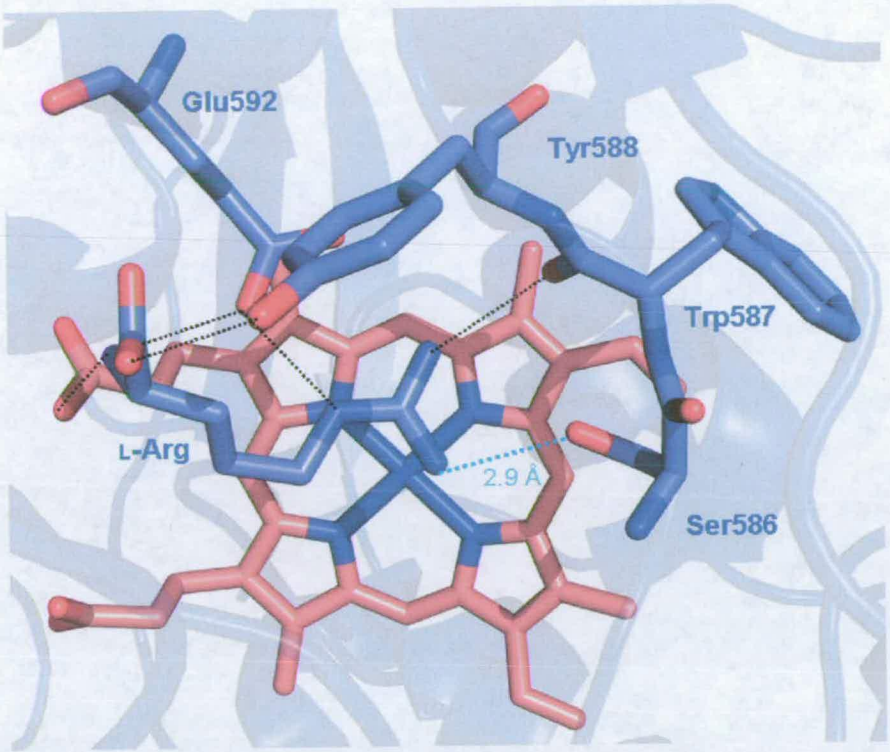

Figure 6.10 The active site of the $nNOS_{oxy}$ G586S mutant, showing some of the interactions between the bound L-Arg and the active site residues, that are the same as observed in the wild-type enzyme structure. The new hydrogen bond between L-Arg and Ser586 is represented in cyan as a dotted line.

As discussed in chapter 3, the affinities of NOS_{oxy} wild-type for L-arginine and NOHA are very similar (table 3.1), while the G586S mutant displays increased affinities for both substrates. The stabilizing effect in the G586S enzyme for L-Arg is a factor of 10 greater then in wild-type, while the affinity for NOHA is only doubled in the G586S enzyme.

As said, this comparison suggests a new capability for L-arginine of forming a supplementary hydrogen bond induced by the presence of Ser586. The same hydrogen-bond is likely to be formed in the presence of NOHA, which on the other hand, has a slightly greater volume due to the additional hydroxyl group: this can clash with the oxygen of Ser586 and may negatively affect its binding in the catalytic site.

A model of the active site, built by overlaying NOHA with the L-Arg in the crystal structure, can help to visualize and explain substrate specificities and affinities (figure 6.11).

Such a model has been built only for illustrative purposes, and is obviously not taking into account the residue motion that can occur upon NOHA binding. The crystal structure of $nNOS_{oxy}$ G586S in complex with NOHA would certainly provide more information on the NOHA binding affinity.

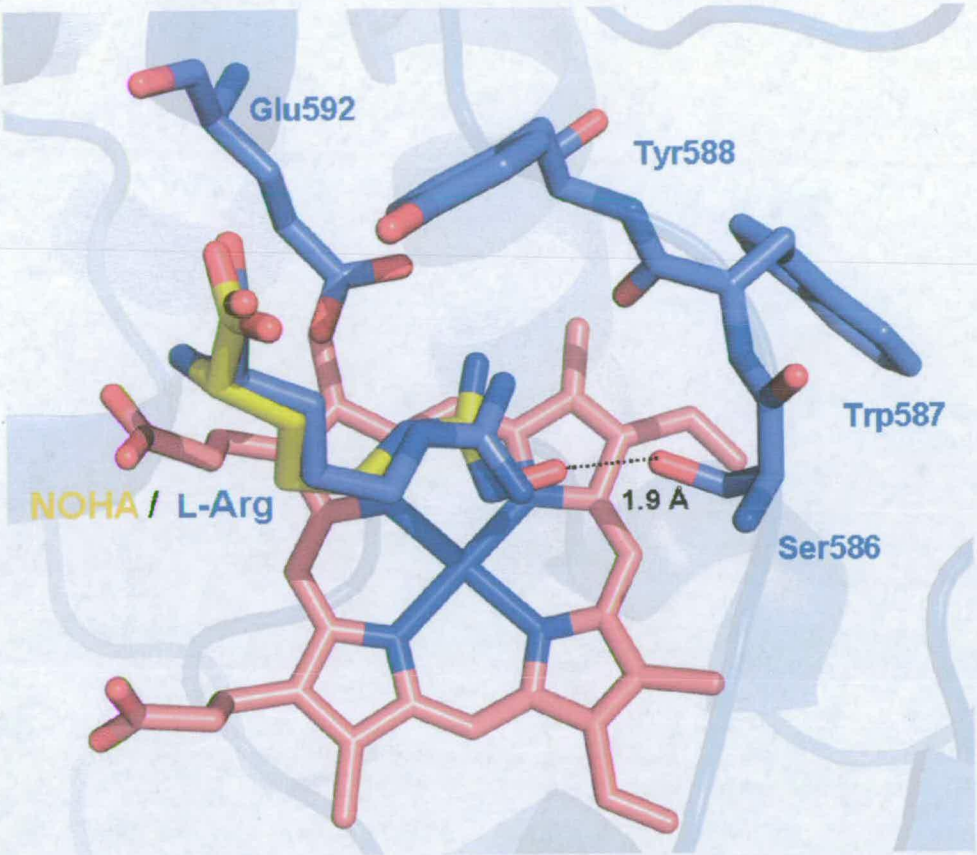

Figure 6.11 Model of $nNOS_{oxy}$ in complex with NOHA created by placing the NOHA over the bound L-Arg. It is possible to observe that in this model the additional hydroxyl group of NOHA clashes with the oxygen of Ser586

The binding orientation of L-arginine in the active site of the G586S mutant enzyme is very similar to that observed in the wild-type $nNOS_{oxy}$. In the mutant it is noticeable that a slight bending of the guanidinium group plane such that the nitrogen is hanging directly over the heme-iron and is closer to the metal. Figures 6.12 and 6.13 show the active sites of the wild-type and the G586S mutant structures with L-arginine.

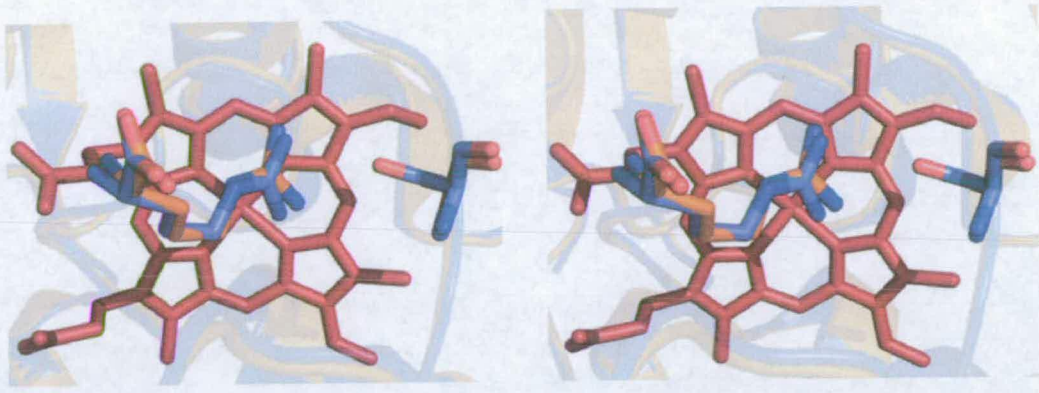

Figure 6.12 Stereoview of an overlay of the active site region of wild-type nNOS (orange) and G586S mutant (blue) viewed from the top. L-Arg from the G586S enzyme (in blue) and L-Arg from the wild-type display the same position in the active site.

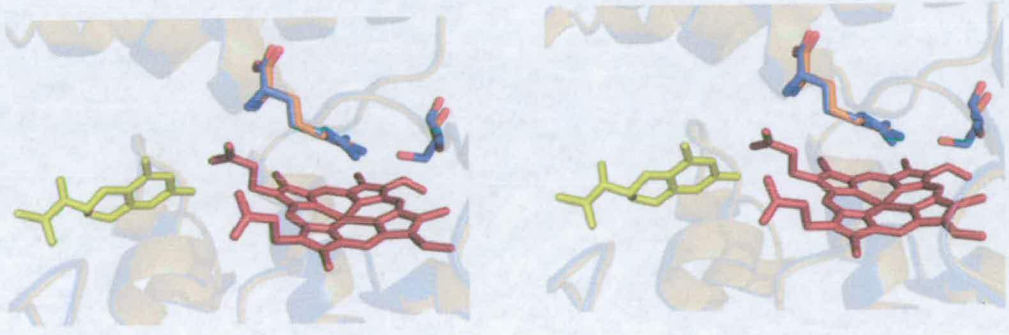

Figure 6.13 Stereoview of an overlay of the active site region of wild-type nNOS (orange) and G586S nNOS (blue) viewed from the side.

As already discussed during the kinetic characterization of the $nNOS_{oxy}$ G586S mutant, the accumulation of a novel reaction intermediate has been observed in the presence of H_4B and substrate, subsequent to oxyferrous species formation. This could be due to a stabilizing effect introduced with the G586S mutation. In particular, as this effect has been observed only in the presence of substrate, it is

possible that it is due to an interaction between the oxy-heme species and substrate determined by a different position assumed by the latter. Also, it has been proposed that the newly formed interaction with the intermediate observed after the oxyferrous compound formation could have the nature of a hydrogen-bond. The shorter distance between the guanidinium-nitrogen and the heme-iron observed in the structure (figure 6.13) support this hypothesis.

Chapter 7

CONCLUSIONS

7 CONCLUSIONS

Nitric Oxide Synthases are important as a consequence of the fact that they produce the key signalling molecule Nitric oxide: this eclectic factor plays a role in a variety of physiological pathways ranging from cytotoxic agent to neurotransmitter and vasodilator. The enzymatic reaction with which NO is produced by NOSs is thought to follow the general pattern of another heme-protein group, cytochrome P450s, with the difference that the complete reaction is performed by NOS in two cycles, which maybe possibly similar. Initially the ferrous heme-iron binds molecular oxygen forming the oxyferrous species which is activated by one-electron reduction to break the O-O bond and produce the putative reactive species which perform the oxygen atom insertion, compound I. In the first cycle the latter inserts a hydroxyl group at the guanidinium terminal of the substrate, L-arginine, forming NOHA. This stays bound in the active site and undergoes the second cycle where, through the insertion of an oxygen atom is cleaved to form citrulline and NO. The globally accepted version of the reaction has been inferred by a series of analyses, but the actual reactive species has never been identified. The last accumulating species along the course of the reaction is the oxyferrous compound: the events downstream remain unknown due to the high rate at which they occur, and the next detected species is the resting ferric enzyme. The aim of this PhD project was to contribute to our understanding of the NOS reaction, particularly in identifying intermediates that form in the unknown part of the reaction.

Despite performing very similar reactions to that of P450, NOS has a much higher degree of hydrophobicity in its catalytic site. The reason of this difference is unknown, and we used it as an inspiration in the attempt to find out the details of the chemical mechanism. The idea was to create a $nNOS_{oxy}$ active site environment with some

hydrophilic nature that has the capability to stabilize and allow the accumulation of intermediates during the reaction by means of newly formed interactions. A series of mutants were then generated replacing hydrophobic amino acids with residues capable of forming H-bonds. When tested, not all the mutants were significantly different catalytically in comparison with the wild type enzyme. However the mutant where glycine 586 was replaced by a serine (G586S $nNOS_{oxy}$) had unusual properties when the decay of the oxyferrous compound was observed in the presence of L-arginine and H_4B. The results suggested that the mutation we engineered was effective in stabilizing at least one of the reaction intermediates by means of a newly formed interaction. Further catalytic characterization of the mutant reaction, using the enzyme inhibitor amino-H_4B, proved that formation of the new intermediate relies on the second electron being transferred from H_4B to the oxy-ferrous compound: this suggests that the newly stabilized intermediate is possibly a species involved in the normal catalytic cycle forming downstream from the oxyferrous complex, and results from its activation.

In order to understand the nature of the newly formed active site interactions, we characterized the way the G586S $nNOS_{oxy}$ mutant binds its substrates. Several susbtrate-analogues and diatomic ligands that mimic O_2 behaviour, such as CO and NO were tested. We then compared the results with those characterizing the wild type enzyme. We observed a ten-fold higher affinity of the mutant for L-arginine, compared to that of the wild type; the stabilizing effect was smaller in the presence of NOHA, due possibly to a steric clash between the new residue and the bulkier ligand. This type of behaviour was confirmed by analogue affinity titrations. Through the diatomic ligands affinities measurements it was evident that a direct interaction between the mutated residue and the heme is to be ruled out. The stabilizing effect induced by the serine 586

was exerted only in the presence of the substrate. It is then possible that the ligand binding is optimized by a new interaction caused by a repositioning of the substrate. Considering the importance of structural data to corroborate these speculations, we embarked on the effort to obtain the crystal structure of the mutant in the presence of L-arginine, and managed to solve the structure at a 2.59 Å resolution. This showed that the new serine residue is at a suitable distance and orientation to form a hydrogen bond with the guanidinium terminal of the substrate. Furthermore, the distance between one of the guanidinium nitrogens and the heme iron was shorter, suggesting a better position to influence diatomic ligand binding to the heme-iron. Finally we measured the reduction potential of the G586S $nNOS_{oxy}$ in the presence and absence of L-arginine by potentiometric titrations: a comparison with the data relative to the WT enzyme showed that the absolute values of the potential and the 10 mV shift caused by the substrate binding are consistent with the mutant enzyme conserving the heme native electrical properties.

Understanding the nature of the new interaction gain insight into the mechanism. The shorter distance between the heme iron and the guanidinium nitrogen just above it shown by the enzyme structure. However, even with the highest possible resolution of the structure it wouldn't be possible to incontrovertibly claim that the distance is significantly shorter than in the WT enzyme. Nevertheless it is likely that this is the case and that the newly formed interaction affects the catalytic behaviour of the enzyme. Resolution of the G586S $nNOS_{oxy}$ structure in the presence of either the other substrate, NOHA, or of substrate-analogues, would provide further useful information on the binding orientation of substrates.

Another important issue, in the attempt to understand the stabilizing effect due to the mutation, is the protonation state of the serine residue itself. Although the pK_a of the amino acid in solution (~13) would suggest that the serine is likely to be in its protonated form, in the active site framework this may not be the case. The H-bond network could favour the stabilization of its unprotonated form: in this case the H-bond would be formed between the substrate terminal oxygen and one of the protons on the guanidinium nitrogen.

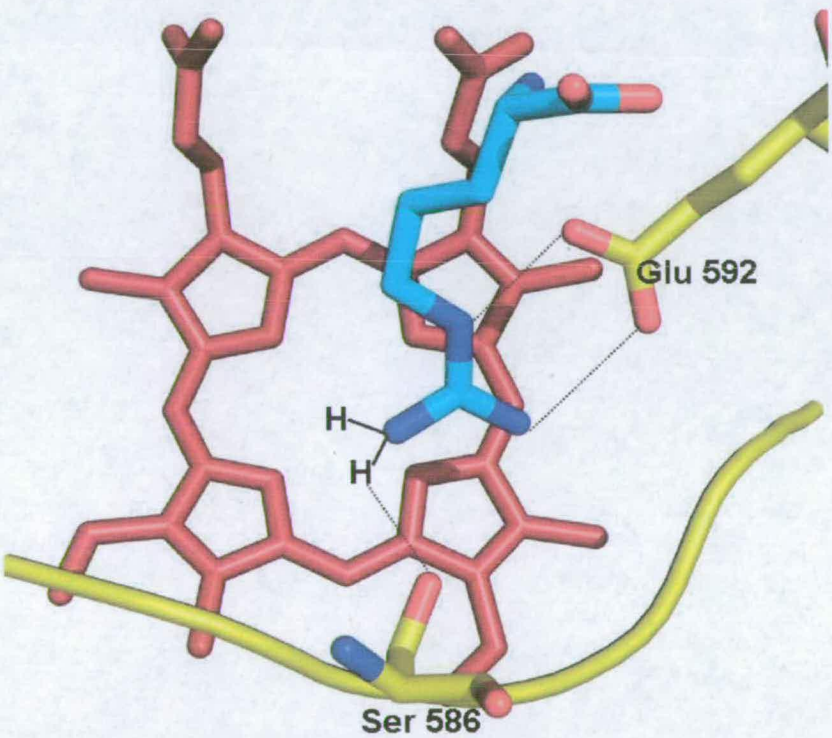

On the other hand, if the serine is protonated an interaction can be formed between its proton and the peptide carbonyl of tryptophan 587, as well as between the serine terminal oxygen and one of the substrate guanidinium protons.

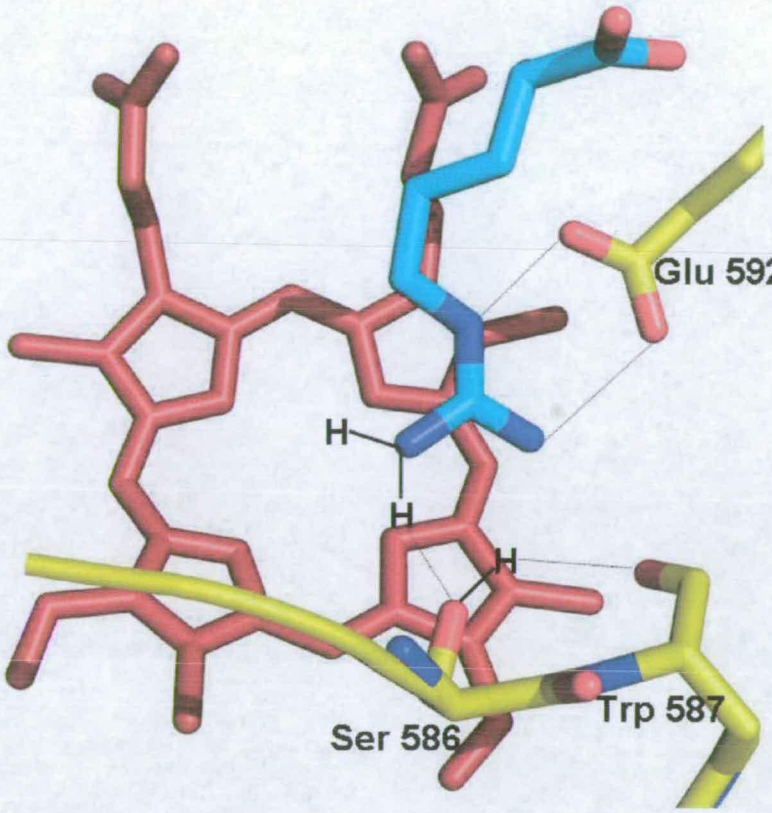

The oxyferrous species, after its activation by the second electron transfer, is thought to undergo two consecutive protonations in order to form the actual reactive species that perform the reaction in both cycles: consequently the easiness with which both protons are transferred has an impact on the overall rate and mechanism of the reaction. It has been speculated that the source of one or either both protons could be the active site bound substrate. The serine 586, if in a protonated state would probably favour at least one of the protonation steps by promptly replacing the substrate donated proton. On the other hand if the serine is unprotonated, the interaction formed with the guanidinium group could be seen as one of a stronger kind if compared with a H-bond: the proton between the guanidinium nitrogen and the serine oxygen could bridge the two atoms

causing an overall stabilization of the guanidinium proton. This would in turn disfavour the transfer of a proton from the substrate to the oxygen-heme intermediate.

The importance of speculating about the protonation state of the mutated serine is related to the different ways this would affect the observed catalytic behaviour, and would provide insights about the mechanism with which the new intermediate is stabilized and its identity. It is difficult to give an interpretation about the mechanism taking place ignoring the identity of the newly detected intermediate. Hence, its identification, for example by means of spectroscopic techniques such as EPR, would constitute an important step towards completing the puzzle of the mutant reaction course. Equally useful would be the analysis of the G586S $nNOS_{oxy}$ catalytic behaviour in a range of different pHs, paying attention though to the stability of the enzyme.

It is also important to know if the newly observed intermediate is part of a normal NOS cycle, in particular concerning the production of NO: hence, either by detection of NO as a product of the G586S nNOS holo-enzyme reaction by enzymatic assays, or by FPLC analysis of the reaction products, proof of the normal enzyme reaction is a key piece of information to obtain.

References

1. Ignarro LJ, Buga GM, Wood KS, Byrns RE, Chaudhuri G.
Endothelium-derived relaxing factor produced and released from artery and vein is nitric oxide.
Proc Natl Acad Sci U S A. 1987;84(24):9265-9.

2. Furchgott, RF, MT Khan, D Jothianandan. Comparison of Endothelium-Dependent Relaxation and Nitric Oxide-Induced Relaxation in Rabbit Aorta. Federation Proceedings. 1987; 46:385-385.

3. Hess DT, Matsumoto A, Kim SO, Marshall HE, Stamler JS.
Protein S-nitrosylation: purview and parameters.
Nat Rev Mol Cell Biol. 2005;6(2):150-66. Review.

4. Gow AJ, Stamler JS. Reactions between nitric oxide and haemoglobin under physiological conditions. Nature. 1998 8;391(6663):169-73.

5. Zhang YY, Xu AM, Nomen M, Walsh M, Keaney JF Jr, Loscalzo J.
Nitrosation of tryptophan residue(s) in serum albumin and model dipeptides. Biochemical characterization and bioactivity.
J Biol Chem. 1996 14;271(24):14271-9.

6. Lincoln TM. Cyclic GMP and mechanisms of vasodilation. Pharmacol Ther. 1989;41(3):479-502. Review.

7. O'Dell TJ, Hawkins RD, Kandel ER, Arancio O.
Tests of the roles of two diffusible substances in long-term potentiation: evidence for nitric oxide as a possible early retrograde messenger.
Proc Natl Acad Sci U S A. 1991 Dec 15;88(24):11285-9.

8. DeKock RL, Gray HB, Chemical structure and bonding. The Benjamin/Cummings Publishing Company 1980

9. Stuehr DJ. Mammalian nitric oxide synthases.
Biochim Biophys Acta. 1999 5;1411(2-3):217-30. Review

10. Alderton WK, Cooper CE, Knowles RG. Nitric oxide synthases: structure, function and inhibition. Biochem J. 2001 1;357(Pt 3):593-615. Review

11. Kone BC. Protein-protein interactions controlling nitric oxide synthases. Acta Physiol Scand. 2000;168(1):27-31. Review.

12. Cho HJ, Martin E, Xie QW, Sassa S, Nathan C. Inducible nitric oxide synthase: identification of amino acid residues essential for dimerization and binding of tetrahydrobiopterin. Proc Natl Acad Sci U S A. 1995 5;92(25):11514-8.

13. Pant K, Bilwes AM, Adak S, Stuehr DJ, Crane BR. Structure of a nitric oxide synthase heme protein from Bacillus subtilis. Biochemistry. 2002 Sep 17;41(37):11071-9

14. Adak, S, Bilwes, AM, Panda, K, Hosfield, D, Aulak, KS, McDonald, JF, Tainer, JA, Getzoff, ED, Crane, BR, Stuehr, DJ. Proc. Natl. Acad. Sci. USA 2002 99, 107–112

15. Förstermann U, Kleinert H. Nitric oxide synthase: expression and expressional control of the three isoforms. Naunyn Schmiedebergs Arch Pharmacol. 1995 352(4):351-64. Review.

16. Daff S, Sagami I, Shimizu T. The 42-amino acid insert in the FMN domain of neuronal nitric-oxide synthase exerts control over Ca(2+)/calmodulin-dependent electron transfer.
J Biol Chem. 1999 22;274(43):30589-95

17. Xie Q, Nathan C. The high-output nitric oxide pathway: role and regulation.
J Leukoc Biol. 1994 Nov;56(5):576-82.

18. Lowenstein CJ, Alley EW, Raval P, Snowman AM, Snyder SH, Russell SW, Murphy WJ. Macrophage nitric oxide synthase gene: two upstream regions mediate induction by interferon gamma and lipopolysaccharide.
Proc Natl Acad Sci U S A. 1993 15;90(20):9730-4.

19. Crane BR, Arvai AS, Gachhui R, Wu C, Ghosh DK, Getzoff ED, Stuehr DJ, Tainer JA. The structure of nitric oxide synthase oxygenase domain and inhibitor complexes.
Science. 1997 17;278(5337):425-31

20. Fischmann TO, Hruza A, Niu XD, Fossetta JD, Lunn CA, Dolphin E, Prongay AJ, Reichert P, Lundell DJ, Narula SK, Weber PC. Structural characterization of nitric oxide synthase isoforms reveals striking active-site conservation.
Nat Struct Biol. 1999;6(3):233-42

21. Raman CS, Li H, Martásek P, Král V, Masters BS, Poulos TL. Crystal structure of constitutive endothelial nitric oxide synthase: a paradigm for pterin function involving a novel metal center. Cell. 1998 23;95(7):939-50.

22. Li H, Shimizu H, Flinspach M, Jamal J, Yang W, Xian M, Cai T, Wen EZ, Jia Q, Wang PG, Poulos TL. The novel binding mode of N-alkyl-N'-hydroxyguanidine to neuronal nitric oxide synthase provides mechanistic insights into NO biosynthesis. Biochemistry. 2002 26;41(47):13868-75

23. Garcin ED, Bruns CM, Lloyd SJ, Hosfield DJ, Tiso M, Gachhui R, Stuehr DJ, Tainer JA, Getzoff ED. Structural basis for isozyme-specific regulation of electron transfer in nitric-oxide synthase. J Biol Chem. 2004 3;279(36):37918-27.

24. Watenpaugh KD, Sieker LC, Herriott JR, Jensen LH. The structure of a non-heme iron protein: rubredoxin at 1.5 Angstrom resolution. Cold Spring Harb Symp Quant Biol. 1972;36:359-67.

25. Karplus PA, Daniels MJ, Herriott JR. Atomic structure of ferredoxin-NADP+ reductase: prototype for a structurally novel flavoenzyme family.
Science. 1991 Jan 4;251(4989):60-6

26. Abu-Soud HM, Stuehr DJ. Nitric oxide synthases reveal a role for calmodulin in controlling electron transfer. Proc Natl Acad Sci U S A. 1993 Nov 15;90(22):10769-72.

27. Masters BS. Nitric oxide synthases: why so complex? Annu Rev Nutr. 1994;14:131-45. Review

28. Salerno JC, Harris DE, Irizarry K, Patel B, Morales AJ, Smith SM, Martasek P, Roman LJ, Masters BS, Jones CL, Weissman BA, Lane P, Liu Q, Gross SS. An autoinhibitory control element defines calcium-regulated isoforms of nitric oxide synthase. J Biol Chem. 1997 21;272(47):29769-77.

29. Matsuda H, Iyanagi T. Calmodulin activates intramolecular electron transfer between the two flavins of neuronal nitric oxide synthase flavin domain. Biochim Biophys Acta. 1999 27;1473(2-3):345-55.

30. Sheta EA, McMillan K, Masters BS. Evidence for a bidomain structure of constitutive cerebellar nitric oxide synthase. J Biol Chem. 1994 27;269(21):15147-53.

31. Roman LJ, Martásek P, Miller RT, Harris DE, de La Garza MA, Shea TM, Kim JJ, Masters BS. The C termini of constitutive nitric-oxide synthases control electron flow through the flavin and heme domains and affect modulation by calmodulin.
J Biol Chem. 2000 22;275(38):29225-32.

32. Zhang J, Martàsek P, Paschke R, Shea T, Siler Masters BS, Kim JJ. Crystal structure of the FAD/NADPH-binding domain of rat neuronal nitric-oxide synthase. Comparisons with NADPH-cytochrome P450 oxidoreductase. J Biol Chem. 2001 5;276(40):37506-13.

33. Deng Z, Aliverti A, Zanetti G, Arakaki AK, Ottado J, Orellano EG, Calcaterra NB, Ceccarelli EA, Carrillo N, Karplus PA. A productive NADP+ binding mode of ferredoxin-NADP + reductase revealed by protein engineering and crystallographic studies.
Nat Struct Biol. 1999;6(9):847-53.

34. Siddhanta U, Presta A, Fan B, Wolan D, Rousseau DL, Stuehr DJ. Domain swapping in inducible nitric-oxide synthase. Electron transfer occurs between flavin and heme groups located on adjacent subunits in the dimer. J Biol Chem. 1998 24;273(30):18950-8.

35. Bredt DS, Hwang PM, Glatt CE, Lowenstein C, Reed RR, Snyder SH. Cloned and expressed nitric oxide synthase structurally resembles cytochrome P-450 reductase. Nature. 1991 27;351(6329):714-8.

36. Stuehr DJ, Cho HJ, Kwon NS, Weise MF, Nathan CF. Purification and characterization of the cytokine-induced macrophage nitric oxide synthase: an FAD- and FMN-containing flavoprotein. Proc Natl Acad Sci U S A. 1991 1;88(17):7773-7

37. Sheta EA, McMillan K, Masters BS. Evidence for a bidomain structure of constitutive cerebellar nitric oxide synthase. J Biol Chem. 1994 27;269(21):15147-53.

38. Bredt DS, Snyder SH. Isolation of nitric oxide synthetase, a calmodulin-requiring enzyme. Proc Natl Acad Sci U S A. 1990;87(2):682-5.

39. Yui Y, Hattori R, Kosuga K, Eizawa H, Hiki K, Ohkawa S, Ohnishi K, Terao S, Kawai C. Calmodulin-independent nitric oxide synthase from rat polymorphonuclear neutrophils.
J Biol Chem. 1991 25;266(6):3369-71.

40. Roman LJ, Martásek P, Miller RT, Harris DE, de La Garza MA, Shea TM, Kim JJ, Masters BS. The C termini of constitutive nitric-oxide synthases control electron flow through the flavin and heme domains and affect modulation by calmodulin. J Biol Chem. 2000 22;275(38):29225-32

41. Nishida CR, Ortiz de Montellano PR. Autoinhibition of endothelial nitric-oxide synthase. Identification of an electron transfer control element. J Biol Chem. 1999 21;274(21):14692-8

42. Craig DH, Chapman SK, Daff S. Calmodulin activates electron transfer through neuronal nitric-oxide synthase reductase domain by releasing an NADPH-dependent conformational lock. J Biol Chem. 2002 13;277(37):33987-94.

43. Fischmann TO, Hruza A, Niu XD, Fossetta JD, Lunn CA, Dolphin E, Prongay AJ, Reichert P, Lundell DJ, Narula SK, Weber PC. Structural characterization of nitric oxide synthase isoforms reveals striking active-site conservation. Nat Struct Biol. 1999;6(3):233-42

44. Crane BR, Arvai AS, Ghosh DK, Wu C, Getzoff ED, Stuehr DJ, Tainer JA. Structure of nitric oxide synthase oxygenase dimer with pterin and substrate. Science. 1998 27;279(5359):2121-6.

45. Wang ZQ, Wei CC, Ghosh S, Meade AL, Hemann C, Hille R, Stuehr DJ. A conserved tryptophan in nitric oxide synthase regulates heme-dioxy reduction by tetrahydrobiopterin. Biochemistry. 2001 30;40(43):12819-25.

46. Wang ZQ, Wei CC, Stuehr DJ. A conserved tryptophan 457 modulates the kinetics and extent of N-hydroxy-L-arginine oxidation by inducible nitric-oxide synthase. J Biol Chem. 2002 12;277(15):12830-7.

47. Lewis DF, Dickins M, Eddershaw PJ, Tarbit MH, Goldfarb PS. Cytochrome P450 substrate specificities, substrate structural templates and enzyme active site geometries. Drug Metabol Drug Interact. 1999;15(1):1-49. Review

48. Lewis DF. Structural characteristics of human P450s involved in drug metabolism: QSARs and lipophilicity profiles. Toxicology. 2000 3;144(1-3):197-203. Review

49. Estabrook RW, Cooper DY, Rosenthal O. The light reversible carbon monoxide inhibition of the steroid C21-hydroxylase system of the adrenal cortex. Biochem. Zeits. 1963; 338, 741-55.

50. Poulos TL, Finzel BC, Gunsalus IC, Wagner GC, Kraut J. The 2.6-.ANG. crystal structure of Pseudomonas putida cytochrome P-450. J. Biol. Chem. 1985, 260(30), 16122-16130.

51. Ravichandran KG, Boddupalli SS, Hasermann CA, Peterson JA, Deisenhofer J. Crystal structure of hemoprotein domain of P450BM-3, a prototype for microsomal P450's. Science 1993, 261(5122), 731-736.

52. Li H; Poulos TL. The structure of the cytochrome p450BM-3 hemedomain complexed with
the fatty acid substrate, palmitoleic acid. Nat. Struct. Biol. 1997, 4(2), 140-146.

53. Lewis, David F. V.; Pratt, John M. The P450 catalytic cycle and oxygenation mechanism. Drug Metab. Rev. 1998, 30(4), 739-786.

54. Yano JK; Blasco F; Li H; Schmid RD; Henne A; Poulos TL. Preliminary characterization and crystal structure of a thermostable cytochrome P450 from Thermus thermophilus. J. Biol. Chem. (2003), 278(1), 608-616.

55. Poulos TL. The role of the proximal ligand in heme enzymes. J. Bio. Inorg. Chem. 1996, 1(4), 356-359.

56. Ryan, K. J.; Engel, L. L Hydroxylation of steroids at carbon 21. J. biol. Chem. (1957), 225(1), 103-114.

57. Werck-Reichhart D, Feyereisen R. Cytochromes P450: a success story. Genome Biol. 2000;1(6):3003. Review

58. Abu-Soud HM, Gachhui R, Raushel FM, Stuehr DJ. The ferrous-dioxy complex of neuronal nitric oxide synthase. Divergent effects of L-arginine and tetrahydrobiopterin on its stability. J Biol Chem. 1997 11;272(28):17349-53

References

58. Abu-Soud HM, Gachhui R, Raushel FM, Stuehr DJ. The ferrous-dioxy complex of neuronal nitric oxide synthase. Divergent effects of L-arginine and tetrahydrobiopterin on its stability. J Biol Chem. 1997 11;272(28):17349-53

59. Ledbetter AP, McMillan K, Roman LJ, Masters BS, Dawson JH, Sono M. Low temperature stabilization and spectroscopic characterization of the dioxygen complex of the ferrous neuronal nitric oxide synthase oxygenase domain. Biochemistry. 1999 22;38(25):8014-21.

60. Tuckey RC, Kamin H.The oxyferro complex of adrenal cytochrome P-450scc. Effect of cholesterol and intermediates on its stability and optical characteristics. J Biol Chem. 1982 Aug 25;257(16):9309-14

61. Bec N, Gorren AC, Voelker C, Mayer B, Lange R. Reaction of neuronal nitric-oxide synthase with oxygen at low temperature. Evidence for reductive activation of the oxy-ferrous complex by tetrahydrobiopterin. J Biol Chem. 1998 29;273(22):13502-8

62. Stuehr DJ, Santolini J, Wang ZQ, Wei CC, Adak S. Update on mechanism and catalytic regulation in the NO synthases. J Biol Chem. 2004 27;279(35):36167-70. Epub 2004 May 7. Review

63. Ost TW, Daff S.Thermodynamic and kinetic analysis of the nitrosyl, carbonyl, and dioxy heme complexes of neuronal nitric-oxide synthase. The roles of substrate and tetrahydrobiopterin in oxygen activation. J Biol Chem. 2005 14;280(2):965-73.

64. Davydov R, Ledbetter-Rogers A, Martásek P, Larukhin M, Sono M, Dawson JH, Masters BS, Hoffman BM. EPR and ENDOR characterization of intermediates in the cryoreduced oxy-nitric oxide synthase heme domain with bound L-arginine or N(G)-hydroxyarginine.
Biochemistry. 2002 20;41(33):10375-81

65. Davydov R, Makris TM, Kofman V, Werst DE, Sligar SG, Hoffman BM.Hydroxylation of camphor by reduced oxy-cytochrome P450cam: mechanistic implications of EPR and ENDOR studies of catalytic intermediates in native and mutant enzymes. J Am Chem Soc. 2001 21;123(7):1403-15.

66. Huang H, Hah JM, Silverman RB. Mechanism of nitric oxide synthase. Evidence that direct hydrogen atom abstraction from the O-H bond of NG-hydroxyarginine is not relevant to the mechanism. J Am Chem Soc. 2001 Mar 21;123(11):2674-6.

67. Wei CC, Wang ZQ, Hemann C, Hille R, Stuehr DJ. A tetrahydrobiopterin radical forms and then becomes reduced during Nomega-hydroxyarginine oxidation by nitric-oxide synthase.
J Biol Chem. 2003 21;278(47):46668-73.

68. Rusche KM, Spiering MM, Marletta MA. Reactions catalyzed by tetrahydrobiopterin-free nitric oxide synthase. Biochemistry. 1998 3;37(44):15503-12.

69. Hurshman AR, Krebs C, Edmondson DE, Huynh BH, Marletta MA. Formation of a pterin radical in the reaction of the heme domain of inducible nitric oxide synthase with oxygen.
Biochemistry. 1999 30;38(48):15689-96

70. Wei CC, Wang ZQ, Arvai AS, Hemann C, Hille R, Getzoff ED, Stuehr DJ. Structure of tetrahydrobiopterin tunes its electron transfer to the heme-dioxy intermediate in nitric oxide synthase. Biochemistry. 2003 Feb 25;42(7):1969-77

71. Wang ZQ, Wei CC, Stuehr DJ. A conserved tryptophan 457 modulates the kinetics and extent of N-hydroxy-L-arginine oxidation by inducible nitric-oxide synthase.
J Biol Chem. 2002 12;277(15):12830-7

72. Wang ZQ, Wei CC, Ghosh S, Meade AL, Hemann C, Hille R, Stuehr DJ. A conserved tryptophan in nitric oxide synthase regulates heme-dioxy reduction by tetrahydrobiopterin. Biochemistry. 2001 30;40(43):12819-25

73. Wei CC, Wang ZQ, Wang Q, Meade AL, Hemann C, Hille R, Stuehr DJ. Rapid kinetic studies link tetrahydrobiopterin radical formation to heme-dioxy reduction and arginine hydroxylation in inducible nitric-oxide synthase. J Biol Chem. 2001 Jan 5;276(1):315-9.

74. Davydov R, Kofman V, Fujii H, Yoshida T, Ikeda-Saito M, Hoffman BM. Catalytic mechanism of heme oxygenase through EPR and ENDOR of cryoreduced oxy-heme oxygenase and its Asp 140 mutants. J Am Chem Soc. 2002 27;124(8):1798-808

75. Stuehr DJ, Kwon NS, Nathan CF, Griffith OW, Feldman PL, Wiseman J. N omega hydroxy-L-arginine is an intermediate in the biosynthesis of nitric oxide from L-arginine. J Biol Chem. 1991 Apr 5;266(10):6259-63.

76. Garnaud PE, Koetsier M, Ost TW, Daff S. Redox properties of the isolated flavin mononucleotide- and flavin adenine dinucleotide-binding domains of neuronal nitric oxide synthase. Biochemistry. 2004 31;43(34):11035-44

77. Roman LJ, Miller RT, de La Garza MA, Kim JJ, Siler Masters BS. The C terminus of mouse macrophage inducible nitric-oxide synthase attenuates electron flow through the flavin domain. J Biol Chem. 2000 21;275(29):21914-9.

78. Roman LJ, Martásek P, Miller RT, Harris DE, de La Garza MA, Shea TM, Kim JJ, Masters BS. The C termini of constitutive nitric-oxide synthases control electron flow through the flavin and heme domains and affect modulation by calmodulin. J Biol Chem. 2000 22;275(38):29225-32

79. Roman LJ, Masters BS. Electron transfer by neuronal nitric-oxide synthase is regulated by concerted interaction of calmodulin and two intrinsic regulatory elements. J Biol Chem. 2006 11;281(32):23111-8. Epub 2006 Jun 16.

80. Li H, Poulos TL. Structure-function studies on nitric oxide synthases. J Inorg Biochem. 2005 ;99(1):293-305. Review.

81. Shiro Y, Fujii M, Iizuka T, Adachi S, Tsukamoto K, Nakahara K, Shoun H Spectroscopic and kinetic studies on reaction of cytochrome P450nor with nitric oxide. Implication for its nitric oxide reduction mechanism. J. Biol. Chem. 1995, 270(4), 1617-23.

82. Nagano S, Li H, Shimizu H, Nishida C, Ogura H, Ortiz de Montellano PR, Poulos T L. Crystal Structures of Epothilone D-bound, Epothilone B-bound, and Substrate-free Forms of Cytochrome P450epoK. J. Biol. Chem. 2003, 278(45), 44886-44893.

83. Meharenna Y T, Li H, Hawkes DB, Pearson AG, De Voss J, Poulos TL. Crystal structure of P450cin in a complex with its substrate, 1,8-cineole, a close structural homologue to D-camphor, the substrate for P450cam. Biochemistry (2004), 43(29), 9487-9494.

84. Hawkes B, Adams GW, Burlingame AL, Ortiz de Montellano PR, de Voss JJ. Cytochrome P450cin (CYP176A), isolation, expression, and characterization. J. Biol. Chem. (2002), 277(31), 27725-27732.

85. Gunsalus, IC, Pederson TC, Sligar SG. Oxygenase-catalyzed biological hydroxylations. Ann. Rev. Biochem. (1975), 44, 377-407.

86. Lambeth JD, Kamin H. Adrenodoxin reductase.adrenodoxin complex. Flavin to iron-sulfur electron transfer as the rate-limiting step in the NADPH-cytochrome c reductase reaction. J. Biol. Chem. (1979), 254(8), 2766-2774.

87. Williams PA, Cosme J, Sridhar V, Johnson EF, McRee DE. Microsomal cytochrome P450 2C5: comparison to microbial P450s and unique features. J. Inorg. Biochem. (2000), 81(3), 183-190.

88. Raag R, Poulos TL. Crystal structure of the carbon monoxide-substrate-cytochrome P-450CAM ternary complex. Biochemistry (1989), 28(19), 7586-7592.

89. Schlichting, Ilme; Jung, Christiane; Schulze, Heike. Crystal structure of cytochrome P450cam complexed with the (1S)-camphor enantiomer. FEBS Lett. (1997), 415(3), 253-257.

90. Modi S; Sutcliffe M J; Primrose W U; Lian L Y; Roberts G C The catalytic mechanism of cytochrome P450 BM3 involves a 6 A movement of the bound substrate on reduction. Nat. struct. Boil. (1996), 3(5), 414-417.

91. Jin, Shengxi; Bryson, Thomas A.; Dawson, John H. Hydroperoxo-ferric heme intermediate as a second electrophilic oxidant in cytochrome P450-catalyzed reactions. J. Biol. Inorg. Chem. (2004), 9(6), 644-653.

92. Nam, Wonwoo; Ryu, Yon Ok; Song, Woon Ju. Oxidizing intermediates in cytochrome P450 model reactions J. Biol. Inorg. Chem. (2004), 9(6), 654-660.

93 Davydov R, Kappl R, Hüttermann J, Peterson JA. EPR-spectroscopy of reduced oxyferrous-P450cam. FEBS Lett. 1991 Dec 16;295(1-3):113-5.

94. Davydov R, Macdonald IDG, Makris TM, Sligar SG, Hoffman BM. EPR and ENDOR of -catalytic intermediates in cryoreduced native and mutant oxy-cytochromes P450cam: mutation-induced changes in the proton delivery system. J.Am.Chem.Soc. 121 1999 10654-10655

95. Davydov R, Makris TM, Kofman V, Werst DE, Sligar SG, Hoffman BM. Hydroxylation of camphor by reduced oxy-cytochrome P450cam: mechanistic implications of EPR and ENDOR studies of catalytic intermediates in native and mutant enzymes. J Am Chem Soc. 2001 Feb 21;123(7):1403-15

96. Schlichting I, Berendzen J, Chu K, Stock AM, Maves SA, Benson DE, Sweet RM, Ringe D, Petsko GA, Sligar SG. The catalytic pathway of cytochrome p450cam at atomic resolution. Science. 2000 Mar 3;287(5458):1615-22

97. Yeom H; Sligar S G; Li H; Poulos T L; Fulco A J The role of Thr268 in oxygen activation of cytochrome P450BM-3. Biochemistry (1995), 34(45), 14733-14740.

98. Aikens, John; Sligar, Stephen G.. Kinetic Solvent Isotope Effects during Oxygen Activation by Cytochrome P-450cam. J. Am. Chem. Soc.(1994), 116(3), 1143-1144.

99. Obayashi, E.; Shimizu, H.; Park, S.-Y.; Shoun, H.; Shiro, Y. Mutation effects of a conserved threonine (Thr243) of cytochrome P450nor on its structure and function. J. Inorg. Biochem.(2000), 82(1-4), 103-111.

100. Truan, Gilles; Peterson, Julian A. Thr268 in substrate binding and catalysis in P450BM-3. Arch. Biochem. Biophys. (1998), 349(1), 53-64.

101. Haines D C; Tomchick D R; Machius M; Peterson J A Pivotal role of water in the mechanism of P450BM-3. Biochemistry (2001), 40(45), 13456-13465

102. Nagano, Shingo; Poulos, Thomas L. Crystallographic study on the dioxygen complex of wild-type and mutant cytochrome P 450cam: Implications for the dioxygen activation mechanism. J. Biol. Chem. (2005), 280(36), 31659-31663.

103. Guengerich FP, Ballou DP, Coon MJ. Spectral intermediates in the reaction of oxygen with purified liver microsomal cytochrome P-450. Biochem Biophys Res Commun. 1976 Jun 7;70(3):951-6.

104. Tyson CA, Lipscomb JD, Gunsalus IC. The role of putidaredoxin and P450 cam in methylene hydroxylation. J Biol Chem. 1972 Sep 25;247(18):5777-84

105. Kunkel T A Rapid and efficient site-specific mutagenesis without phenotypic selection. *Proc. Natl. Acad. Sci. USA* (1985), 82(2), 488-92.

106. Newton, D.C., H.J. Montgomery, and J.G. Guillemette. 1998. *Archives of Biochemistry and Biophysics* 359:249-257.

107 McMillan K, Masters BS. Optical difference spectrophotometry as a probe of rat brain nitric oxide synthase heme-substrate interaction. Biochemistry. 1993 28;32(38):9875-80.

108 Binding of L-arginine and imidazole suggests heterogeneity of rat brain neuronal nitric synthase Gorren Schmidt and Mayer

109 Li H, Igarashi J, Jamal J, Yang W, Poulos TL. Structural studies of constitutive nitric oxide synthases with diatomic ligands bound. J Biol Inorg Chem. 2006;11(6):753-68.

110 Housecroft C E, Sharpe A G. "Inorganic Chemistry". Pearson Education Limited 2001, 2005

111 Hurshman AR, Krebs C, Edmondson DE, Marletta MA. Ability of tetrahydrobiopterin analogues to support catalysis by inducible nitric oxide synthase: formation of a pterin radical is required for enzyme activity. Biochemistry. 2003 18;42(45):13287-303

112 Egawa T, Shimada H, Ishimura Y. Evidence for compound I formation in the reaction of cytochrome P450cam with m-chloroperbenzoic acid. Biochem Biophys Res Commun. 1994 30;201(3):1464-9.

113 Zhang R, Nagraj N, Lansakara-P DS, Hager LP, Newcomb M. Kinetics of two-electron oxidations by the compound I derivative of chloroperoxidase, a model for cytochrome P450 oxidants. Org Lett. 2006 22;8(13):2731-4.

114 Kellner DG, Hung SC, Weiss KE, Sligar SG. Kinetic characterization of compound I formation in the thermostable cytochrome P450 CYP119. J Biol Chem. 2002 22;277(12):9641-4.

115 Sorlie M, Gorren AC, Marchal S, Shimizu T, Lange R, Andersson KK, Mayer B. Single-turnover of nitric-oxide synthase in the presence of 4-amino-tetrahydrobiopterin: proposed role for tetrahydrobiopterin as a proton donor. J Biol Chem. 2003 5;278(49):48602-10.

116 Mayer B, Klatt P, Werner ER, Schmidt K. Identification of imidazole as L-arginine-competitive inhibitor of porcine brain nitric oxide synthase. FEBS Lett. 1994 22;350(2-3):199-202

117 Ost TW, Miles CS, Munro AW, Murdoch J, Reid GA, Chapman SK. Phenylalanine 393 exerts thermodynamic control over the heme of flavocytochrome P450 BM3. Biochemistry. 2001 13;40(45):13421-9

118 Sagami I, Shimizu T. The crucial roles of Asp-314 and Thr-315 in the catalytic activation of molecular oxygen by neuronal nitric-oxide synthase. A site-directed mutagenesis study.J Biol Chem. 1998 23;273(4):2105-8

119 Li H, Shimizu H, Flinspach M, Jamal J, Yang W, Xian M, Cai T, Wen EZ, Jia Q, Wang PG, Poulos TL. The novel binding mode of N-alkyl-N'-hydroxyguanidine to neuronal nitric oxide synthase provides mechanistic insights into NO biosynthesis. Biochemistry. 2002 26;41(47):13868-75.

120 Leslie, A. G. W. CCP4 Newslett. Protein Crystallogr. 32, 7-8 (1996).

121 Kabsch W. Evaluation of Single-Crystal X-ray Diffraction Data from Position Sensitive Detectors. J. Appl. Crystallography. 21, 916-924 (1988).

122 McCoy A. Phaser crystallographic software. J. Appl. Cryst. 40, 658-674 (2007).

123 Roussel, A and Cambillau, C. (eds.) In Silicon Graphics Geometry Partners Directory 86 (Mountain View, CA, USA: Silicon Graphics, 1991).

124 Emsley, P and Cowtan, K Coot: model-building tools for molecular graphics. Acta Crystallographica D60, 2126-2132 (2004).

125 Adams, P D PHENIX: building new software for automated crystallographic structure determination. Acta Cryst. D58, 1948-1954 (2002).

126 McPherson, A., ed. Preparation and Analysis of Protein Crystals. 1982, John Wiley & Sons.: New York.

127 McPherson A ed. Crystallization of Biological Macromolecules. 1999, Cold Spring Harbor Laboratory Press, New York.

128 Segal, D R D D M Protein crystallization. Micro techniques involving vapor diffusion. Methods Enzymol., 1971. 22: p. 266-269.

129 Murshudov, G., A.A. Vagin, and E. Dodson, Refinement of macromolecular structures by the maximum-likelihood method. Acta Cryst. , 1997. D53: p. 240-255.

130 Vernède X, J C Fontecilla-Camps A method to stabilize reduced and/or gas-treated protein crystals by flash-cooling under a controlled atmosphere. J. Appl. Cryst. , 1999 32: p. 505-509.

131 Ingledew WJ, Smith SM, Salerno JC, Rich PR. Neuronal nitric oxide synthase ligand and protein vibrations at the substrate binding site. A study by FTIR. Biochemistry. 2002 Jul 2;41(26):8377-84

132 Ingledew WJ, Smith SM, Gao YT, Jones RJ, Salerno JC, Rich PR. Ligand, cofactor, and residue vibrations in the catalytic site of endothelial nitric oxide synthase. Biochemistry. 2005 Mar 22;44(11):4238-46